Argonne NATIONAL LABORATORY

ANL-GenIV-124

Analysis of Supercritical CO_2 Cycle Control Strategies and Dynamic Response for Generation IV Reactors

Nuclear Engineering Division

About Argonne National Laboratory

Argonne is a U.S. Department of Energy laboratory managed by UChicago Argonne, LLC under contract DE-AC02-06CH11357. The Laboratory's main facility is outside Chicago, at 9700 South Cass Avenue, Argonne, Illinois 60439. For information about Argonne, see www.anl.gov.

Availability of This Report

This report is available, at no cost, at http://www.osti.gov/bridge. It is also available on paper to the U.S. Department of Energy and its contractors, for a processing fee, from:

U.S. Department of Energy
Office of Scientific and Technical Information
P.O. Box 62
Oak Ridge, TN 37831-0062
phone (865) 576-8401
fax (865) 576-5728
reports@adonis.osti.gov

ANL-GenIV-124

Analysis of Supercritical CO_2 Cycle Control Strategies and Dynamic Response for Generation IV Reactors

by
A. Moisseytsev and J. J. Sienicki
Nuclear Engineering Division, Argonne National Laboratory

September 15, 2009

TABLE OF CONTENTS

Abstract 3
1. Introduction 5
2. S-CO_2 Cycle Development for the VHTR 6
   2.1. Steady State Analysis of S-CO_2 Cycle for the VHTR 6
   2.2. Control Analysis of the S-CO_2 Cycle for the VHTR 16
3. S-CO_2 Cycle Control Analysis for the SFR 21
   3.1. Quasi-Static S-CO_2 Cycle Control Analysis for the SFR 21
   3.2. Dynamic Simulation of S-CO_2 Cycle Control for the SFR 22
4. Plant Dynamics Code Development 34
   4.1. Modifications to the Plant Dynamics Code for Generation IV Systems Analysis 34
   4.2. Incompressible Flow Treatment Option 34
5. Summary 39
References 41
Appendix A Quasi-Static S-CO_2 Cycle Control Analysis for a SFR ..... A
Appendix B A Utility for Piecewise Linear Fitting of Transient Data ..... B

LIST OF TABLES

Table 4-1. Effect of the Incompressible Flow Treatment in S-CO_2 Cycle 37

LIST OF FIGURES

Figure 2-1. Traditional Recompression S-CO_2 Cycle Application to VHTR..... 7
Figure 2-2. Cascaded S-CO_2 Cycle Configuration for the VHTR..... 9
Figure 2-3. Cascaded S-CO_2 Cycles for the VHTR - Top Section..... 10
Figure 2-4. Cascaded S-CO_2 Cycles for the VHTR - Middle Section..... 10
Figure 2-5. Cascaded S-CO_2 Cycles for the VHTR - Bottom Section. 11
Figure 2-6. T-s Diagram of S-CO_2 Cycle with Precooling..... 13
Figure 2-7. S-CO_2 Cycle with 3.5 MPa Minimum Pressure and Precooling..... 13
Figure 2-8. T-s Diagram for S-CO_2 Cycle with Two-Stage Precooling. 15
Figure 2-9. S-CO_2 Cycle with 1 MPa Minimum Pressure..... 15
Figure 2-10. Results of VHTR Transient Control Analysis. 18
Figure 3-1. Coupled Transient Calculations of S-CO_2 Cycle for SFR Using SAS4A/SASSYS-1 and Plant Dynamics Codes..... 24
Figure 3-2. Convergence of the Sodium Temperature in the Reactor Scram Simulation. 27
Figure 3-3. Convergence of the Sodium Flow Rate in the Reactor Scram Simulation. ... 28
Figure 3-4. Results of the Reactor Scram Transient – Reactor Side. 29
Figure 3-5. Results of the Reactor Scram Transient – S-CO_2 Cycle Side. 30
Figure 4-1. CO_2 Compressibility in the S-CO_2 Cycle..... 35
Figure 4-2. Error from Incompressible Flow Treatment in Transient. 38

Abstract

The analysis of specific control strategies and dynamic behavior of the supercritical carbon dioxide (S-CO_2) Brayton cycle has been extended to the two reactor types selected for continued development under the Generation IV Nuclear Energy Systems Initiative; namely, the Very High Temperature Reactor (VHTR) and the Sodium-Cooled Fast Reactor (SFR). Direct application of the standard S-CO_2 recompression cycle to the VHTR was found to be challenging because of the mismatch in the temperature drop of the He gaseous reactor coolant through the He-to-CO_2 reactor heat exchanger (RHX) versus the temperature rise of the CO_2 through the RHX. The reference VHTR features a large temperature drop of 450 °C between the assumed core outlet and inlet temperatures of 850 and 400 °C, respectively. This large temperature difference is an essential feature of the VHTR enabling a lower He flow rate reducing the required core velocities and pressure drop. In contrast, the standard recompression S-CO_2 cycle wants to operate with a temperature rise through the RHX of about 150 °C reflecting the temperature drop as the CO_2 expands from 20 MPa to 7.4 MPa in the turbine and the fact that the cycle is highly recuperated such that the CO_2 entering the RHX is effectively preheated. Because of this mismatch, direct application of the standard recompression cycle results in a relatively poor cycle efficiency of 44.9 %. However, two approaches have been identified by which the S-CO_2 cycle can be successfully adapted to the VHTR and the benefits of the S-CO_2 cycle, especially a significant gain in cycle efficiency, can be realized. The first approach involves the use of three separate cascaded S-CO_2 cycles. Each S-CO_2 cycle is coupled to the VHTR through its own He-to-CO_2 RHX in which the He temperature is reduced by 150 °C. The three respective cycles have efficiencies of 54, 50, and 44 %, respectively, resulting in a net cycle efficiency of 49.3 %. The other approach involves reducing the minimum cycle pressure significantly below the critical pressure such that the temperature drop in the turbine is increased while the minimum cycle temperature is maintained above the critical temperature to prevent the formation of a liquid phase. The latter approach also involves the addition of a precooler and a third compressor before the main compressor to retain the benefits of compression near the critical point with the main compressor. For a minimum cycle pressure of 1 MPa, a cycle efficiency of 49.5 % is achieved. Either approach opens up the door to applying the S-CO_2 cycle to the VHTR. In contrast, the SFR system typically has a core outlet-inlet temperature difference of about 150 °C such that the standard recompression cycle is ideally suited for direct application to the SFR. The ANL Plant Dynamics Code has been modified for application to the VHTR and SFR when the reactor side dynamic behavior is calculated with another system level computer code such as SAS4A/SYSSYS-1 in the SFR case. The key modification involves modeling heat exchange in the RHX, accepting time dependent tabular input from the reactor code, and generating time dependent tabular input to the reactor code such that both the reactor and S-CO_2 cycle sides can be calculated in a convergent iterative scheme. This approach retains the modeling benefits provided by the detailed reactor system level code and can be applied to any reactor system type incorporating a S-CO_2 cycle. This approach was applied to the particular calculation of a scram scenario for a SFR in which the main and intermediate sodium pumps are not tripped and the generator is not disconnected from the electrical grid in

order to enhance heat removal from the reactor system thereby enhancing the cooldown rate of the Na-to-CO_2 RHX. The reactor side is calculated with SAS4A/SASSYS-1 while the S-CO_2 cycle is calculated with the Plant Dynamics Code with a number of iterations over a timescale of 500 seconds. It is found that the RHX undergoes a maximum cooldown rate of ~ -0.3 °C/s. The Plant Dynamics Code was also modified to decrease its running time by replacing the compressible flow form of the momentum equation with an incompressible flow equation for use inside of the cooler or recuperators where the CO_2 has a compressibility similar to that of a liquid. Appendices provide a quasi-static control strategy for a SFR as well as the self-adaptive linear function fitting algorithm developed to produce the tabular data for input to the reactor code and Plant Dynamics Code from the detailed output of the other code.

1. Introduction

The Argonne National Laboratory (ANL) FY 2009 work on supercritical carbon dioxide (S-CO_2) Brayton cycle development has been focused on the applicability of the cycle and investigation of the cycle control aspects for the two reactor systems selected for continued development under the Generation IV Nuclear Energy Systems Initiative - the gas-cooled Very High Temperature Reactor (VHTR) and the Sodium-Cooled Fast Reactor (SFR).

It has been found that the direct application of the standard recompression S-CO_2 Brayton cycle to the VHTR is challenging because the relatively large temperature change of the helium reactor coolant makes the direct application of the traditional recompression S-CO_2 cycle relatively inefficient for the VHTR. Thus, alternative cycle configurations were explored for the VHTR. Two such alternative configurations were found that overcome the difficulties with attempting to use the standard recompression cycle on a VHTR and make it possible to use the S-CO_2 Brayton cycle as a power converter for the VHTR. A significant cycle efficiency of 49 % is achieved for a VHTR core outlet temperature of 850 °C. On the other hand, the standard recompression cycle configuration suits the SFR application very well. Due to these differences, the development of S-CO_2 cycles for VHTR and SFR applications, including the cycle control and dynamic response, has been carried out as two mainly independent tasks. The results of the analyses for these two tasks are presented below in separate Sections 2 and 3 of this report.

The report also presents the continued development and improvement of the ANL Plant Dynamics Code carried out during the course of this work. The code development is discussed in Section 4, but is also partly covered in the relevant parts of Sections 2 and 3, where a code modification was needed to continue the analysis. Appendix A documents initial control strategy development for the SFR while Appendix B documents an essential part of the code modifications.

2. S-CO_2 Cycle Development for the VHTR

Under the Generation IV Initiative, the S-CO_2 cycle has been also proposed as an energy converter for the Very High Temperature Reactor (VHTR). Earlier analysis of the S-CO_2 cycle by MIT [1] has demonstrated significant efficiency gain compared to the ideal gas helium cycle. However, later investigation by MIT [2] has shown that the S-CO_2 cycle may not be suited to gas-cooled reactor applications for which a large reactor coolant temperature change is a feature of the reactor system. A similar mismatch problem has been identified for S-CO_2 cycle applications to a solar power tower concentrating solar plant system utilizing liquid salts as the primary coolant [3]. For both applications, a cascaded cycle arrangement, also investigated in this work, has been proposed.

2.1. *Steady State Analysis of S-CO_2 Cycle for the VHTR*

Because of the difficulties with direct application of the S-CO_2 cycle to gas-cooled reactors, work on S-CO_2 cycle control analysis for the VHTR has been started with a steady-state analysis to explore and identify an optimum cycle configuration (or configurations). It was assumed in this work that the VHTR reactor would operate with helium coolant with temperatures of 850 °C at the He-CO_2 HX inlet and 400 °C at the HX outlet, and a pressure of 7 MPa at the HX inlet. The power for the reactor is assumed to be 600 MWt with the helium flow rate calculated from the power and the temperature change. The assumed temperature change of the reactor coolant (450 °C) does not suit the S-CO_2 cycle application utilizing the traditional recompression supercritical cycle in which the S-CO_2 temperature change in the reactor heat exchanger (RHX) is about 150 °C reflecting the temperature drop associated with expansion in the turbine. Therefore, a direct application of the recompression S-CO_2 cycle to the VHTR was expected to provide a relatively low efficiency. Figure 2-1 demonstrates that when the recompression S-CO_2 cycle is applied to the VHTR conditions described above, the CO_2 temperature at the turbine inlet can only reach about 550 °C even though 850 °C is available from the reactor side. This limitation comes from the temperature change in the turbine which is limited to about 150 °C when CO_2 expands, in the optimal cycle configuration, from 20 MPa to 7.6 MPa. Since the CO_2 temperature at the RHX inlet could not exceed the He cold leg temperature (400 °C), the CO_2 temperatures at the high temperature recuperator hot end are also limited to values close to 400 °C leading to the maximum turbine inlet temperature of about 550 °C. As a result, an efficiency of only 45 % is calculated for the VHTR application, compared to about 50 % and 54 % calculated in a previous analysis [1] for an assumed turbine inlet temperature of 850 °C for helium and S-CO_2 cycles (without limitations on the RHX temperatures), respectively. It also follows from Figure 2-1 that the calculated effectiveness of the RHX on the S-CO_2 side is only (556 °C – 398 °C)/ (850 °C – 398 °C) = 35 % even though it reaches almost 100 % on the helium side. This low HX effectiveness on the S-CO_2 side imposes an additional restriction on the input data. When fixed HX dimensions were specified for the

calculations (as it has been done in all previous steady state analysis of S-CO_2 cycle), the CO_2 temperature at the turbine inlet tended to approach 800-850 °C such that the CO_2 temperature at the RHX inlet was calculated on each iterative step to be above the helium outlet temperature. As a result, no converged solution was found and the code provided unrealistic results, such as efficiency in the range of 20-35%, when the iterations were terminated by reaching the maximum allowable number of steps.

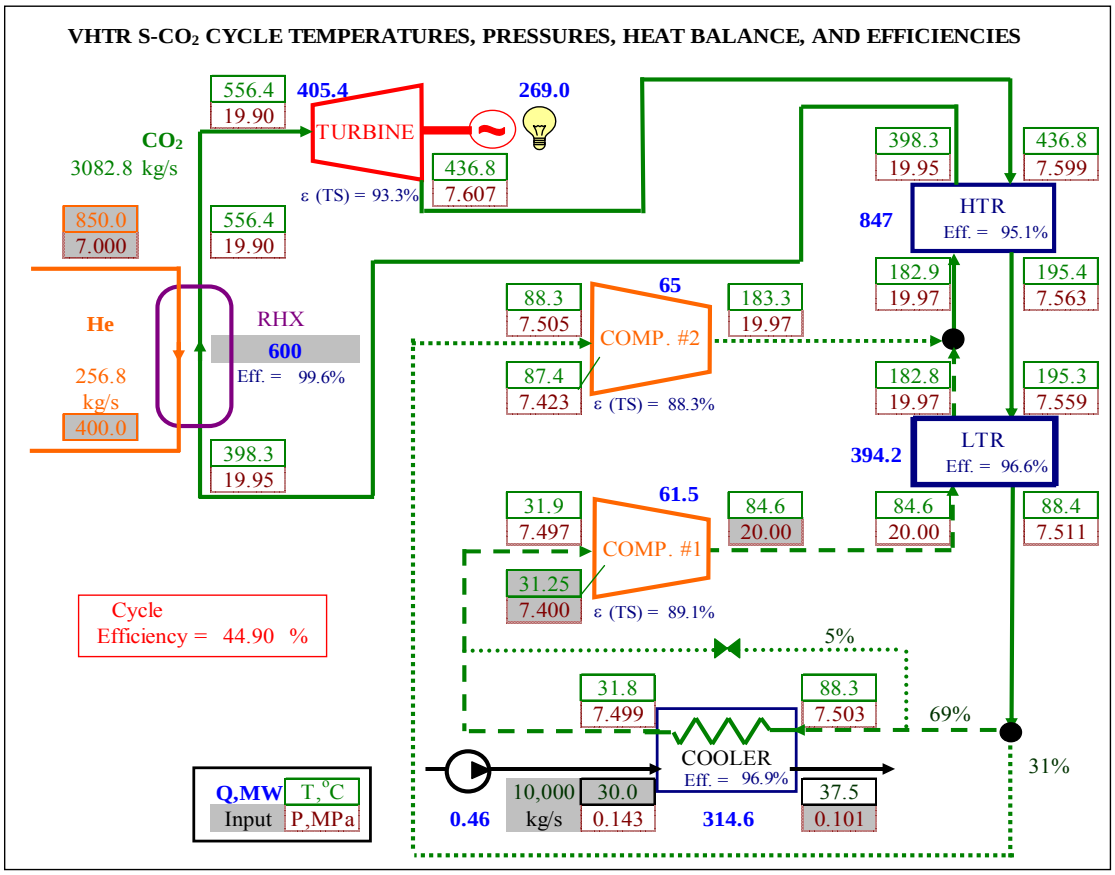

Figure 2-1. Traditional Recompression S-CO_2 Cycle Application to VHTR.

To avoid the limits of the different temperature changes on the helium and S-CO_2 sides of the reactor heat exchanger, a cascaded cycle configuration has been proposed previously for similar applications involving a mismatch in temperature drops between the primary coolant and the CO_2 [2, 3]. In this configuration (Figure 2-2), the entire temperature change on the helium side is divided into several regions such that the temperature change for each region would be close to 150 °C, optimal for S-CO_2 cycle. Separate independent S-CO_2 cycles are coupled to each section of the divided RHX. This way, the S-CO_2 can be heated in each individual RHX unit more effectively reaching about 850 °C at the turbine inlet in the top cycle. Figures 2-3 through 2-5 show in greater detail the S-CO_2 temperatures and calculated cycle efficiencies for the top, middle, and bottom cascading cycles, respectively. The CO_2 temperature for the top cycle reaches

about 830 °C at the turbine inlet providing a cycle efficiency of about 54 % (this result agrees with previous finding from Dostal [1]).

The calculated cycle efficiencies for the middle and bottom sections are about 50 % and 44 %, respectively. In fact, the bottom section represents closely the single cycle configuration for the VHTR (Figure 2-1) except for the heat duties and the flow rates. Since the heat duties of the three sections of the RHX in the cascaded arrangement are the same, the net efficiency of the three cascading cycles can be simply calculated as an average of the cycle efficiencies, i.e. net efficiency = (54 %+50 %+44 %)/3 = 49.3 %.

Thus, the overall cycle efficiency is much higher that that of the single S-CO_2 cycle (45 % in Figure 2-1) making this cascaded cycle arrangement clearly a preferable option for VHTR at least from the standpoint of efficiency. However, there are potential complexities of such a configuration coming from the fact that three independent S-CO_2 cycles would need to be constructed and operated. For example, three sets of the turbomachinery, each having a turbine and two compressors on one shaft, would be needed. (The generator arrangement could be more flexible such that either each cycle could have its own generator or all there turbomachines could be located on a single shaft driving a common generator). Also, three sets of the heat exchangers, high and low temperature recuperators, and coolers, would be needed. Considering the high temperature recuperator for example, the total heat duty of the heat exchangers in the there cycles would be about 1084 MWt compared to 847 MWt for the single cycle arrangement. However, since the cascading cycle arrangement provides higher efficiency, the recuperator heat duty per kWe would be close to that of the single cycle, 3.66 MWt/MWe for the cascade arrangement versus 3.14 MWt/MWe for the single cycle. In addition, the overall plant control strategy must deal with simultaneously controlling three S-CO_2 cycles.

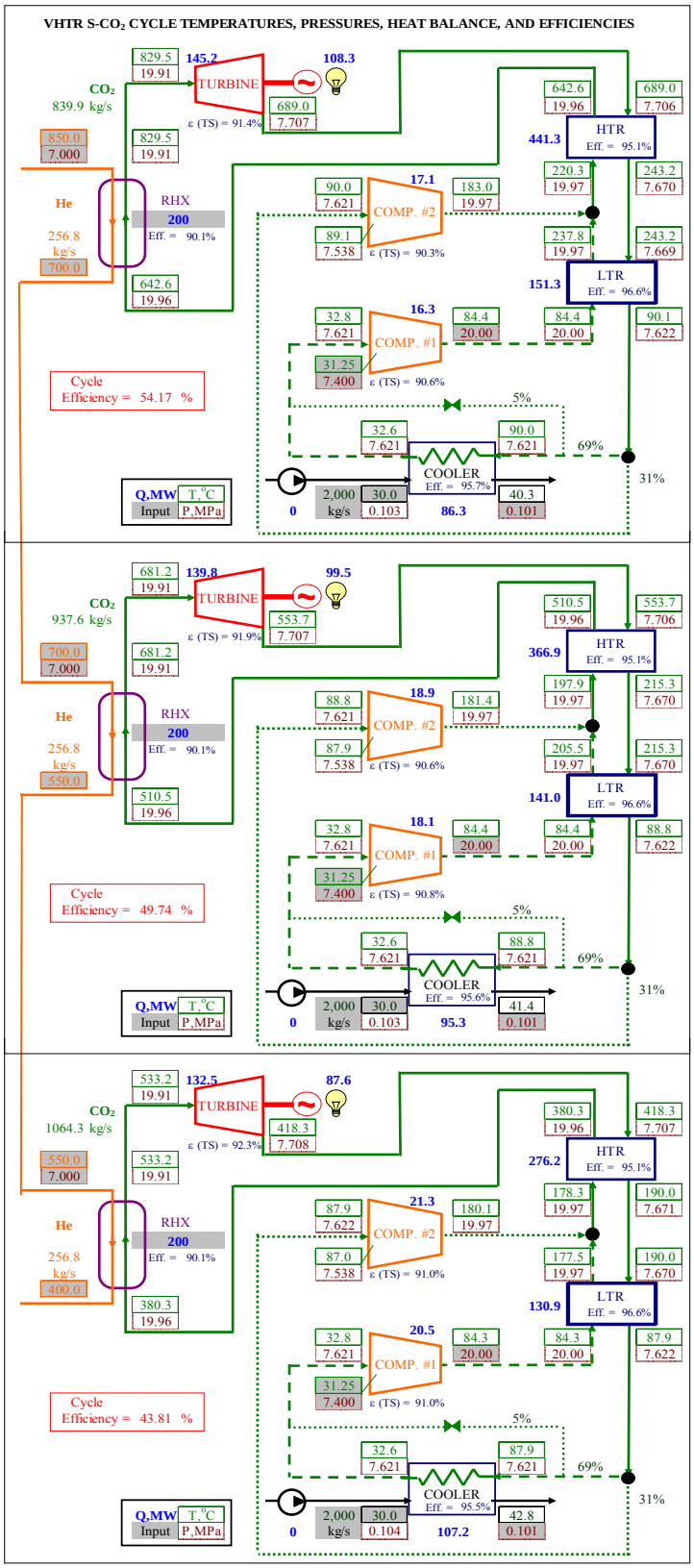

Figure 2-2. Cascaded S-CO$_2$ Cycle Configuration for the VHTR.

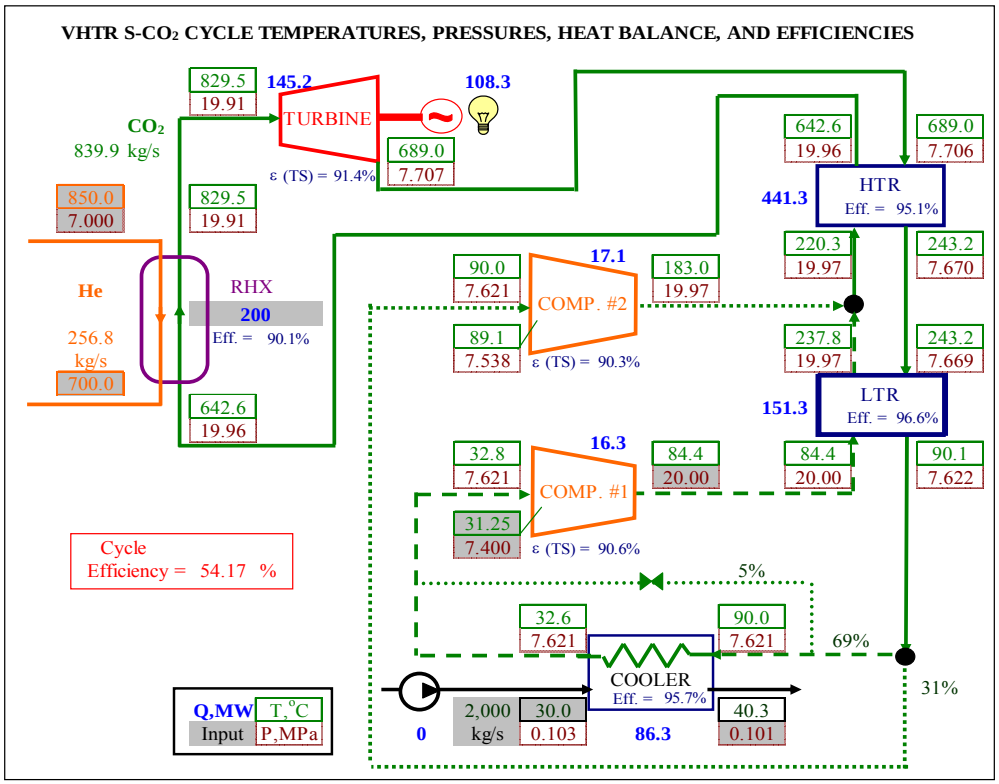

Figure 2-3. Cascaded S-CO$_2$ Cycles for the VHTR - Top Section.

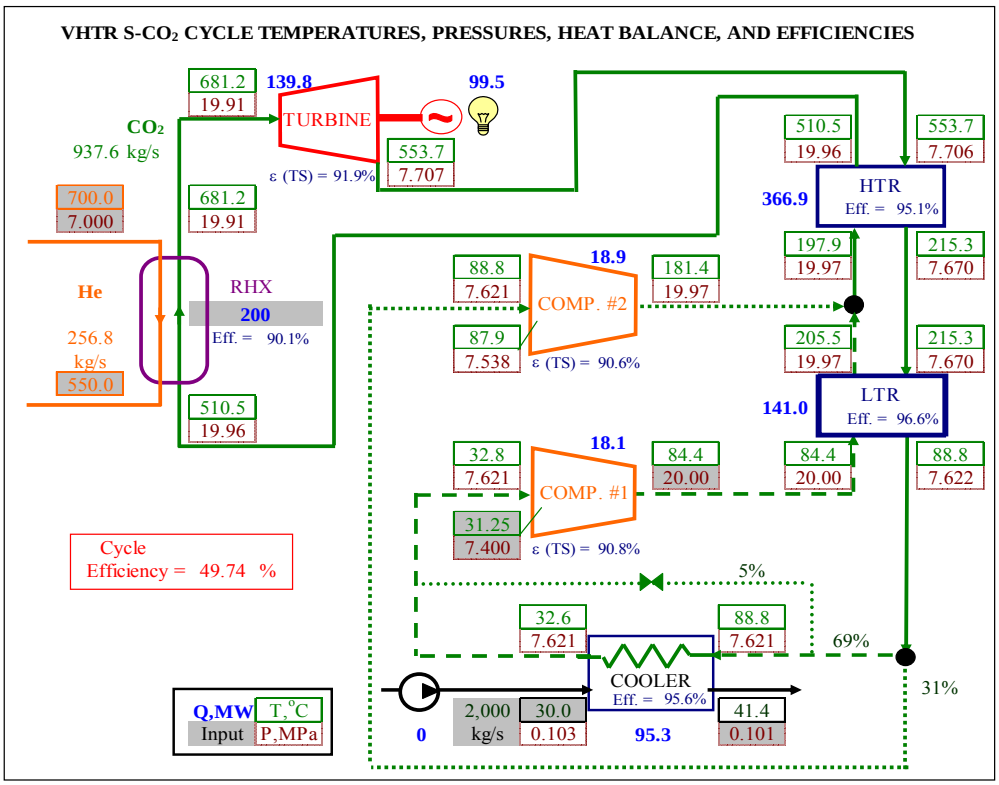

Figure 2-4. Cascaded S-CO$_2$ Cycles for the VHTR - Middle Section.

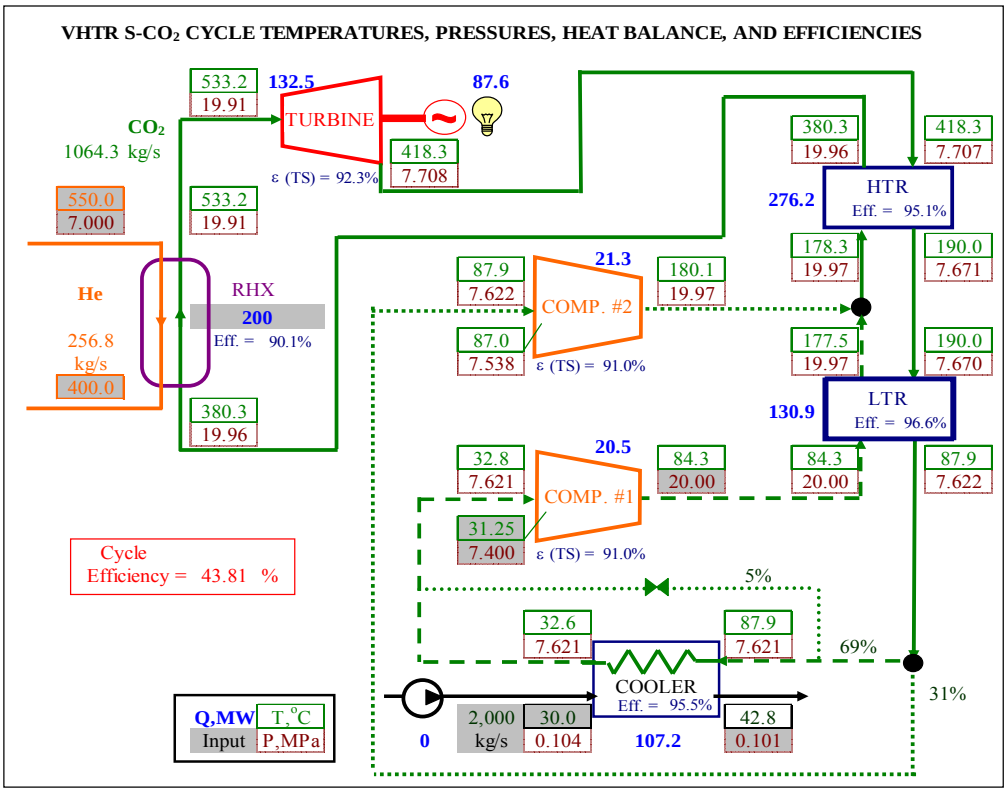

Figure 2-5. Cascaded S-CO_2 Cycles for the VHTR - Bottom Section.

Another limitation for S-CO_2 cycle analysis has been observed during the analysis for the VHTR. As it is mentioned above, the S-CO_2 temperature can reach about 830 °C in the top section of the cascading cycles. At the same time, the calculations were done based on the S-CO_2 properties subroutines recommended by NIST [4]. Those subroutines have a stated temperature range of up to 1100 °K or 827 °C. Thus, even at the steady state conditions, the range of the properties subroutines was exceeded; it might be expected that in some specific transients the S-CO_2 temperature can increase even further. The fact that the calculations proceeded without failure suggests that the properties subroutines still work at the calculated temperatures. However, it is understood that the results in this report, and possibly further analyses for this application, are based on the calculations of properties in a regime where those properties subroutines may not have been verified.

The cascaded cycle configuration described above is one of the options to compensate for the mismatch of the temperature changes on two sides of the reactor heat exchanger. Another option would be to increase the temperature change on the S-CO_2 side of the heat exchanger. The optimal temperature change, 150 °C, obtained in previous calculation is a function of the pressure change in the turbine. For the pressures considered optimal for the recompression cycle – 20 MPa and 7.8 MPa – the temperature change in the turbine is limited to about 150 °C. If those pressures were to vary, then the temperature change could be increased. An example of such variation would be operating of CO_2 cycle at the conditions of an ideal gas Brayton cycle (i.e., in the gas, not

supercritical, regime). However, at those conditions, the main benefit of the S-CO_2 cycle – reduced compressional work near the critical point – would be lost and the cycle would provide little if any benefit compared to the ideal gas (helium) cycle. So, it was decided in the current work to configure the S-CO_2 cycle in such a way that:

1) the compression near the critical point still occurs, and
2) the pressure ratio across the turbine is increased.

One obvious way to satisfy the above criteria would be to increase maximum cycle pressure up from the original 20 MPa. However, in order to approach the temperature change of 450 °C, the pressure difference in the turbine would need to be roughly 3 times the original value, or about 36 MPa, resulting in a maximum pressure in excess of 40 MPa. This pressure would clearly complicate the design and fabrication of the heat exchangers, pipes, and turbomachinery, if the use of such a high pressure is even feasible.

The other option to increase pressure drop in the turbine would be to decrease the turbine outlet pressure. To investigate the benefits of such approach, a value of 3.5 MPa (about half of the original value) was assumed for the minimum cycle pressure for further analysis. Still, in order to take advantage of the compression near the critical point, the pressure at the main compressor inlet should be raised back to around 7.7 MPa. This could be done by splitting the compressor in two parts, where the first part would boost the pressure to 7.7 MPa such that the benefits of compression near the critical point would be realized in the second part of the compressor. In addition, the temperature at the main compressor inlet should be brought to just above the critical value such that an precooling between those compression stages would be needed. The temperature - specific entropy (T-s) diagram of such cycle is schematically shown in Figure 2-6 with corresponding cycle arrangement shown in Figure 2-7.

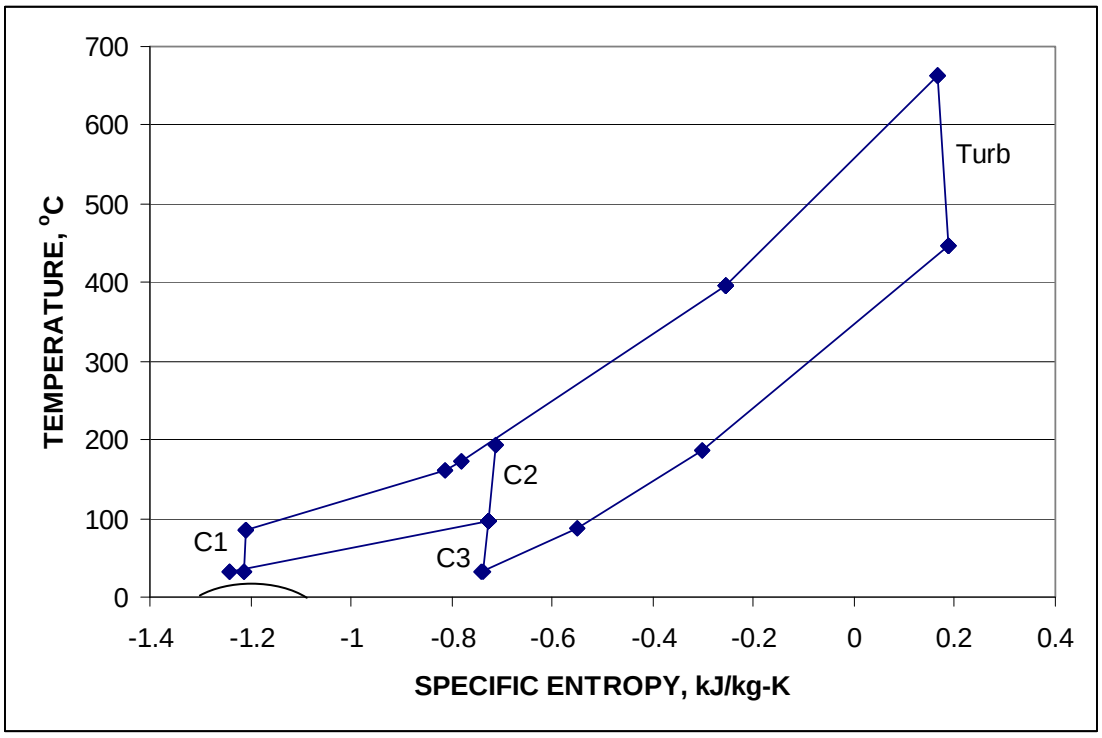

Figure 2-6. T-s Diagram of S-CO_2 Cycle with Precooling.

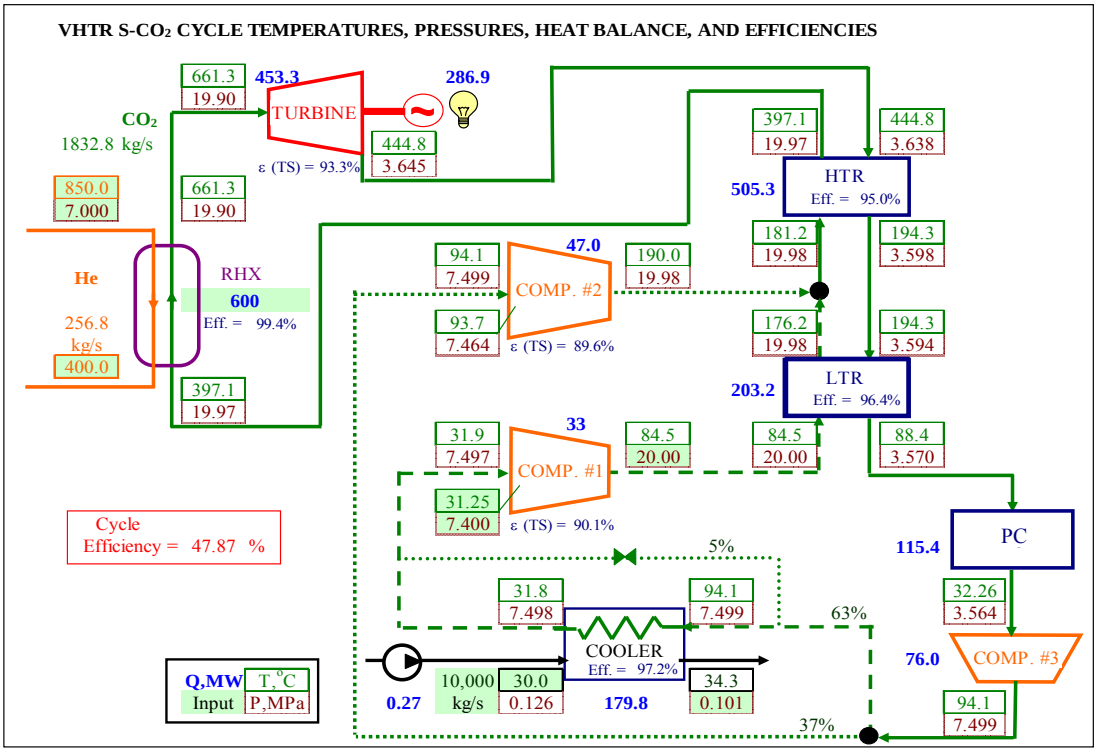

Figure 2-7. S-CO_2 Cycle with 3.5 MPa Minimum Pressure and Precooling.

The cycle configuration (Figure 2-7) is the same as for the traditional recompression cycle, except that an additional compressor (Comp #3 or C3) and an additional precooler (PC) are added before the flow split point. These changes allow decreasing the turbine outlet temperature down to a value representing expansion to a pressure of about 3.6 MPa while keeping the inlet and outlet conditions for both main and recompression compressors about the same as in the original configuration. Increasing the turbine pressure change leads to an increased temperature change in the turbine such that the temperature change at the S-CO_2 side of the reactor heat exchanger could correspondingly be increased. The calculations have shown (Figure 2-7) that the turbine inlet temperature can be increased to about 660 °C (from about 550 °C in the original configuration in Figure 2-1) and the cycle efficiency could be increased to about 48 % (compared to 45 %). The drawbacks would be an addition of extra compressor and cooler as well as the increased pressure difference in the recuperators. Compared to the cascaded cycles, this cycle configuration would only add one compressor and one cooler compared to the three sets of turbine with two compressors, three coolers, and three sets of the recuperators. Still, the cycle efficiency for this configuration is calculated to be only about 1 % lower than that for the cascaded cycles. It also simplifies the plant control strategy from having to deal with simultaneously controlling three S-CO_2 cycles.

This cycle efficiency increase provided by somewhat minor variation of the cycle layout is promising such that investigation in this direction was continued. First, further increase in the turbine pressure ratio was investigated by increasing the maximum cycle pressure to 25 MPa. The resulting pressure change in the turbine would be from 25 MPa to 3.6 MPa, or more than 20 MPa. A cycle efficiency of about 48.3 % is calculated in this case, i.e. about a 0.3 % increase from the 20 MPa pressure in Figure 2-7. The other option would be to further decrease the turbine outlet pressure. A case with 20 MPa maximum cycle pressure and 1 MPa minimum cycle pressure was investigated. It was found that in this case it would be beneficial to add another set of compressor and precooler such that the compression from 1 MPa to 7.7 MPa is performed in two stages rather than in the one stage shown in Figure 2-6. The temperature - specific entropy diagram of the cycle with a 1 MPa minimum pressure and two additional compressors is shown in Figure 2-8. Compared to Figure 2-6, this configuration achieves an even greater temperature change in the turbine such that the turbine inlet temperature can be increased above 800 °C while the RHX inlet temperature is still kept below 400 °C. An optimization of this cycle configuration, including the optimal flow split between the main and recompressing compressor as well as optimal pressure changes in two additional compressors, was carried out and an optimal cycle efficiency of 49.5 % has been calculated. Note that this cycle efficiency is even higher than that calculated for the cascaded cycles.

From the steady state design analysis, the two most promising S-CO_2 cycle configurations for the VHTR conditions are the cascaded recompression supercritical cycle arrangement and a single recompression cycle with the minimum pressure below the critical pressure with one or more stages of precooling. Since there are no clear benefits of one concept over the other from the standpoint of efficiency, it is recommended that the further analysis of the S-CO_2 cycle for VHTR applications, including cycle control strategy, should retain these two options.

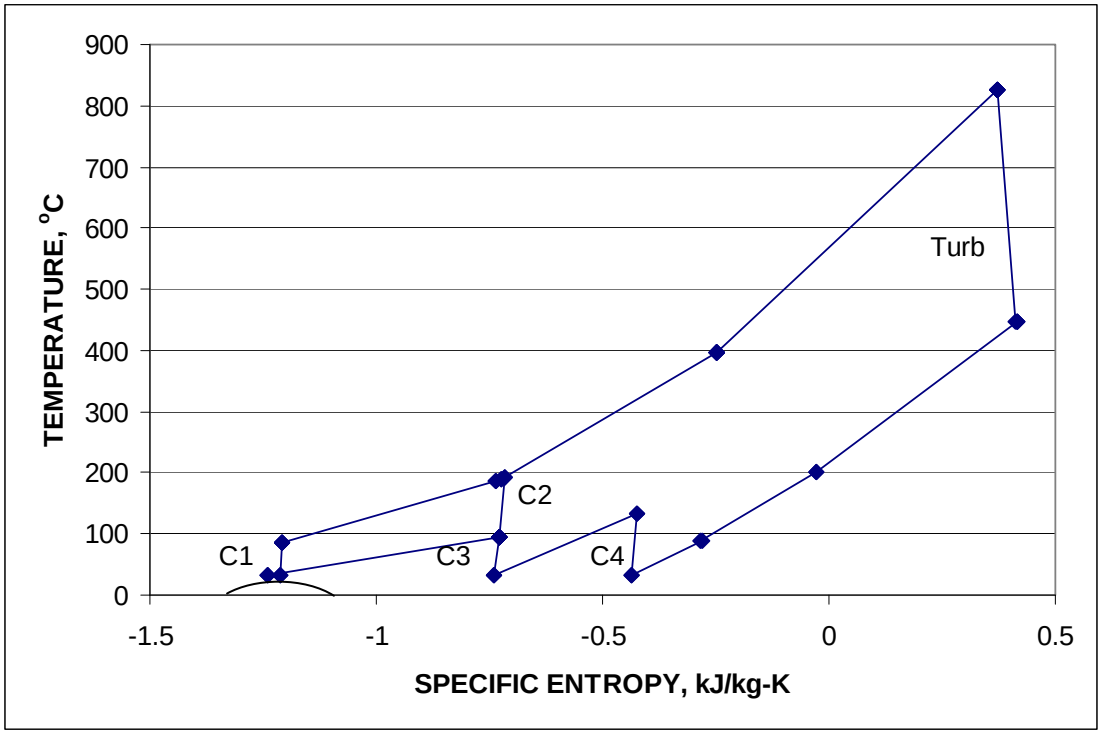

Figure 2-8. T-s Diagram for S-CO_2 Cycle with Two-Stage Precooling.

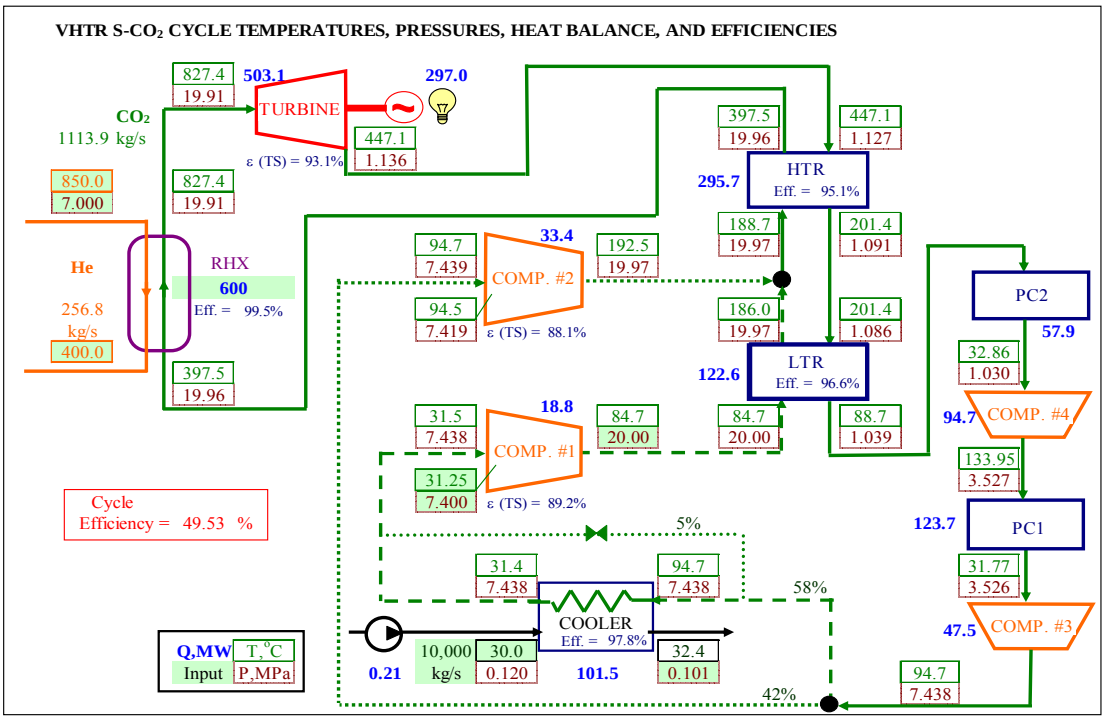

Figure 2-9. S-CO_2 Cycle with 1 MPa Minimum Pressure.

2.2. *Control Analysis of the S-CO_2 Cycle for the VHTR*

During the steady state analysis of the S-CO_2 cycle for VHTR application, two promising concepts were identified: cascaded cycles and a cycle with a subcritical minimum pressure with one or more stages of precooling.

In the cascaded arrangement, the configuration of each section is exactly the same as for the traditional recompression cycle. Also, the pressures and the temperatures at the bottom of the cycle, including those around the compressor near the critical point, are almost identical to those in the traditional recompression cycle. Therefore, it is expected that the control and transient response of each section would be very similar to that of the recompression S-CO_2 cycle analyzed in previous work. In fact, the control of the cascaded configuration may be even simpler than for a single cycle. Since there are three independent cycles in the plant, one or two cycles may be disconnected from the reactor to achieve 33 % or 67 % power reduction, providing additional flexibility in the plant control. On the other hand, variation in operation in one cycle may affect the helium temperatures in the corresponding section of the RHX which in turn could affect helium temperatures in the other sections of the RHX and therefore the operation of other cycles. Even though this effect needs to be studied for the control analysis, it is not expected to significantly affect controllability of the cycles. For these reasons, no analysis on the control of the cascaded cycles was carried out for this report.

The work on control and transient analysis of the S-CO_2 cycle configuration with precooling stages has been started. The Plant Dynamics Code and the control mechanisms have been modified to take into account the additional components and control requirements. Among those, the most significant ones are the presence of an additional compressor and cooler with the need to control the compressor inlet temperature. Since the inlet pressure for this additional compressor is below the critical value (3.5 MPa and 1.0 MPa in the examples considered above), the compressor inlet temperature needs to be controlled to stay above the critical temperature to avoid two-phase flow into the compressor blades.

Transient calculations investigating control have been initiated for the cycle layout with a 3.5 MPa minimum pressure and one additional compressor and precooler (Figure 2-7). The turbomachinery performance maps were generated for the turbine and the three compressors. The initial transient calculations to investigate the control of this cycle configuration were carried out using the Plant Dynamics Code. Figure 2-10 shows the first results of the transient calculations for an example of electrical grid load reduction in a linear fashion from 100 % to 50 %. It is assumed in the calculations that the helium RHX inlet pressure and temperature and its flow rate remain constant during the transient at the steady state level. The generator power adjustment to match the grid demand is accomplished by turbine bypass control. The main compressor inlet temperature is controlled by a combination of cooler bypass and cooler flow rate control, as in the previous analyses. The inlet temperature for the additional compressor (Compressor #3) is controlled only by precooler water flow rate control (precooler bypass control has not yet been implemented in the Plant Dynamics Code).

The results of the transient control analysis in Figure 2-10 show some oscillations after about 350 s into the transient. A cause for these oscillations has not yet been determined; more work is needed to investigate the transient cycle behavior. Some observations of possible cause for the oscillations were made based on the results of the steady state analysis. The results (Figure 2-7) show significant variation of the temperature difference between helium and CO_2 flows along the RHX length. At the hot end, this temperature difference reaches about 200 °C while at the cold end this temperature difference is less than 3 °C. This discrepancy results in a very nonlinear heat flow distribution along the heat exchanger length complicating the numerical calculations of heat transfer in both the steady state and transient calculations. Moreover, the very small temperature difference at the cold end of RHX degrades the convergence on the CO_2 flow rate in the steady state calculations. The CO_2 flow rate is calculated from the heat balance and performance of the RHX given the CO_2 temperature at the RHX inlet. That inlet temperature is calculated by the cycle analysis (HTR performance) given the CO_2 flow rate and RHX outlet temperature. Due to small temperature difference at the cold end of the RHX, even a small variation of the RHX inlet temperature resulted in significant variation of the calculated CO_2 flow rate. As a result, the steady state calculations failed to completely converge to a solution within the specified number of iterative steps. Although variations in the flow rate towards the end of the iterations were small enough to report the steady state conditions in Figure 2-7, this lack of complete convergence in flow rate might be significant for the dynamic calculations (PDC relies on the steady state solution for the initial conditions). This difference in the flow rate results in a calculated mismatch in the RHX heat balance during the first few seconds in a transient (Figure 2-10). It is also responsible for the difference in the calculated main compressor inlet temperature with the design value of 31.25 °C even at steady state conditions. More analysis is needed to investigate whether this convergence problem eventually causes the oscillations of the transient results. A smooth solution obtained with the same code for the SFR system (reported in Section 3 of this report) suggests that the oscillations are not caused by the numerical algorithm.

Aside from the oscillations, effective S-CO_2 cycle control for VHTR has been demonstrated in Figure 2-10. The generator load follows the grid demand, the choke and surge in the compressors are avoided, and the inlet temperature for two compressors operating near the critical temperature is maintained above the critical value. The compressor inlet pressure is calculated to remain above the critical value for the main compressor and below the critical value for the precooler compressor.

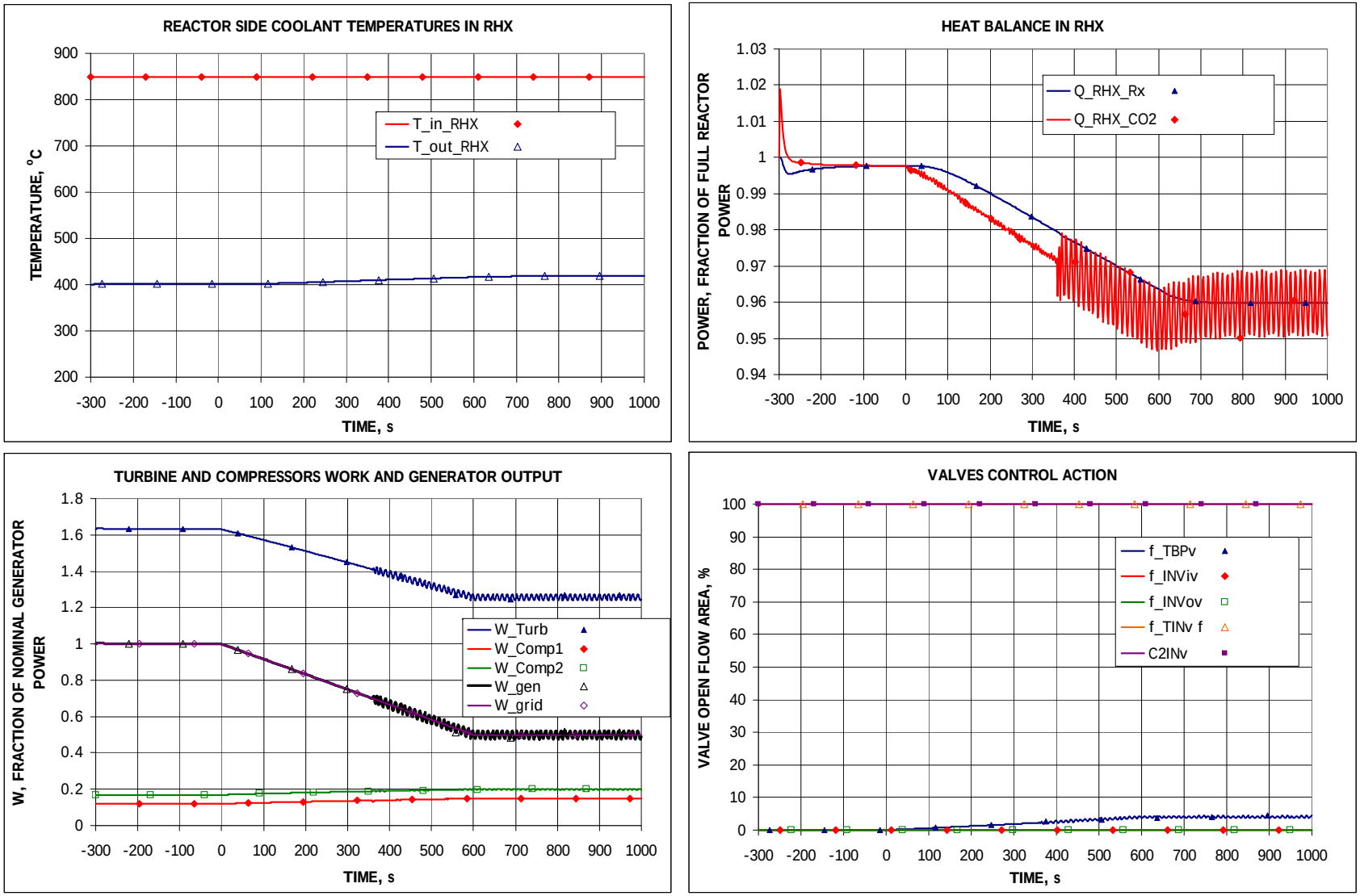

Figure 2-10. Results of VHTR Transient Control Analysis.

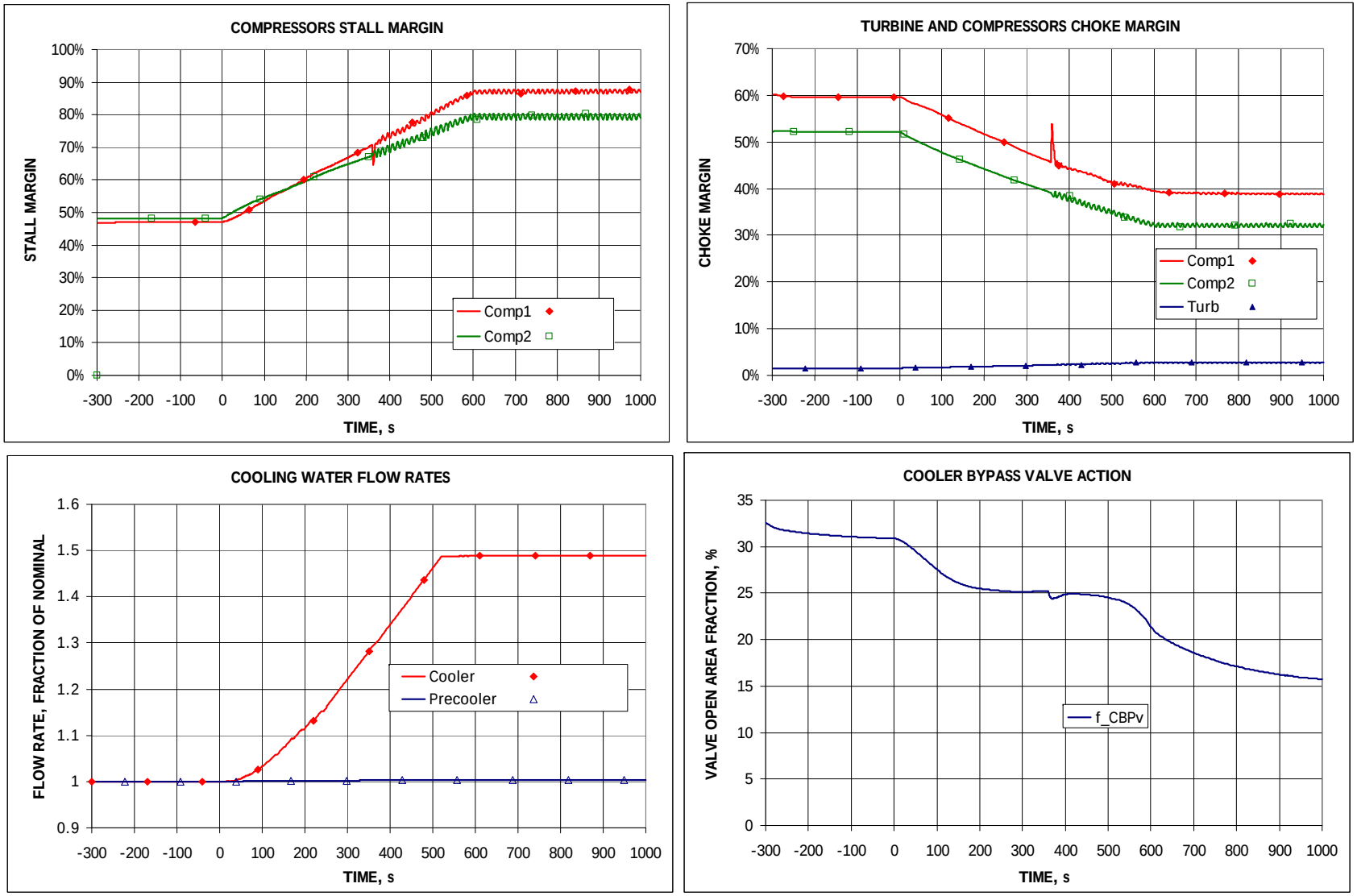

Figure 2-10. Results of VHTR Transient Control Analysis. (Continued)

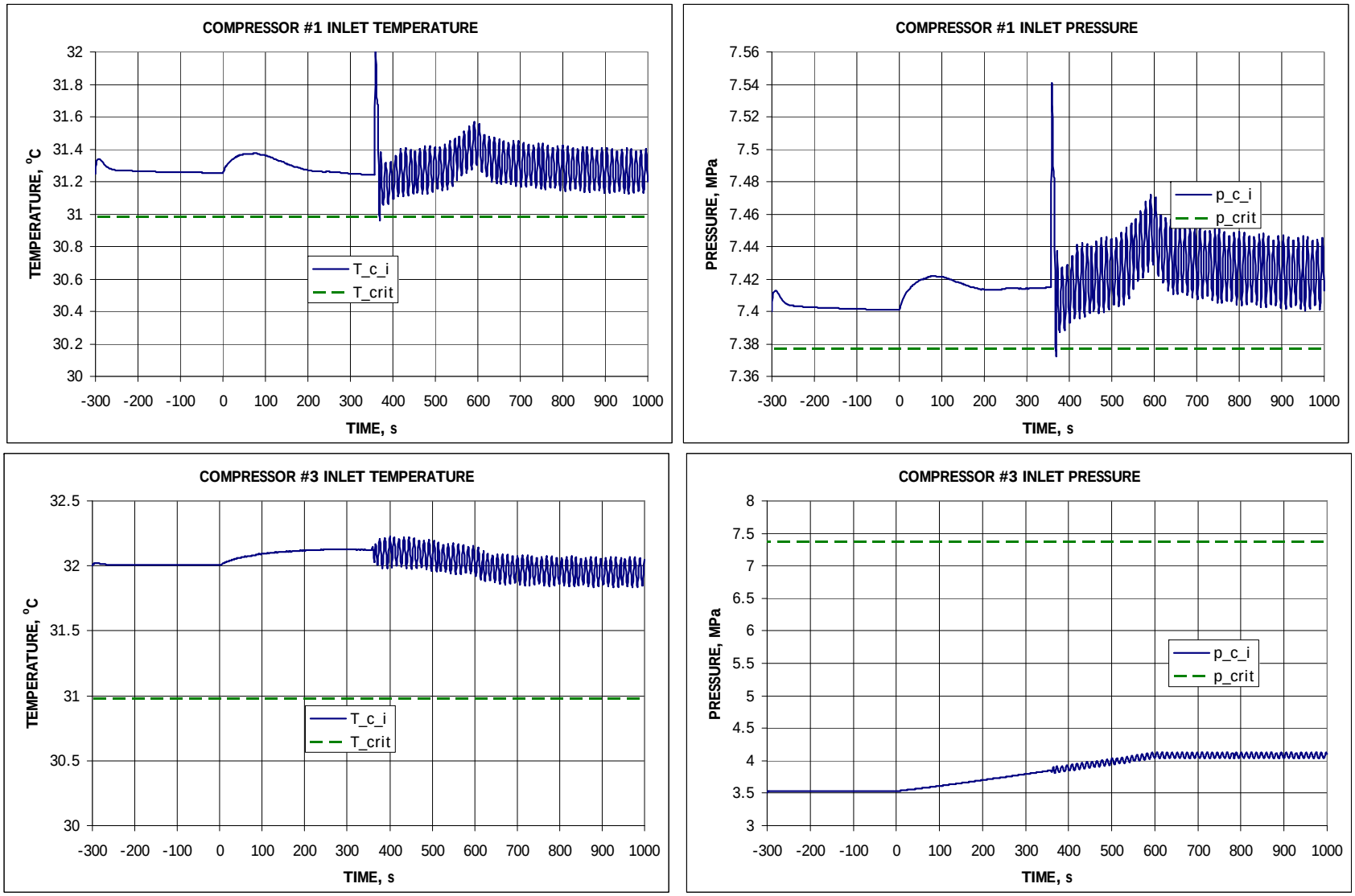

Figure 2-10. Results of VHTR Transient Control Analysis. (Continued)

3. S-CO_2 Cycle Control Analysis for the SFR

The development of the S-CO_2 Brayton cycle for SFR applications has been ongoing at ANL for several years. Work was started in 2004 when the S-CO_2 cycle was adopted as an advanced energy converter for the KALIMER SFR as part of a U.S. DOE/Republic of Korea I-NERI project between ANL and the Korea Atomic Energy Research Institute (KAERI). The S-CO_2 cycle was selected as the reference power converter for the 125 MWt Small Modular Fast Reactor (SMFR) [5]. The SMFR preconceptual design evolved into the 250 MWt Advanced Burner Test Reactor (ABTR) preconceptual design which also incorporates a S-CO_2 cycle power converter [6]. A S-CO_2 cycle was also subsequently developed as a power converter for a 1000 MWt Advanced Burner Reactor (ABR) [7].

It was demonstrated that the traditional recompression S-CO_2 cycle configuration, where the CO_2 flow is split between two compressors and part of the flow bypasses the low temperature part of a recuperator, provides optimal performance of the S-CO_2 cycle for SFR applications. The calculated cycle efficiency, close to 40 %, is at least comparable to that of the superheated steam cycle while S-CO_2 cycle provides other benefits, such as elimination of sodium-water reactions and smaller turbomachinery. Several other cycle configurations have been analyzed for SFR applications [8,9] in order to further increase the cycle efficiency. Even though several configurations were found to produce higher cycle efficiency, those configurations may require higher capital cost or special operating conditions. For example, it was found that condensation cycles would provide higher cycle efficiency, but at the same time would require the availability of a significantly colder heat sink. For these reasons, the recompression cycle configuration which has become somewhat standard is still considered optimal for the SFR applications.

3.1. *Quasi-Static S-CO_2 Cycle Control Analysis for the SFR*

The quasi-static control analysis of a S-CO_2 cycle coupled to a SFR has been carried out as a part of the S-CO_2 cycle development for ABTR reactor. That analysis was not included in the ABTR report [6] nor in any other report or publication. Thus, the results of the cycle control analysis for ABTR are presented in this report in Appendix A.

Overall, the S-CO_2 cycle control results are close to those obtained previously for Lead-Cooled Fast Reactor (LFR) systems [10,11,12]. Inventory control is a preferable control mechanism since it provides the highest efficiency at reduced loads. However, the range of applicability of inventory control is limited by the available volume of the inventory control system tanks (i.e., storage vessels). It was estimated that the ABTR inventory control would operate between 30 % and 100 % loads based on a reasonably sized total tank volume. Unlike the STAR LFR reactors considered in the previous work, ABTR employs a possibility of a direct reactor power control by means of deliberate control rod movement as well as direct control of the primary and intermediate coolant flow rates through the coolant pump speed controls. These two additional control options

were included in the S-CO_2 cycle control analysis for the ABTR (Appendix A). It was found that direct reactor power control might be a preferable choice for plant control for the loads below 30 %.

3.2. *Dynamic Simulation of S-CO_2 Cycle Control for the SFR*

The ANL Plant Dynamics Code [13] used for transient analysis of the S-CO_2 cycle was originally developed for the Secure Transportable Autonomous Lead-cooled Fast Reactors (STAR LFRs). Sodium-Cooled reactors have several features which prohibit direct application of a transient code developed for the STAR LFR systems to a SFR. These features include:

- Reactor power control by means of the control rod movements (STAR reactors rely solely on the core reactivity feedbacks for the power control enabling autonomous load following with deliberate rod insertions to shut down the reactor when necessary),
- Presence of the intermediate sodium loop in contrast to the LFRs which do not incorporate intermediate circuits, and
- Forced circulation of both the primary and intermediate sodium coolants.

In order to apply the Plant Dynamics Code to a SFR S-CO_2 cycle, significant code modifications would be required to simulate the primary and intermediate sodium loops with all the additional SFR control mechanisms. The necessary modifications to the code were started last fiscal year [14], but have not been completed. It has been realized that in order to accurately represent the reactor core, primary and intermediate sodium loops with sodium pumps, and the corresponding control mechanisms, a code would need to have a capability similar to that developed in the SAS4A/SASSYS-1 code [15]. Development of such capability would be a complex, possibly multi-year, task. Consequently, a different approach was adopted during the current fiscal year.

It was decided to modify the Plant Dynamics Code such that it would only need to analyze the S-CO_2 cycle part of the plant. The reactor coolant conditions at the heat-supply heat exchanger[1] would be specified as an input for the S-CO_2 cycle analysis. Those conditions would include the coolant itself (helium, sodium, etc.), its flow rate, inlet temperature, and inlet pressure, and should be provided for both steady state and transient calculations. For steady state design calculations, the coolant outlet temperature should also be specified. For transient calculations, a table of the inlet coolant conditions as a function of time is needed. Such modifications to the Plant Dynamics Code were

[1] Depending on the analyzed system, this heat supply heat exchanger could be a Pb-to-CO_2 HX inside the reactor vessel (for STAR LFR systems), a Na-to-CO_2 HX either outside the reactor vessel or inside the vessel (for SFR system concepts with or without an intermediate sodium loop), or a He-to-CO_2 HX (for the VHTR). This HX is usually referred to as Reactor Heat Exchanger (RHX) in this report.

implemented and the code was used for the steady state and transient analyses of both the SFR described in this chapter and the VHTR presented in the following chapter.

For transient calculations with the Plant Dynamics Code, the inlet conditions for the reactor side coolant at the Na-CO_2 HX are given. These conditions are either assumed (such as constant flow rate and inlet temperature) or calculated by another code (such as SAS4A/SASSYS-1, as described below). The Plant Dynamics Code calculates the transient response of the S-CO_2 cycle. Among the parameters calculated by the Plant Dynamics Code are reactor coolant conditions at the outlet of the Na-CO_2 HX (temperature and pressure or pressure drop). These conditions, if necessary, should be provided back to the reactor code and the iterations on the reactor coolant temperature and pressure change should be carried out, as presented below.

For the transient analysis of the S-CO_2 cycle coupled to a SFR, an ABR concept developed at ANL under the Advanced Fuel Cycle Initiative (AFCI) program has been selected. The selection is based on the fact that the ABR reactor model for the SAS4A/SASSYS-1 code was available to the authors and could be readily used for the current analysis with some minor modifications. The modifications include the flow parameters (flow areas, hydraulic diameter, and length) on the sodium side of the Na-CO_2 HX. These parameters are calculated by the steady state part of the Plant Dynamics Code. Since the SAS4A/SASSYS-1 code does not model a S-CO_2 Brayton cycle power converter, a simplified steam generator model was used in the current calculations. In this simplified model, only the geometric flow parameters (flow areas, hydraulic diameter, and length) and the temperature change are specified for the intermediate sodium side of the steam generator. As described above, the geometric parameters are calculated by the Plant Dynamics Code to simulate a Na-CO_2 Printed Circuit Heat Exchanger (PCHE). To calculate the sodium temperature change in the steam generator, transient calculations using the Plant Dynamics Code are utilized.

The overall calculational approach is schematically illustrated in Figure 3-1. Given the specified sodium temperature change[1] in the steam generator (Na-CO_2 HX), the SAS4A/SASSYS-1 code calculates all the transient results for the reactor side for the entire transient. Among the calculated parameters are the intermediate sodium flow rate and the intermediate sodium temperature at the steam generator (Na-CO_2 HX) inlet. These two parameters are then supplied to the Plant Dynamics Code for the S-CO_2 cycle transient calculations. (Since the sodium properties do not depend on pressure, the sodium pressure at the Na-CO_2 HX inlet was not needed for the S-CO_2 cycle calculations; in other systems, such as the helium-cooled VHTR, the reactor coolant pressure would also be needed for the S-CO_2 cycle calculations). Given the reactor coolant conditions, the Plant Dynamics Code calculates the transient response of the S-CO_2 cycle part of the plant for the entire transient. The Plant Dynamics Code also calculates the time-dependent sodium outlet temperature based on the transient response of the Na-CO_2 HX, sodium flow rate and temperatures, and S-CO_2 flow rate, temperatures, and pressures. The sodium outlet temperature is converted into the sodium temperature change in the

[1] In these calculations, a SAS4A/SASSYS-1 option to specify the temperature changed normalized to the steady state value is used.

Na-CO_2 HX (steam generator) and is supplied to the SAS4A/SASSYS-1 code to update the sodium conditions at the HX inlet during the transient. The iterations are repeated until the required convergence on the input parameters (such as the sodium temperature change in the Na-CO_2 HX) is obtained. To calculate the convergence, the values of the input parameters are stored at each iteration and are compared with the values on the previous iteration. The iterations can be started at any convenient location. For example, the iterations may be started by setting the sodium temperature change in the steam generator equal to that at the steady state conditions, as demonstrated in Figure 3-1 and as adopted for the calculations presented below.

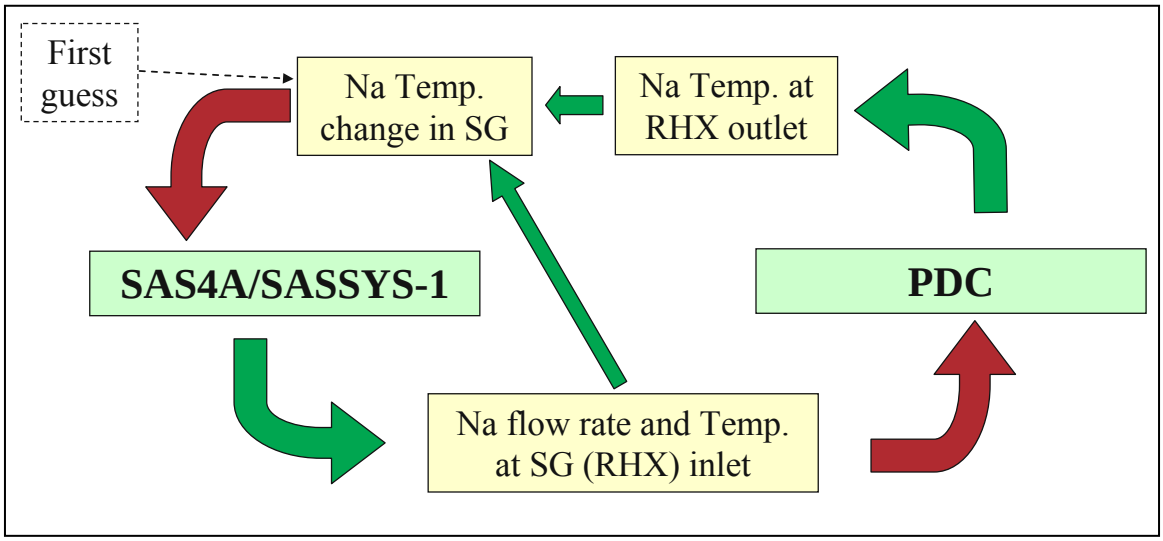

Figure 3-1. Coupled Transient Calculations of S-CO_2 Cycle for SFR Using SAS4A/SASSYS-1 and Plant Dynamics Codes.

A transient initiator can be specified on either the reactor side, the S-CO_2 cycle side, or both, depending on the analyzed transient. For example, in the calculations presented further in this chapter, the initiating event is a reactor scram, such that the transient is initiated on the reactor side and the corresponding input was provided to the SAS4A/SASSYS-1 model. No external transient initiators were necessary on the S-CO_2 cycle (except for the sodium flow rate and temperature).

Both the SAS4A/SASSYS-1 and the Plant Dynamics codes accept input for the transient parameters as a table where a parameter is defined as a piecewise linear function of time (the values are specified at certain time points and linear variation between those points is assumed). Since the transient results calculated by the codes, such as temperature change in the HX, are generally not linear, a special utility was developed for the current analysis. The utility accepts a time history of a parameter, usually as values at each calculated time step, and fits it with a piecewise linear function for a code input. The utility is described in Appendix B. The utility also presents the results in a format suitable for direct code input. The table size for the input parameters is limited to 14 entries in the SAS4A/SASSYS-1 input. There is, however, a restart option which allows interruption of the calculations at any time, modifying the input parameters, and continuing the

calculations. If this option is used, then the entire transient time can be divided into a a number of intervals for each of which a table with 14 values can be used, thus allowing a possibility to provide an input table with as many entries as required. (In the calculations presented below, this restart option was not needed since 14 entries appeared to be sufficient for the analyzed transient.) In the Plant Dynamics Code, the table size is currently limited to 100 entries, but this limit can be easily changed, if necessary. In the calculations below, tables of arbitrary selected 40 entries were used and appeared to be sufficient.

To demonstrate the simultaneous transient analysis of the SFR reactor side and S-CO_2 cycle, an accident scenario of a reactor scram was analyzed. Since the two codes are connected at the Na-CO_2 heat exchanger, the transient conditions were deliberately selected to provide significant variations of the conditions inside the HX during the transient. It was expected that the reactor scram without sodium pump trip would change the sodium temperatures significantly and quickly throughout the reactor side, including those in the Na-CO_2 HX. Thus, a capability of the proposed calculational scheme would be tested on one of the most challenging conditions. In this particular transient, no event initiator is simulated on the S-CO_2 side. It is assumed that the generator would stay connected to the electrical grid providing a constant rotational speed for the S-CO_2 turbine and compressors. Based on a previous analysis of a reactor scram, simulated with the LFR capability in the Plant Dynamics Code [14], a transient time of 500 seconds was selected.

Figure 3-2 shows how a convergence in the sodium temperature at the Na-CO_2 HX (RHX) is achieved. For the first iteration, the outlet temperature was calculated by SAS4A/SASSYS-1 under an assumption that the sodium temperature change in the RHX stays constant. For the second and subsequent iterations, the temperature change was obtained from the Plant Dynamics Code results. As demonstrated in Figure 3-2, the maximum difference in the outlet temperature between two subsequent iterations is decreasing and is reduced to about 1 °C after the fifth iteration. This difference was judged to be adequate for these calculations, so the iterations were stopped after the fifth run. Figure 3-3 shows similar convergence results for the sodium flow rate. In this particular scenario (no trip of the sodium pumps), the flow rate does not change significantly such that the difference between two iterations is reduced to less than about 0.01% after fifth iteration.

The converged results of the analyzed transient are shown in Figure 3-4 for the SAS4A/SASSYS-1 code for the reactor side and in Figure 3-5 for the Plant Dynamics Code for the S-CO_2 side. The reactor scram is simulated by fast insertion of a large negative reactivity (-5 $ in 2 seconds). The core fission power and temperatures drop shortly after the reactivity insertion. However, it takes some time to cool down the hot primary pool (outlet plenum) and an even longer time to communicate this temperature change to the Na-CO_2 HX. At this point, the CO_2 temperature at the HX outlet and turbine inlet start to decrease followed by the decrease in the turbine outlet and HTR inlet temperatures. Reducing the HTR inlet temperature leads to a lower temperature at the HTR cold side outlet which is communicated back to the Na-CO_2 HX and, through the

intermediate sodium loop, to the primary sodium cold pool. This temperature decrease continues throughout the entire transient; sodium temperatures close to 200 °C (i.e., about 100 °C above freezing) are calculated at the end of the simulation. On the S-CO_2 cycle side, the only active control is the cooler bypass control to maintain the compressor inlet temperature. All other controls are inactive since the generator output falls below the grid demand as soon as the CO_2 temperatures start to decrease. Decrease in the CO_2 temperatures also causes a decrease in CO_2 pressures. The sodium flow rates remain approximately constant throughout the entire transient, as shown in Figure 3-3 for the intermediate loop and in Figure 3-4 for the primary loop. The small changes in the flow rates are due to the changing density of the sodium.

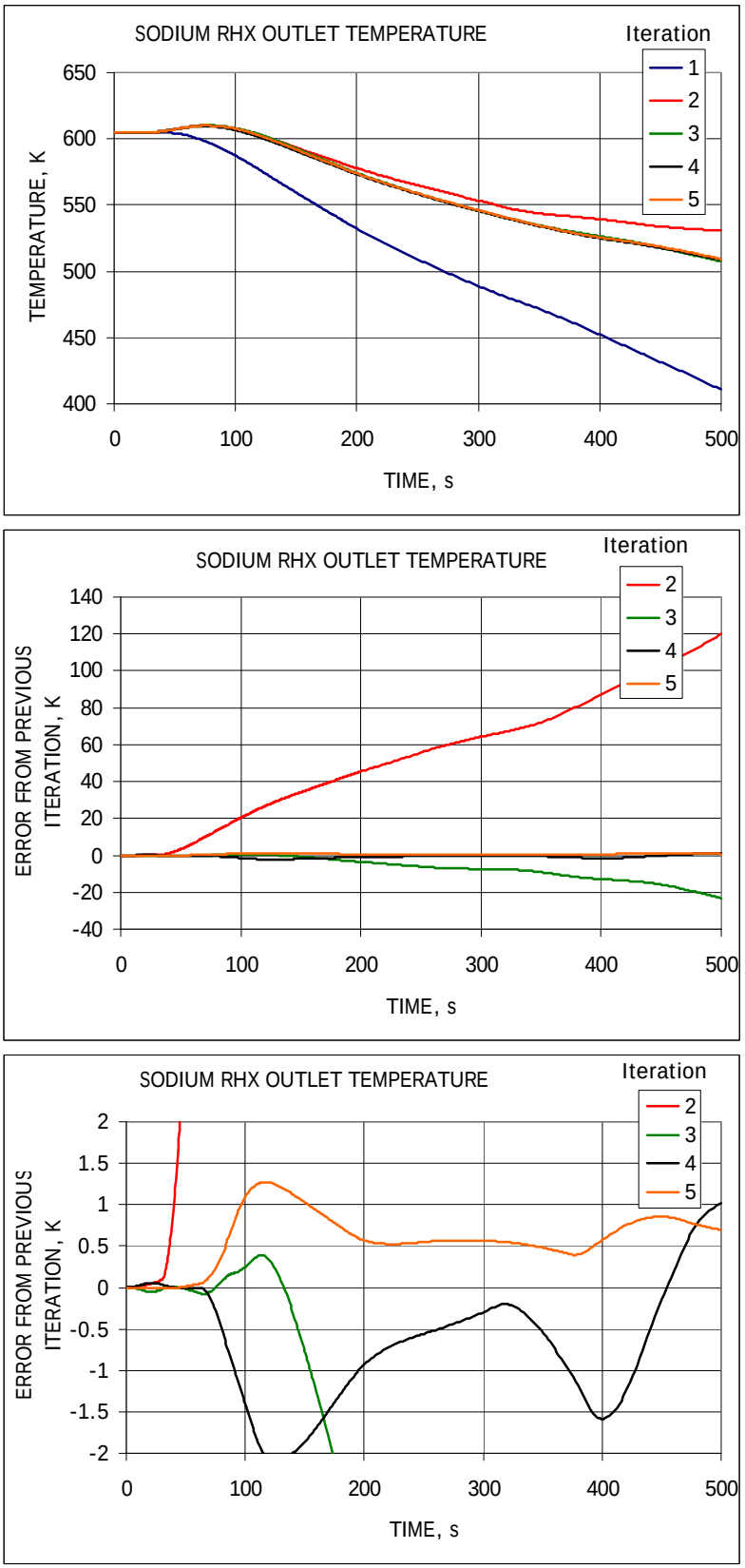

Figure 3-2. Convergence of the Sodium Temperature in the Reactor Scram Simulation.

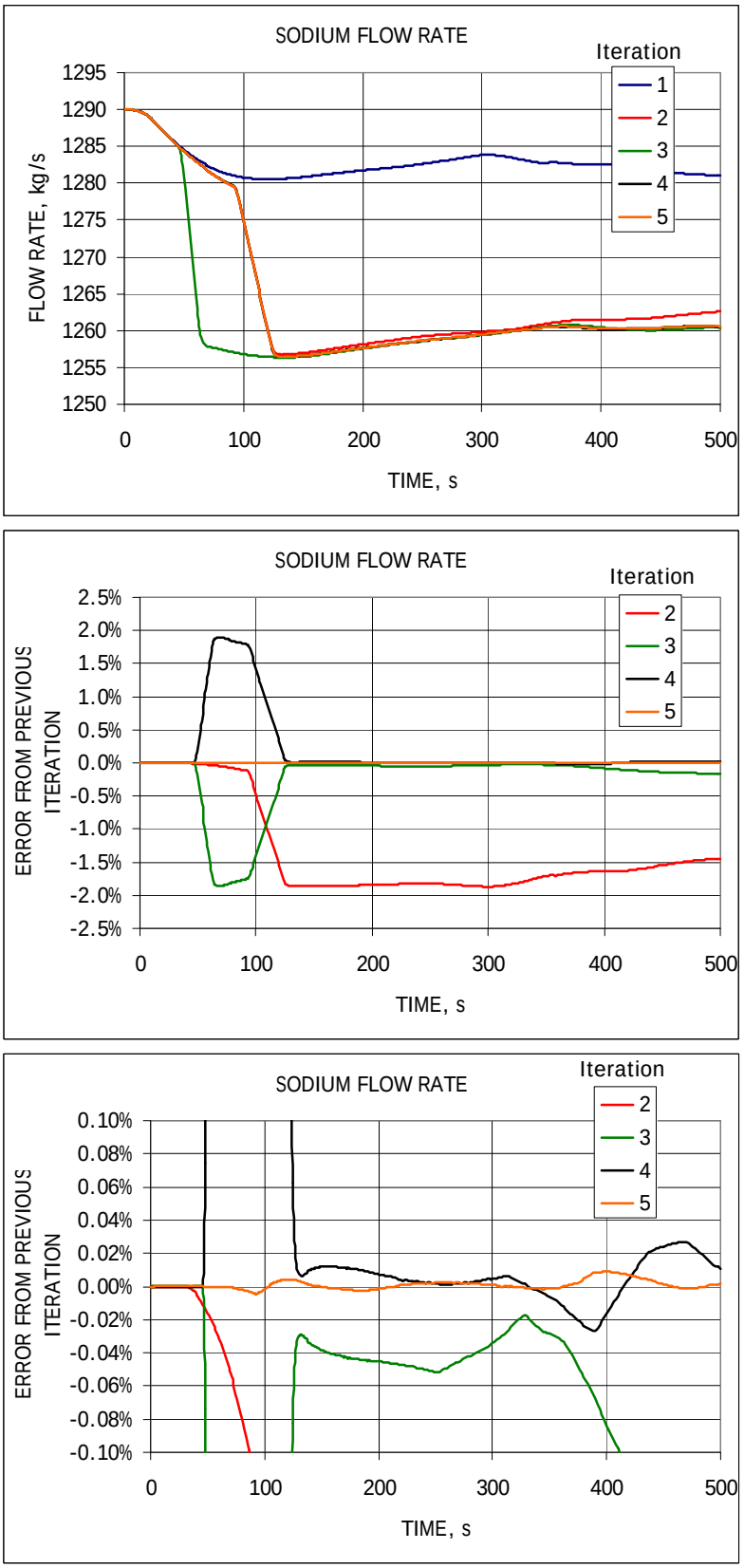

Figure 3-3. Convergence of the Sodium Flow Rate in the Reactor Scram Simulation.

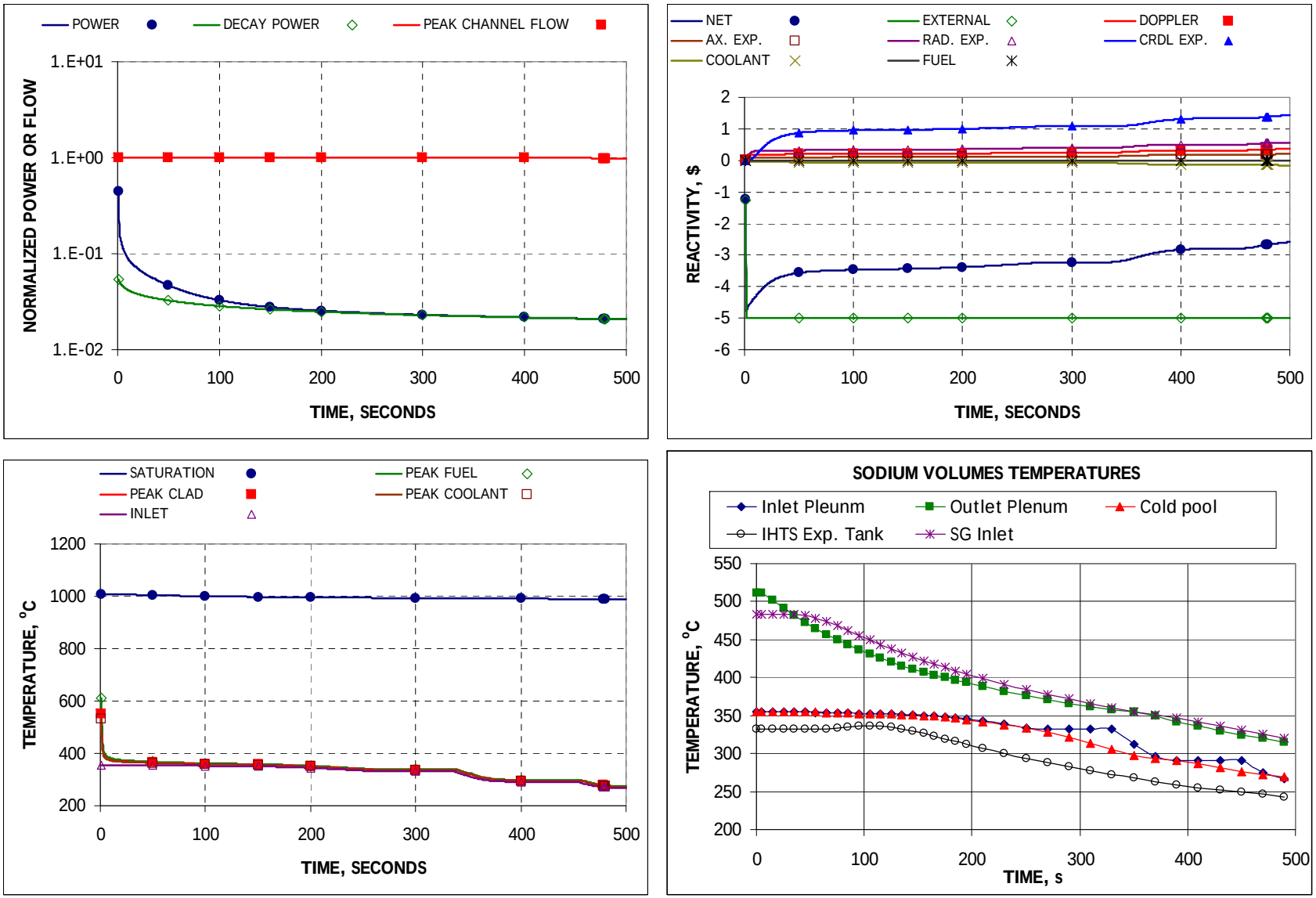

Figure 3-4. Results of the Reactor Scram Transient – Reactor Side.

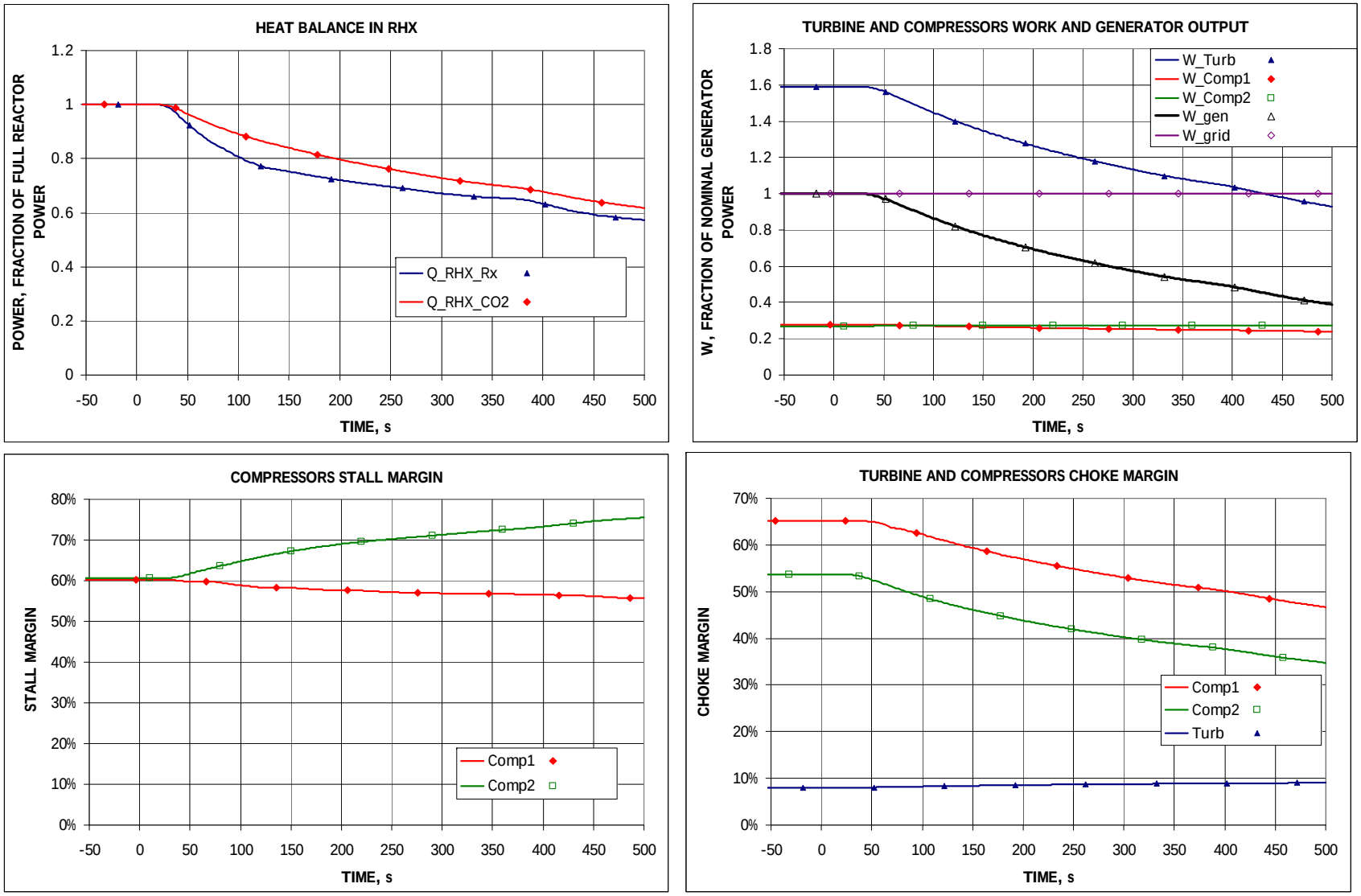

Figure 3-5. Results of the Reactor Scram Transient – S-CO_2 Cycle Side.

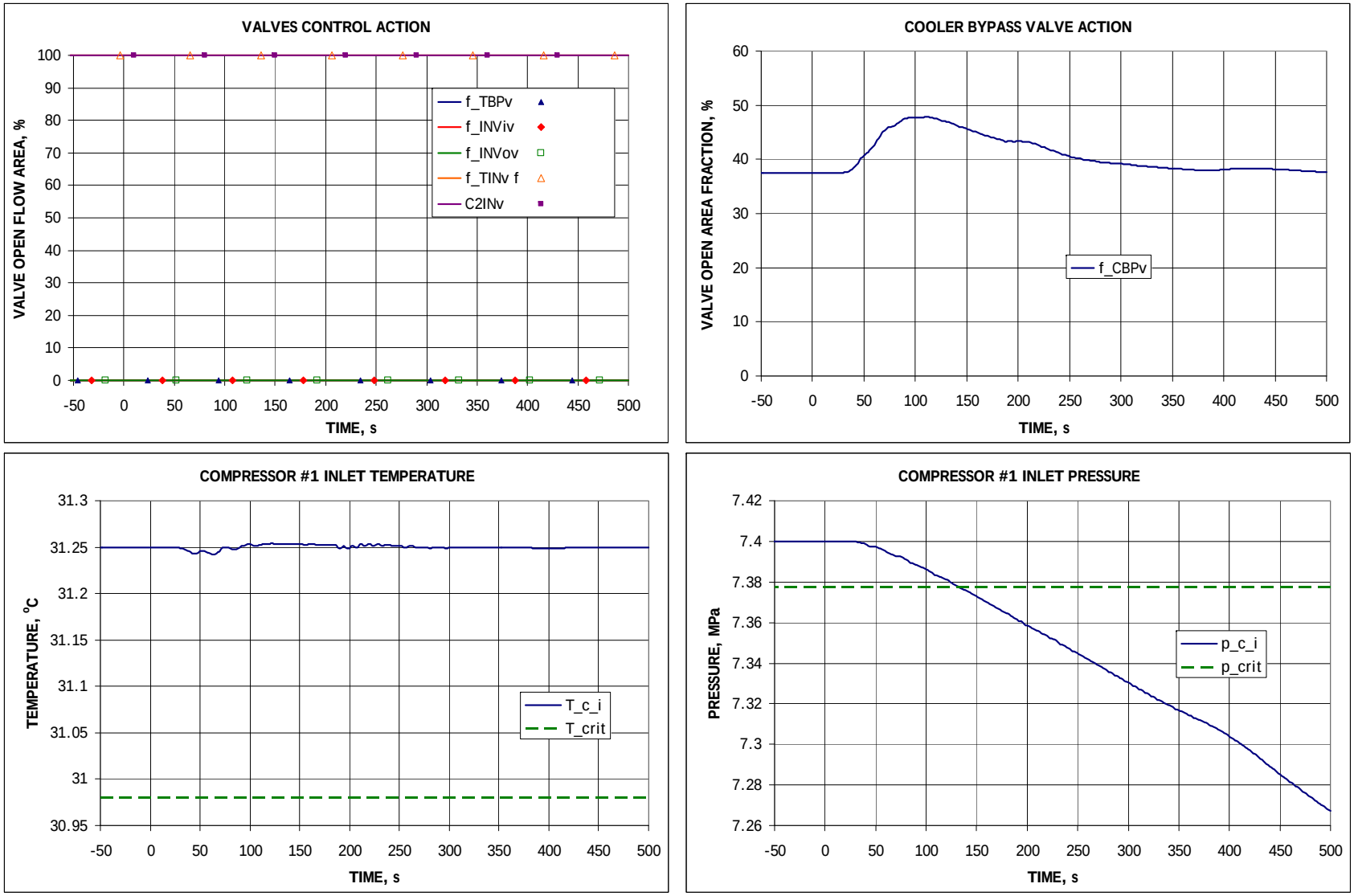

Figure 3-5. Results of the Reactor Scram Transient – S-CO2 Cycle Side. (Continued)

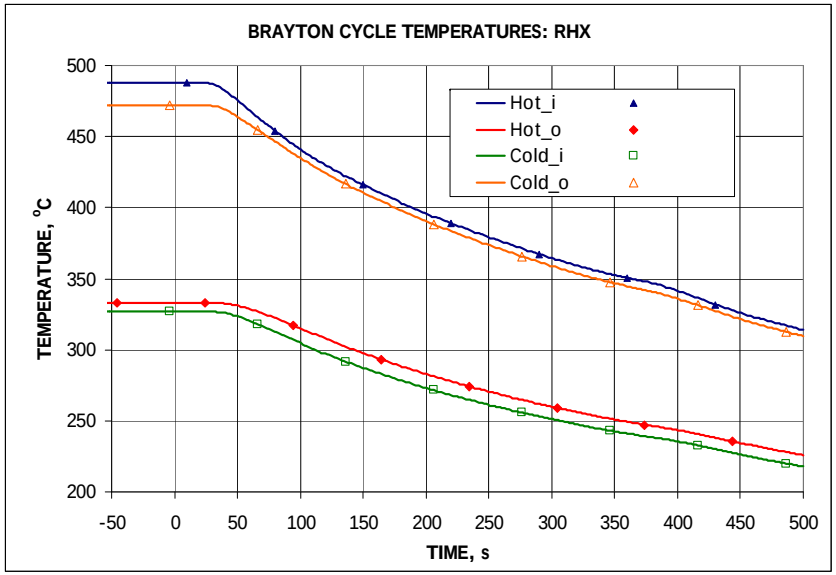

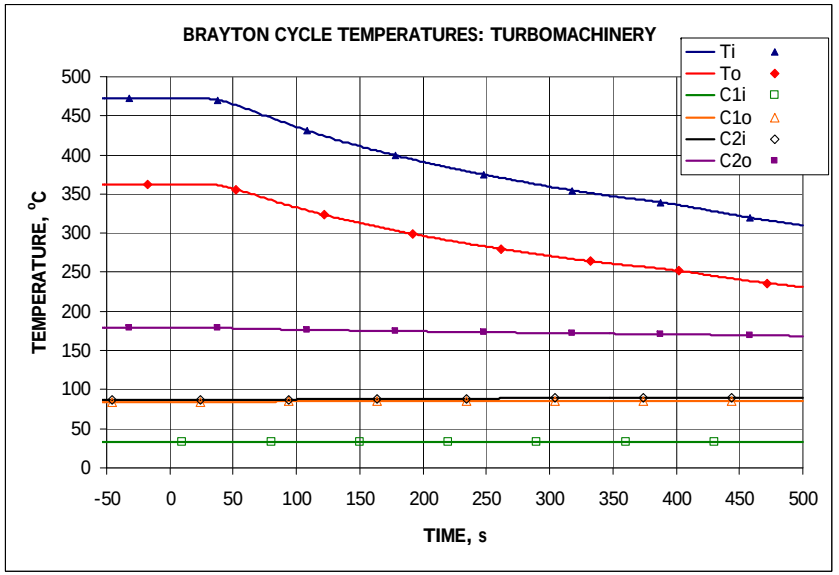

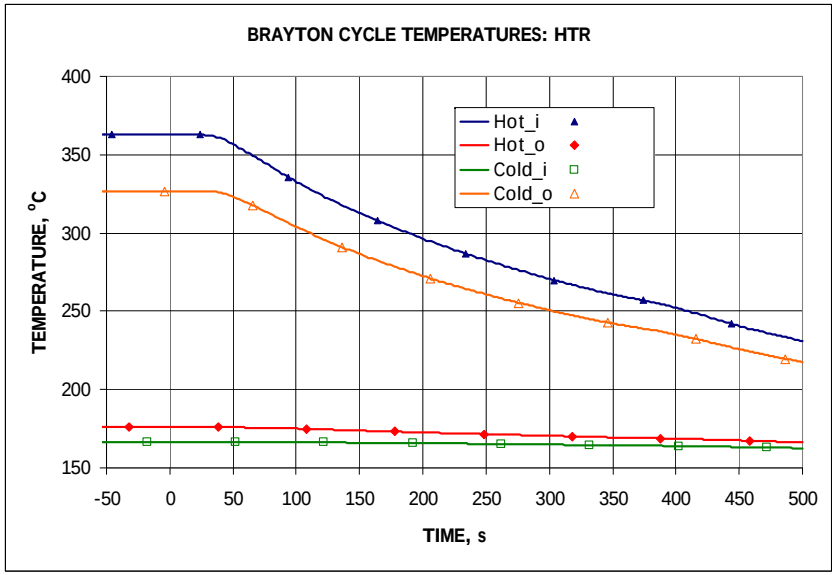

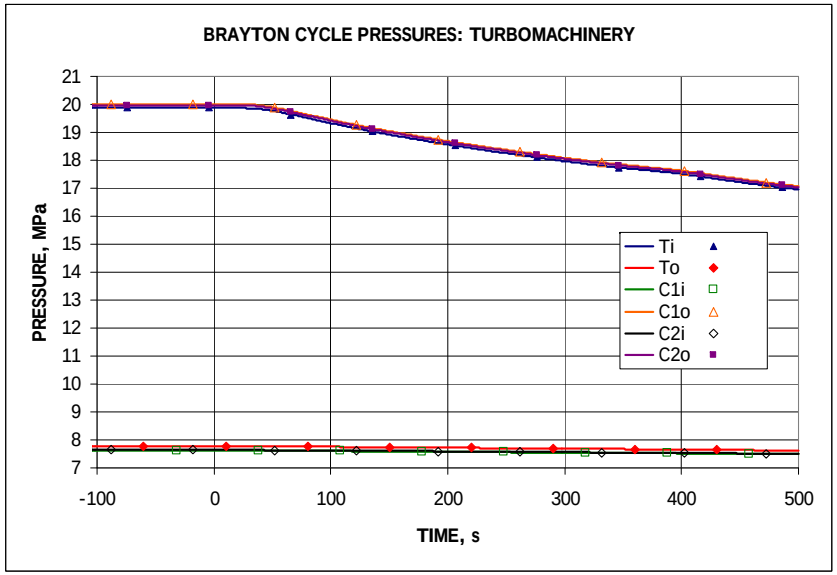

Figure 3-5. Results of the Reactor Scram Transient – S-CO2 Cycle Side. (Continued)

Since the analyzed transient conditions were selected to provide one of the most significant amount of change in the temperature conditions for the Na-CO_2 HX, the results of the analyzed transient would also be useful for the design analysis of the heat exchanger (so far, only steady state conditions have been used for the heat exchanger design). The results of the calculations shows that the temperatures at the hot end of the Na-CO_2 HX in this scenario drop in almost linear fashion by about 160 °C over 500 sec transient, or about 0.32 °C/sec. The temperatures on the cold end also drop almost linearly by about 80 °C, or about 0.16 °C/sec.

The work on the transient analysis of the S-CO_2 cycle for the SFR is expected to continue next fiscal year. It is intended to analyze more transients which could affect the design and operation of the Na-CO_2 HX and other heat exchangers, such as CO_2 pipe break accidents.

4. Plant Dynamics Code Development

During the work on the control analysis for the Generation IV systems reported in previous sections, some improvements and modifications to the Plant Dynamics Code (PDC) have been made. Those modifications are reported in this chapter.

4.1. *Modifications to the Plant Dynamics Code for Generation IV Systems Analysis*

The modifications needed for the PDC in order to allow for the analysis of various Generation IV systems have already been described in previous sections of this report. Those modifications are simply repeated here.

To allow analysis of the S-CO_2 cycle coupled to practically any system, the S-CO_2 part of the PDC was separated from the reactor part. The reactor coolant conditions at the reactor heat exchanger (RHX) are specified as an input for the S-CO_2 cycle analysis for both steady state and transient calculations. Those conditions include specification of the coolant itself (helium, sodium, etc.), its flow rate, inlet temperature, and inlet pressure. For steady state design calculations, the coolant outlet temperature is also specified. For the transient calculations, tables of the inlet coolant conditions as a function of time are required.

For the transient calculations with the Plant Dynamics Code, the inlet conditions for the reactor side coolant at the RHX are given. Those conditions are either assumed (such as constant flow rate and inlet temperature) or calculated by another code (such as SAS4A/SASSYS-1). The Plant Dynamics Code calculates the transient response of the S-CO_2 cycle. Among the parameters calculated by the Plant Dynamics Code are the reactor coolant conditions (temperature and pressure or pressure drop) at the outlet of the RHX. These conditions, if necessary, should be provided back to the reactor code and the iterations on the reactor coolant temperature and pressure change should be carried out, as presented in Section 3.2 of this report. As before, the Plant Dynamics Code still calculates the time dependent temperatures inside of the reactor heat exchanger, including the temperatures of the reactor fluid and CO_2 as well as the wall temperatures.

4.2. *Incompressible Flow Treatment Option*

It has been observed during previous calculations with the PDC that the time step size for the transient calculations of the S-CO_2 cycle is mostly controlled by the momentum equation in the cooler, i.e. close to the critical point. That feature of the PDC can be explained by Figure 4-1 which plots the CO_2 compressibility, defined as $z=p/\rho RT$, around the traditional recompression S-CO_2 cycle. Near the top part of the cycle (RHX, turbine, HTR), the compressibility is close to unity meaning that CO_2 behaves like an ideal gas. However, around the cooler and the main compressor, the compressibility approaches very low values, typical for an incompressible fluid.

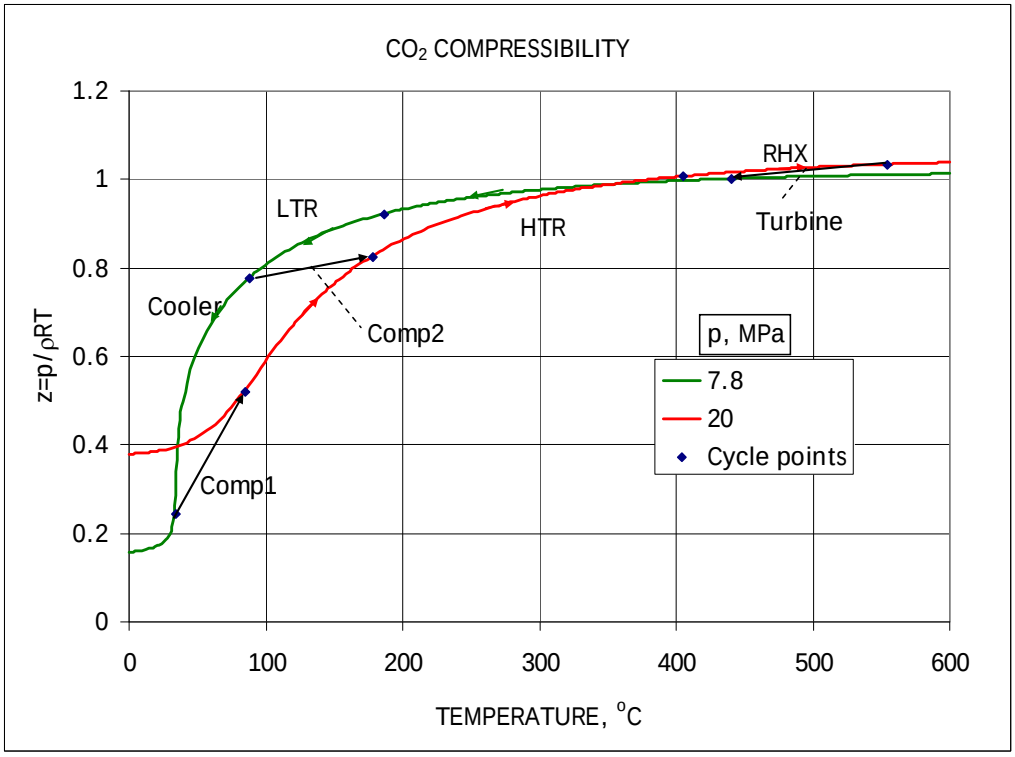

Figure 4-1. CO_2 Compressibility in the S-CO_2 Cycle.

The PDC [13] solves the compressible flow equations throughout the entire cycle. For these equations, the flow rate is found from the momentum equation as a function of the pressure difference. The flow rate is allowed to change from cell to cell and the difference in the flow rates in two adjacent cells defines the density change at the borders of the cell. To relate the density with the pressure needed to solve the momentum equation, a partial derivative of the pressure with respect to density is calculated, as following:

$$\frac{\partial \dot{m}_i}{\partial t} = \frac{A}{\Delta x_i}\left(p_i - p_{i+1}\right) - \frac{2 f_i \Delta x_i}{M_i D_h}\dot{m}_i\left|\dot{m}_i\right|$$

$$\frac{\partial \rho_i}{\partial t} = \frac{1}{A\left(\frac{\Delta x_i}{2} + \frac{\Delta x_{i-1}}{2}\right)}\left(\dot{m}_i - \dot{m}_{i-1}\right)$$

$$\frac{\partial p_{i+1}}{\partial t} = p_{T_{i+1}}\frac{\partial T_{i+1}}{\partial t} + p_{\rho_{i+1}}\frac{\partial \rho_{i+1}}{\partial t}$$

where $p_{\rho_{i+1}} = \left(\frac{\partial p}{\partial \rho}\right)_{T,i+1} = \frac{1}{\left(\frac{\partial \rho}{\partial p}\right)_{T,i+1}}$ = partial derivative of the pressure with respect to density.

For an incompressible fluid, like water in the cooler, density is almost independent of the pressure, such that

$$\left(\frac{\partial \rho}{\partial p}\right)_T \to 0 .$$

The derivative would be equal to zero for a perfectly incompressible fluid.

Since CO_2 shows the fluid-like behavior near the cooler and compressor, the derivative of density with respect to pressure becomes very small in this region such that the derivative of pressure with respect to density becomes very large. As a result, a transition from density (mass) equation to pressure for the momentum equation is done by multiplying by a very large number. In order to compensate for this multiplication, a very small time step (~10^{-3} sec) would be needed to solve the equations even at the steady state (i.e., not changing) conditions.

In an attempt to accelerate the PDC calculations, an option for an incompressible flow treatment in the heat exchangers has been added. At the beginning of each time step, the code now calculates the maximum compressibility of CO_2, z, for each flow in each heat exchanger. If this compressibility is greater than a user-defined threshold for the compressible flow treatment, then the compressible flow equations, as described above, are still applied to that flow. If, however, the compressibility is less than a threshold value, then an incompressible flow treatment is applied to that particular flow.

The incompressible flow treatment is similar to equations solved on the water side on the cooler [16]. It is assumed that the flow rate is the same for all cells of the heat exchanger, and the momentum equation above is integrated over the heat exchanger length to calculate the flow rate:

$$\frac{\partial \dot{m}}{\partial t} = \frac{A}{L}\left(p_{in} - p_{out}\right) - \frac{2}{D_h}\dot{m}\left|\dot{m}\right|\sum_{i=1}^{n}\frac{f_i \Delta x_i}{M_i},$$

where the friction coefficients and masses are calculated for each region at the beginning of each time step and the sum is assumed to be constant during the time step. The pressures inside the heat exchanger are calculated from the pressure drop for a given flow rate:

$$p_{i+1} = p_i - \frac{2 f_i \Delta x_i^2}{A M_i D_h}\dot{m}^2 .$$

Then, the densities needed for the properties calculations are computed from pressure and temperature through the partial derivatives.

A sensitivity study for the incompressible flow treatment threshold was carried out. The tradeoff between the computational time and the calculational error was investigated

on an example of a transient defined by a ramp load change from 100 % to 50 %. The computational times were recorded and the accuracy of the incompressible flow was defined as a maximum error in the transient between the calculated values of the cooler-outlet temperature and pressure and those calculated by the fully compressible flow treatment. The cooler outlet conditions were selected since the accurate calculations of the CO_2 conditions near the critical point is important for the transient behavior of the entire cycle. Table 4-1 shows the results of the sensitivity study. When a threshold is selected such that the incompressible flow treatment is applied only in the cooler, the computational time is reduced significantly while the maximum error in temperature and pressure are very small. When the threshold is increased to add the low and high temperature recuperators, the computational time continues to decrease but at the expense of less accurate cooler outlet conditions. Since the CO_2 properties are very strong functions of temperature and pressure near the critical point, the difference of 0.5 °C, for example, is considered to be significant. Therefore, for the further analysis, it is recommended to include the incompressible flow treatment only in the cooler. To do that, the compressibility threshold is set to 0.8; below this value, an incompressible flow treatment is applied, above this value, a compressible treatment is used. Figure 4-2 shows the transient behavior of the incompressible flow treatment error for the cooler outlet conditions for the case where this treatment was applied for the cooler and the cold side of the low temperature recuperator.

Table 4-1. Effect of the Incompressible Flow Treatment in S-CO_2 Cycle

Incompressible Flow Treatment in	Simulation time	Maximum transient error in cooler outlet conditions	
		Temperature, °C	Pressure, MPa
- (compressible)	4 hr 10 min	-	-
Cooler	1 hr 3 min	0.06	0.019
Cooler + LTR cold side	47 min	0.57	0.176
Cooler + LTR + HTR	25 min	0.89	0.275

The incompressible flow treatment, described above has only been applied so far to the S-CO_2 cycle heat exchangers. The flow outside the heat exchangers (such as in the pipes, turbine, and compressors) is still treated with the compressible flow equations.

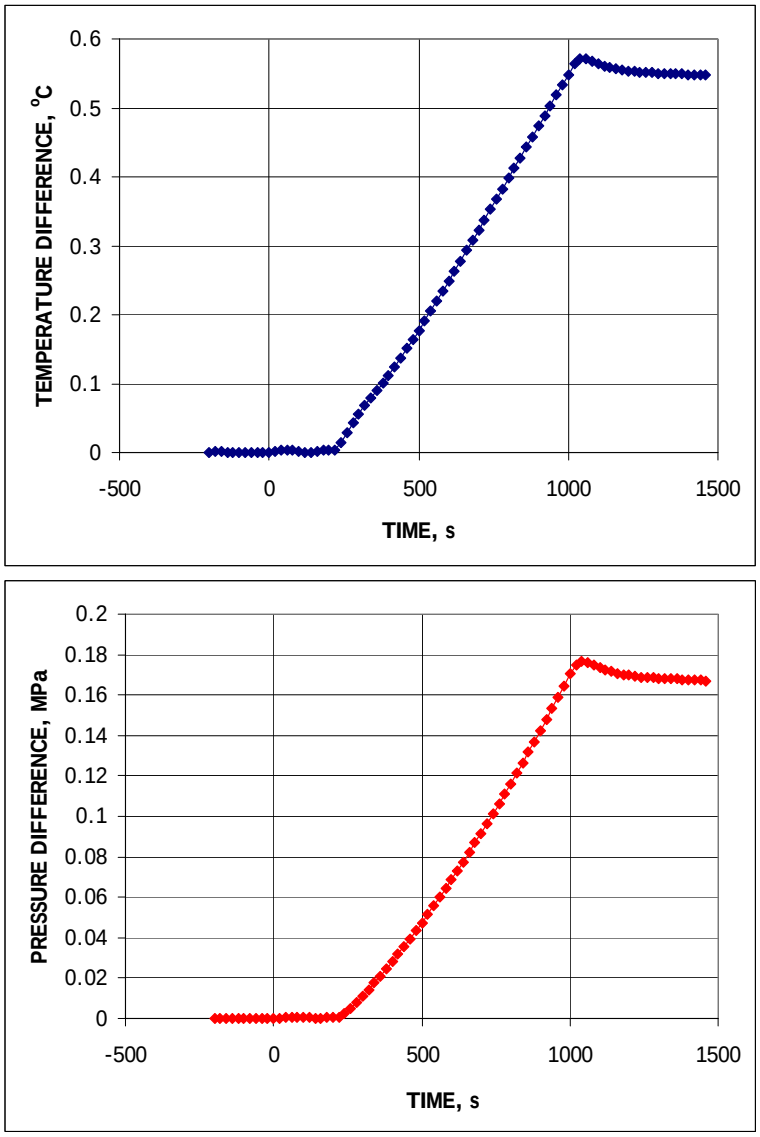

Figure 4-2. Error from Incompressible Flow Treatment in Transient.

5. Summary

The analysis of specific control strategies and dynamic behavior of the supercritical carbon dioxide (S-CO_2) Brayton cycle has been extended to the two reactor types selected for continued development under the Generation IV Nuclear Energy Systems Initiative; namely, the Very High Temperature Reactor (VHTR) and the Sodium-Cooled Fast Reactor (SFR).

An investigation of S-CO_2 cycle applicability to the VHTR confirmed previous findings that the large temperature change on the helium side of the reactor heat exchanger in the VHTR system makes a direct application of the standard recompression S-CO_2 cycle relatively inefficient (44.9 % cycle efficiency). Steady state analyses were carried out to find more efficient ways of coupling the S-CO_2 cycle to the VHTR. As a result of the steady state design analyses, two S-CO_2 cycle configurations have been indentified by which the S-CO_2 cycle can be successfully coupled to the VHTR to realize a high cycle efficiency. The first is a cascaded recompression supercritical cycle arrangement with three separate S-CO_2 cycles each having its own reactor heat exchanger for He-to-CO_2 heat exchange. An overall cycle efficiency of 49.3 % is calculated. The second is a single recompression cycle for which the minimum pressure is selected significantly below the critical pressure with a precooler and additional compressor ahead of the main compressor. A cycle efficiency of 49.5 % is calculated. It is recommended that further analysis of the S-CO_2 cycle for VHTR application, including cycle control, should retain both of these two options to further investigate their relative benefits. Based on the fact that each cycle in the cascaded arrangement is very similar to the traditional standard recompression cycle, it is expected that the control response of the cascaded S-CO_2 cycles would be similar to the response previously calculated for the standard recompression cycle. A transient control analysis of the S-CO_2 cycle for the VHTR for the second configuration with a minimum pressure below the critical pressure plus the additional precooler and third compressor has been initiated; preliminary transient control results have been obtained.

Overall, the results of the quasi-static control analysis for the ABTR SFR are very similar to those previously obtained for S-CO_2 cycle applications to the STAR LFRs. Inventory control is calculated to be the preferable option but has a limited range of applicability. A control strategy for the entire power range was developed for a S-CO_2 cycle coupled to the SFR. To analyze the transient behavior of the S-CO_2 cycle coupled to a SFR, a special approach was developed under which simultaneous runs of a reactor system level transient analysis code (such as SAS4A/SASSYS-1) for the reactor part and the Plant Dynamics Code for the S-CO_2 part are carried out in an iterative scheme. It has been shown that this simultaneous use of two separate codes quickly produces a converged solution such that the detailed system level transient response of the entire plant can be calculated and investigated for different scenarios. The new plant transient response analysis capability was demonstrated for an example of a transient scenario initiated by a reactor scram without tripping the sodium pumps or disconnecting the generator from the electrical grid. The calculations have shown that the sodium

temperatures decrease following the reactor scram resulting in decreasing CO_2 temperatures and pressures in the Na-to-CO_2 heat exchanger (HX). The rates of the temperature decreases at both ends of the Na-to-CO_2 HX are calculated from the results of the transient simulation and can be used in the design analysis of the Na-to-CO_2 HX.

To carry out the calculations described in this report, several modifications to the Plant Dynamics Code were necessary. These modifications include the separation of the S-CO_2 cycle calculations from the reactor part such that the same code can be applied to various reactor systems. In this arrangement, the reactor coolant fluid and its conditions (such as flow rate, temperatures, and pressures) at the reactor heat exchanger need to be defined by input. For the transient calculations, tables of those parameters as functions of time are provided as input. A self-adaptive algorithm has been developed which produces time dependent tabular input through a least squares-based fitting of piecewise linear functions to the detailed output of the reactor system level transient code choosing the location of the time points to capture the time variation in the output. In addition to those modifications, the option of an incompressible flow treatment in the heat exchangers was added to the Plant Dynamics Code. It was demonstrated that if a threshold to switch between the compressible and incompressible treatment is carefully selected, a significant reduction in the already short computational time can be achieved without significant penalties on the accuracy of the calculations.

References

1. Dostal, V., "A Supercritical Carbon Dioxide Cycle for Next Generation Nuclear Reactors," D.Sc. Dissertation, MIT, 2004.

2. Driscoll, M.J., "Monthly Progress Report for Period September 1-30, 2007, on Project: Energy Conversion – S-CO_2 Systems and Dynamic Response Analysis," October 10, 2007.

3. Johnson, G. A. and McDowell, M., "Issues Associated with Coupling Supercritical CO_2 Power Cycles to Nuclear, Solar and Fossil Fuel Heat Sources," presentation at the SC CO_2 Power Cycle Symposium 2009, RPI, Troy, NY, April 29-30, 2009.

4. Span, R. and Wagner, W., "A New Equation of State for Carbon Dioxide Covering the Fluid Region from the Triple-Point Temperature to 1100K at Pressures up to 800 MPa," J. Phys. Chem. Ref. Data, 25 (6), pp. 1509-1596, 1996.

5. Chang, Y.I., et. al., "Small Modular Fast Reactor Design Description," ANL-SMFR-1, Argonne National Laboratory, July 1, 2005.

6. Chang, Y.I., et. al., "Advanced Burner Test Reactor Preconceptual Design Report," ANL-ABR-1 (ANL-AFCI-173), Argonne National Laboratory, September 5, 2006.

7. Kim, T.K., Yang, W.S., Grandy, C., and Hill, R.N., "Core Design Studies for a 1000 MWth Advanced Burner Reactor," Annals of Nuclear Energy, 36, pp. 331–336, 2009.

8. Moisseytsev, A. and Sienicki, J. J., "Performance Improvement Options for the Supercritical Carbon Dioxide Brayton Cycle," ANL-GenIV-103, Argonne National Laboratory, June 6, 2008.

9. Moisseytsev, A. and Sienicki, J. J., "Investigation of Alternative Layouts for the Supercritical Carbon Dioxide Brayton Cycle for a Sodium-Cooled Fast Reactor," Nuclear Engineering and Design, Vol. 239, pp. 1362-1371, 2009.

10. Moisseytsev, A. and Sienicki, J. J., "Supercritical CO_2 Brayton Cycle Control Strategy for Autonomous Liquid Metal-Cooled Reactors," Proceedings of Americas Nuclear Energy Symposium, ANES, Miami Beach, FL, October 3-6, 2004.

11. Moisseytsev, A. and Sienicki, J. J., "Control of Supercritical CO_2 Brayton Cycle for LFR Autonomous Load Following," Transactions of the American Nuclear Society, Vol. 93, p. 342, American Nuclear Society 2005 Winter Meeting, Washington, DC, November 13-17, 2005.

12. Moisseytsev, A. and Sienicki, J. J., "Automatic Control Strategy Development for the Supercritical CO_2 Brayton Cycle for LFR Autonomous Load Following," Paper 6074,

Proceedings of 2006 International Congress on Advances in Nuclear Power Plants, ICAPP'06, Reno, NV, June 4-8, 2006.

13. Moisseytsev, A. and Sienicki, J. J., "Development of a Plant Dynamics Computer Code for Analysis of a Supercritical Carbon Dioxide Brayton Cycle Energy Converter Coupled to a Natural Circulation Lead-Cooled Fast Reactor," ANL-06/27, Argonne National Laboratory, July 2006.

14. Moisseytsev, A. and Sienicki, J. J., "Supercritical Carbon Dioxide Cycle Control Analysis," ANL-GenIV-111, Argonne National Laboratory, September 15, 2008.

15. Cahalan, J. E., Tentner, A. M., and Morris, E. E., "Advanced LMR Safety Analysis Capabilities in the SASSYS-1 and SAS4A Computer Codes," Proceedings of the International Topical Meeting on Advanced Reactor Safety, Pittsburgh, April 17-21, 1994, Vol. 2, p. 1038, American Nuclear Society, La Grange Park (1994).

16. Moisseytsev, A. and Sienicki, J. J., "Control Strategies and Stability Analysis for Supercritical CO_2 Cycles," ANL-GenIV-096, Argonne National Laboratory, September 15, 2007.

Appendix A
Quasi-Static S-CO_2 Cycle Control Analysis for a SFR

The S-CO_2 cycle control analysis for the Advanced Burner Test Reactor (ABTR) [A1] has been carried out using the steady state part of the ANL Plant Dynamics Code (PDC) [A2]. The control calculations are performed in a quasi-static mode where only initial and final states of the system are calculated based on the steady state equations. To carry out quasi-static control calculations, the steady state part of the PDC has been modified. In those calculations, the designs of the components are fixed by the steady state (design) and the performance of each component is calculated based on the changing flow conditions caused by the control action. The most significant difference between the steady state (design) and quasi-static (control) calculations is the use of the turbomachinery models. In steady state calculations, the design subroutines are used for the S-CO_2 turbine and compressors whereas in the control calculations, the turbomachinery off-design performance subroutines are utilized. Those are the same subroutines used by the PDC to generate the performance maps for the dynamic calculations.

The S-CO_2 cycle control calculations for ABTR are similar to those reported previously for lead-cooled natural circulation STAR reactors [A3,A4,A5]. The calculations on the S-CO_2 cycle are almost the same for the SFR and LFR. The difference comes from the reactor side. STAR reactors are designed for autonomous control for autonomous load following where the reactor power and natural circulation flowrate are inherently adjusted by the strong reactivity feedbacks of the LFR core to changes in the lead coolant and fuel temperatures. For the ABTR reactor, the reactor power control is implemented by movement of the control rods. Therefore, an additional control mechanism for independent reactor power variation is present in the ABTR design (compared to the STAR LFRs). In addition, the forced circulation of the primary and intermediate sodium coolants in ABTR (as opposed to the natural circulation of just one primary coolant in STAR) provide another independent control mechanism through the adjustment reactor coolant(s) flow rate(s). Thus, the quasi-static analysis of the S-CO_2 cycle has been expanded from previous works in order to include these additional controls for the ABTR.

Figure A-1 shows the ABTR overall plant configuration, S-CO_2 cycle arrangement and components, and the considered control mechanisms. The control mechanisms simulated in the analysis include the reactor power control (by means of the control rods), primary and intermediate sodium flow rate control (by the control of the sodium pumps), turbine bypass flow (regulated by the turbine bypass valve), S-CO_2 inventory control (provided by the inventory tanks), turbine throttling, Na-CO_2 HX bypass, control of the flow split between two compressors (by compressor throttling valves), and minimum cycle temperature control (by adjusting water flow rate in cooler). The shutdown heat removal loop shown in Figure A-1 is not included in the current control analysis.

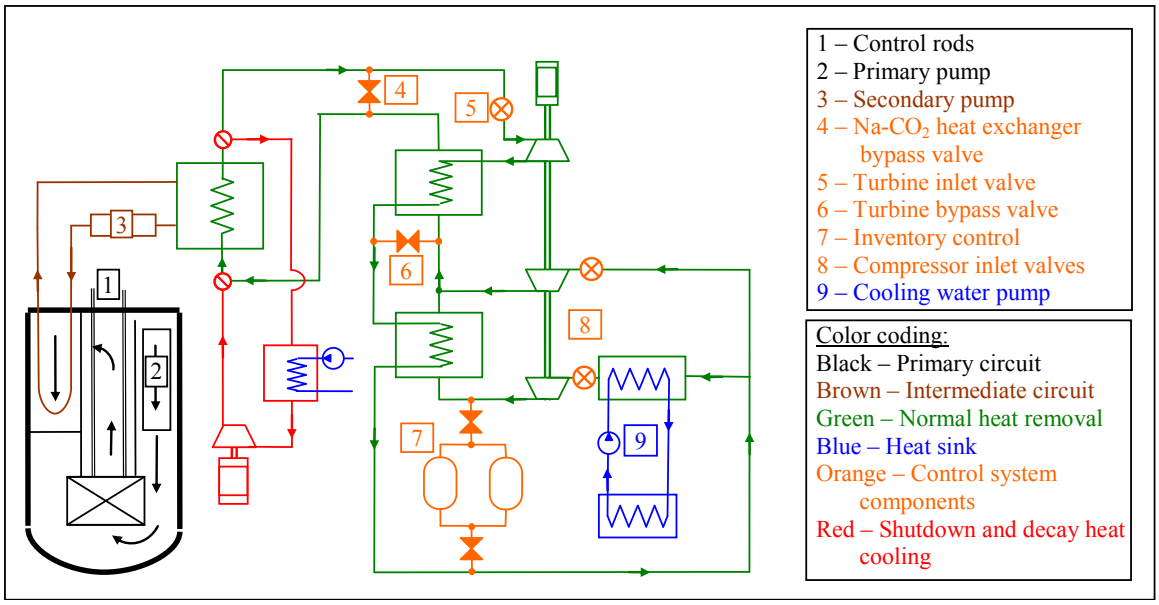

Figure A-1. ABTR Control Mechanisms.

In the quasi-static control analysis, the system response to each individual control action is investigated. It is assumed in the analysis that the water flow rate is adjusted automatically to keep the minimum cycle temperature at the design value (except in the minimum temperature variation option where the minimum cycle temperature is changing). It is also assumed that the conditions on the primary and intermediate loops (coolant flow rates) are adjusted automatically to match the heat removal and sodium temperatures in the Na-CO_2 heat exchanger. In these particular calculations, synchronous generator operation is assumed meaning that the generator rotational speed is fixed by the grid frequency at the steady-state value. Since the turbine and compressors are located on the common shaft with the generator (Figure A-1), this assumption means that the rotational speed of the turbine and compressors is fixed in the calculations. Also, it is generally assumed that only one control action is taken at a time, i.e. a combination of independent controls is not investigated in this work.

For the reactor power control, two options have been identified and analyzed in this work:

- Direct reactor power control, and
- Reactor power adjustment.

Under the direct power control, the reactor power is *specified* as an input parameter. All other parameters, including those on the S-CO_2 side, are calculated. The primary and intermediate sodium flow rates are automatically adjusted in this case to keep the maximum intermediate sodium temperature constant and to maintain the heat balance in the primary and intermediate loops. Since the calculations for the current analysis assumed only one independent control action at a time, when the direct reactor power

control option is selected, no control action is implemented on the S-CO_2 cycle (except for the water flow rate control to maintain the minimum temperature).

The other reactor power control option, reactor power adjustment, is implemented when the control action is taken on the S-CO_2 side. In this case, both the sodium flow rates and the reactor power are automatically adjusted to match the current calculated conditions for the Na-CO_2 heat exchanger. In these calculations, the control logic is set up such that the maximum intermediate sodium temperature is kept constant. The minimum intermediate sodium temperature is either kept constant, if possible, or is otherwise assumed to be 5 °C above the CO_2 temperature at Na-CO_2 HX inlet.

The water flow rate in the cooler is assumed to be automatically adjusted such that the minimum temperature in the S-CO_2 cycle (at the main compressor first stage inlet) is kept just above the critical temperature. This assures that the two-phase flow into compressor blades is avoided all the time even when the compressor inlet pressure falls below the critical value, as it is calculated to do in some cases. In addition to this automatic control, an option to actively change the minimum temperature is investigated as a separate cycle control mechanisms. In all calculations, the water inlet temperature is assumed to be 30 °C and the water cooler outlet pressure is 1 atm. The code then calculates the required water flow rate and the water pumping power. This pumping power, together with the pumping power for the primary and intermediate sodium loops, is subtracted from the generator output to calculate the net plant electrical output. It is assumed in the calculations that the pumping power for sodium pumps is constant at the design value of 0.8 MW for each loop.

In the control calculations presented below, the control action is specified as an input. This input depends on the control action (for example, it could be fraction of total power for the reactor power control or fraction of total flow that bypasses the turbine for the turbine bypass control). The code then calculates the remaining parameters which characterize the system state. The calculated parameters include:

- Intermediate sodium HX outlet temperature and flow rate,
- CO_2 pressures, temperatures, and flow rates in the cycle, from which the turbomachinery power and efficiencies, HX heat duties, and flow split fractions are derived,
- Cooling water inlet and outlet temperatures, pressures, and flow rates, and
- Cycle (generator) power and net plant electrical output.

There are several limits defining the ranges of the control actions. The cycle control is investigated between 0 % and 100 % generator output. Thus, no control action resulting in power output below 0 % or above 100 % is considered in this work. The other limit is provided by the turbomachinery operating range, such as choke and surge in compressors or possible choke in the turbine. In addition, the sodium temperature should be kept above freezing all the time.

The control calculations start from the design (full-power) conditions. The design conditions and component dimensions are presented in the ABTR report [A1].

Figure A-2 shows the results of the reactor power control calculations. As the reactor power is decreased, the CO_2 temperature at the Na-CO_2 HX outlet is reduced. This temperature reduction causes the turbine work to decrease. It also lowers the temperatures at the turbine outlet as well as in the recuperators. As a result, the CO_2 temperature at the Na-CO_2 HX inlet is also reduced. Reduction of the turbine work causes a decrease in the generator output power. The sodium and water flow rates are adjusted for the CO_2 temperatures. Since the generator output decreases faster than the reactor power (generator power reaches zero at about 40 % reactor power), the cycle efficiency quickly reduces from the full power value in this control scheme.

Figure A-3 shows the results for the inventory control calculations. As CO_2 mass is removed from the cycle, the system pressures are reduced causing the CO_2 flow rate to decrease. The turbine and compressor works decrease with the flow; however, the reduction in the turbine work is more significant in an absolute sense than that of the compressors leading to the reduction in the generator output. The sodium temperatures in the Na-CO_2 HX (RHX) are calculated based on the sodium flow rate which is adjusted to provide the heat balance in the heat exchanger. The results in Figure A-3 show that the cycle efficiency decreases only slightly between 100 % and 40 % loads.

The results of the turbine bypass control (Figure A-4) and the turbine inlet throttling (Figure A-5) are similar to those obtained previously for the STAR LFRs [A3,A4,A5]. In the case of turbine bypass control, the turbine work decreases while the compressor work increases slightly resulting in fast drop of the generator output. The reactor power changes more slowly than the generator output requiring significant increase in the water flow rate to dump the excess heat into atmosphere (through the cooling towers). This leads to a significant increase in the water flow rate and water pumping power such that the plant efficiency drops even faster than the turbine work. A similar effect is observed with the minimum temperature control (Figure A-6). As the conditions in the cooler pass through the pseudo-critical point, significant increase in the water flow rate and pumping power is required resulting in a drop in the plant efficiency.

Figure A-7 compares the control mechanisms in terms of cycle efficiency, sodium flow rate, and water flow rate for the reduced loads. It is apparent from Figure A-7 that inventory control provides the highest efficiency at reduced loads while turbine bypass yields the lowest efficiency. The water flow rate is defined by how much excessive heat needs to be removed from the plant and therefore is reversely proportional to the cycle efficiency. The required adjustment of the sodium flow rate is very similar for all control mechanisms except for reactor power control where a significant change in the flow rate is needed.

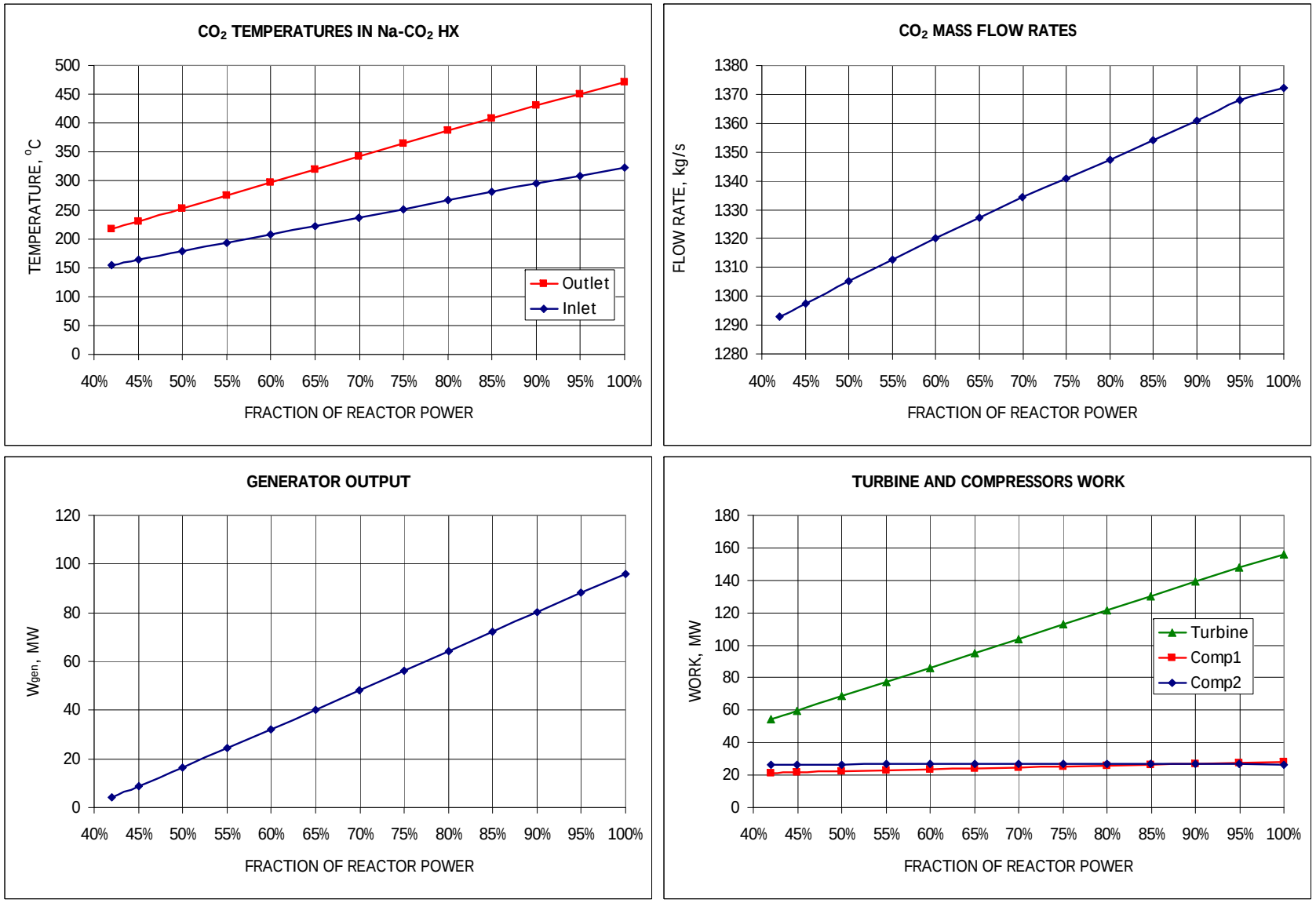

Figure A-2. Results of Reactor Power Control.

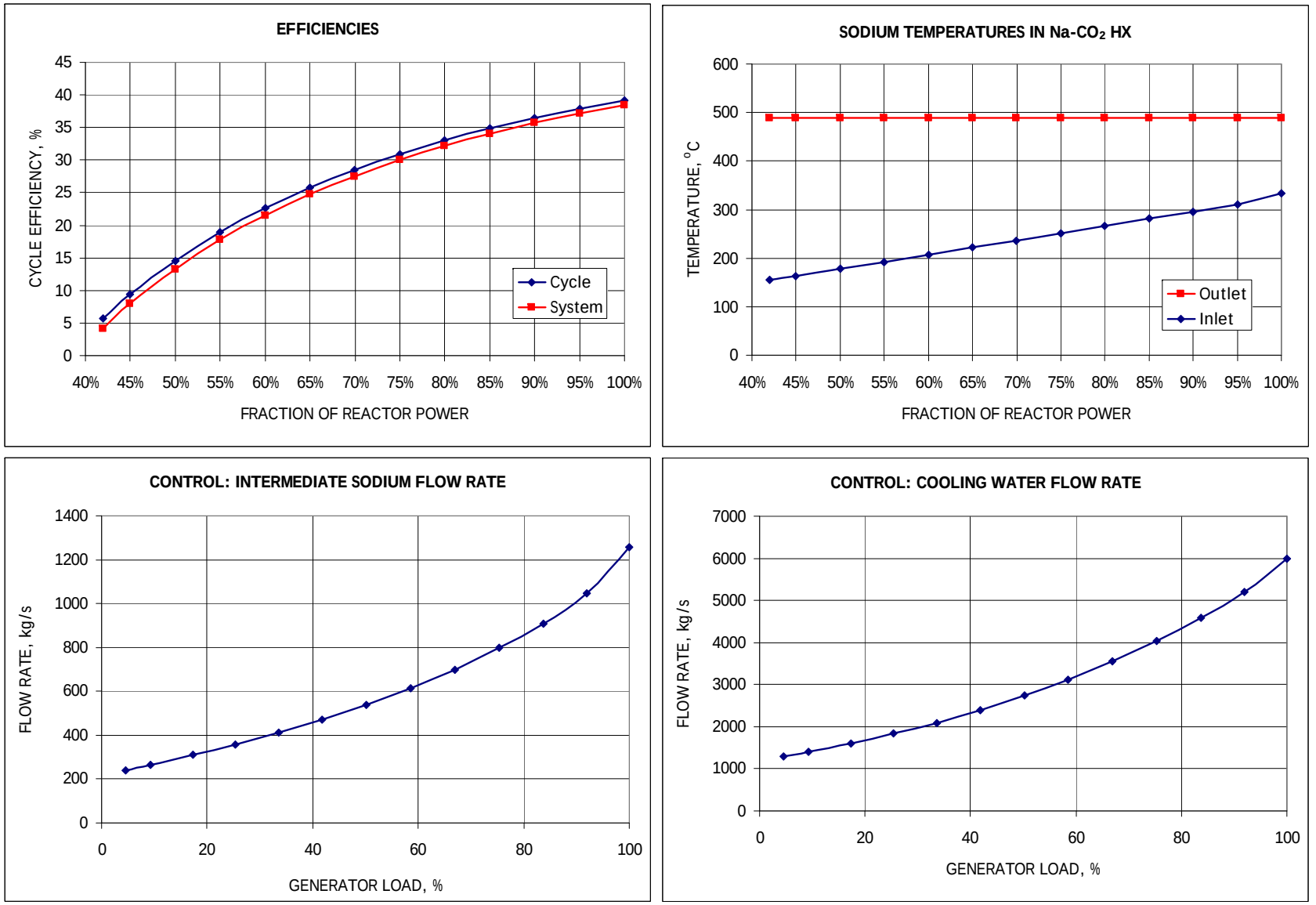

Figure A-2. Results of Reactor Power Control. (Continued)

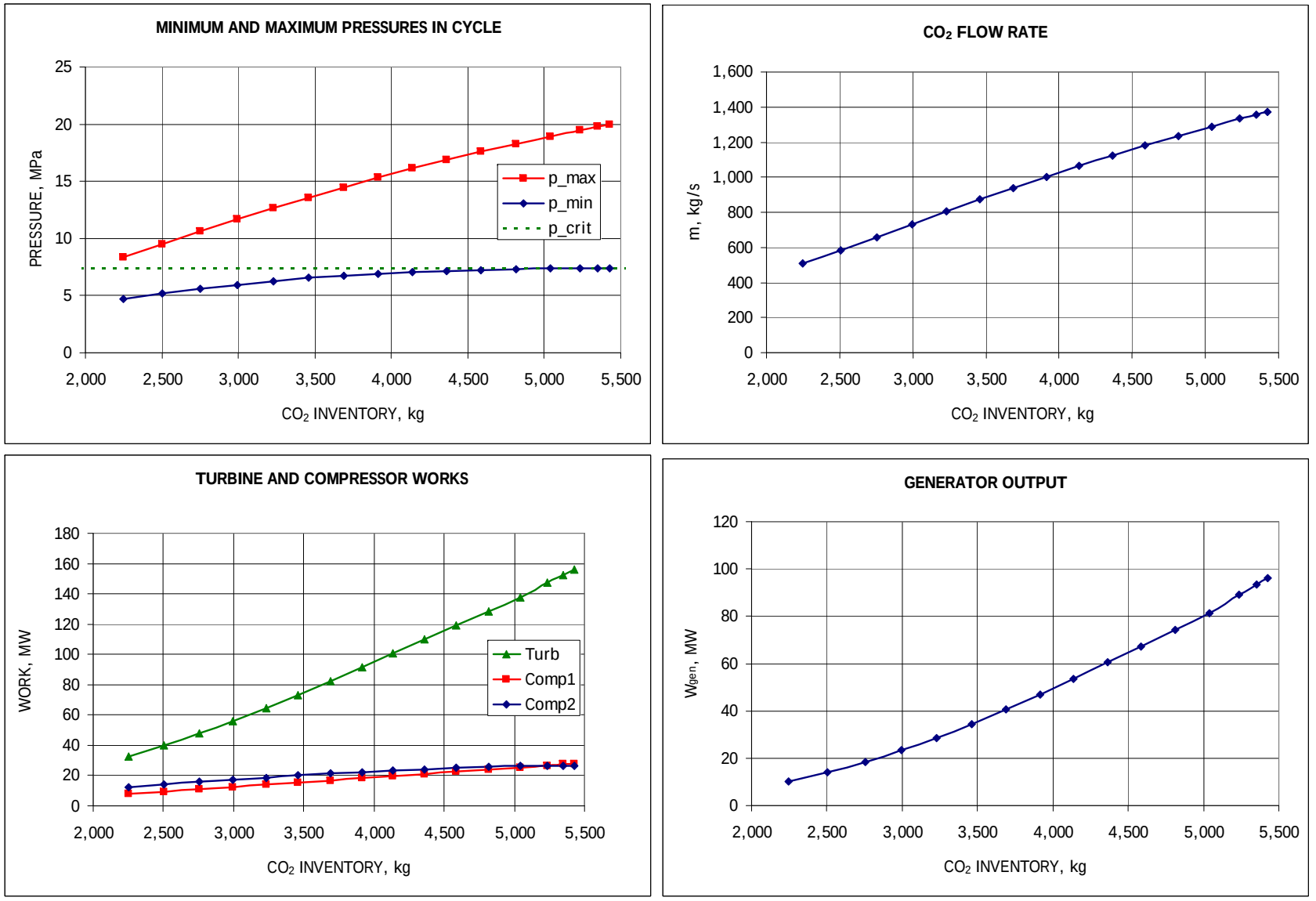

Figure A-3. Results of Inventory Control.

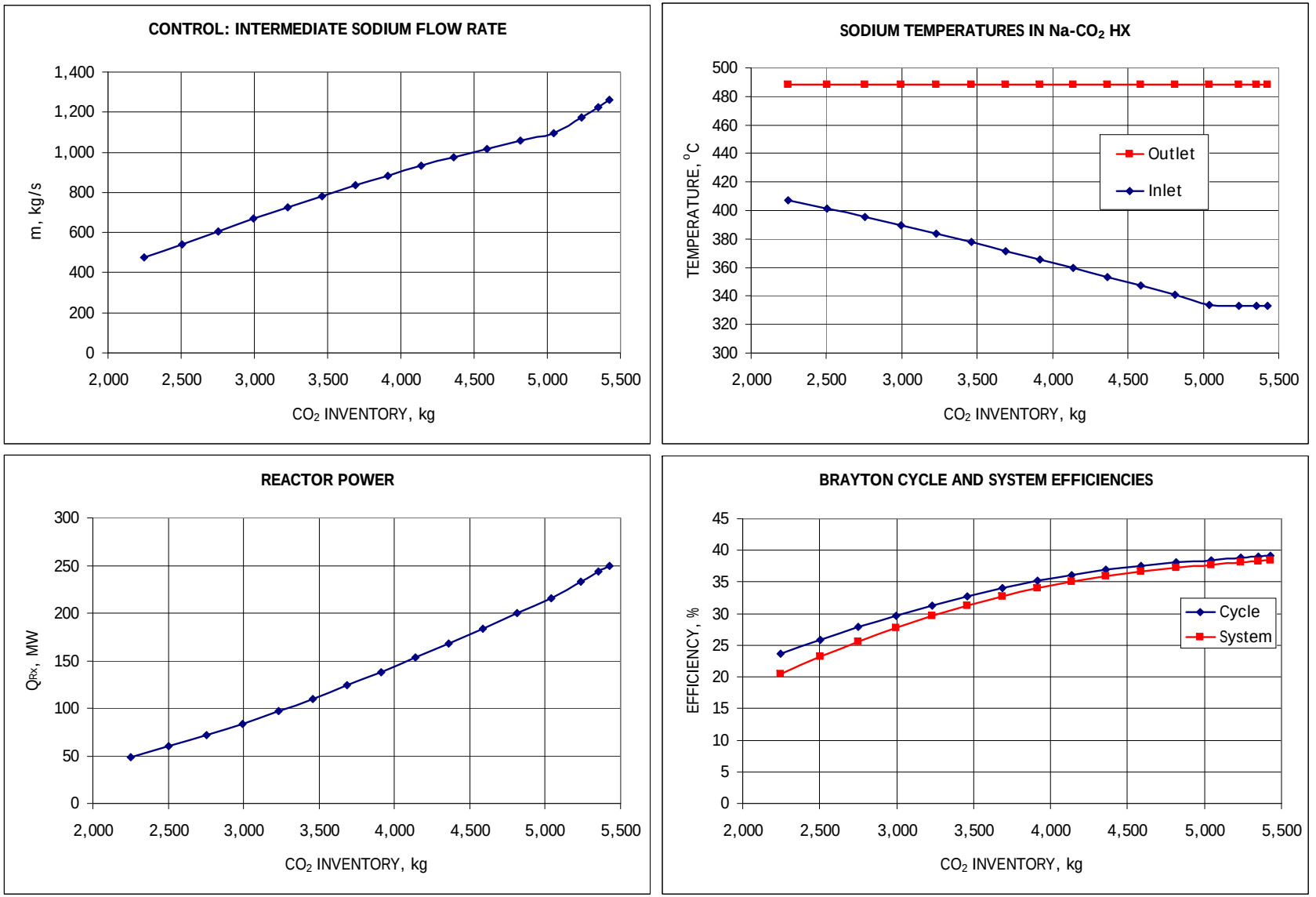

Figure A-3. Results of Inventory Control. (Continued)

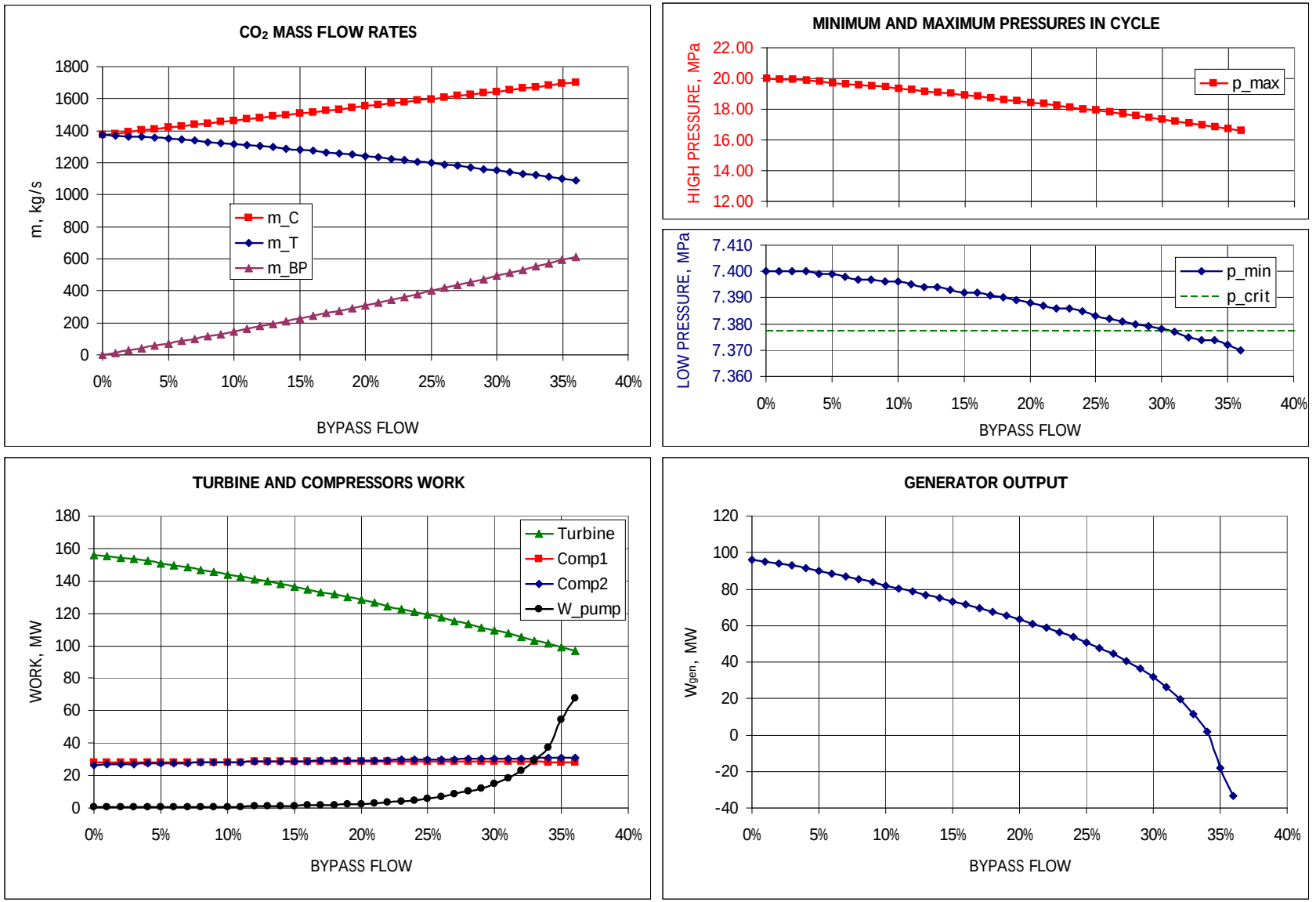

Figure A-4. Results of Turbine Bypass Control.

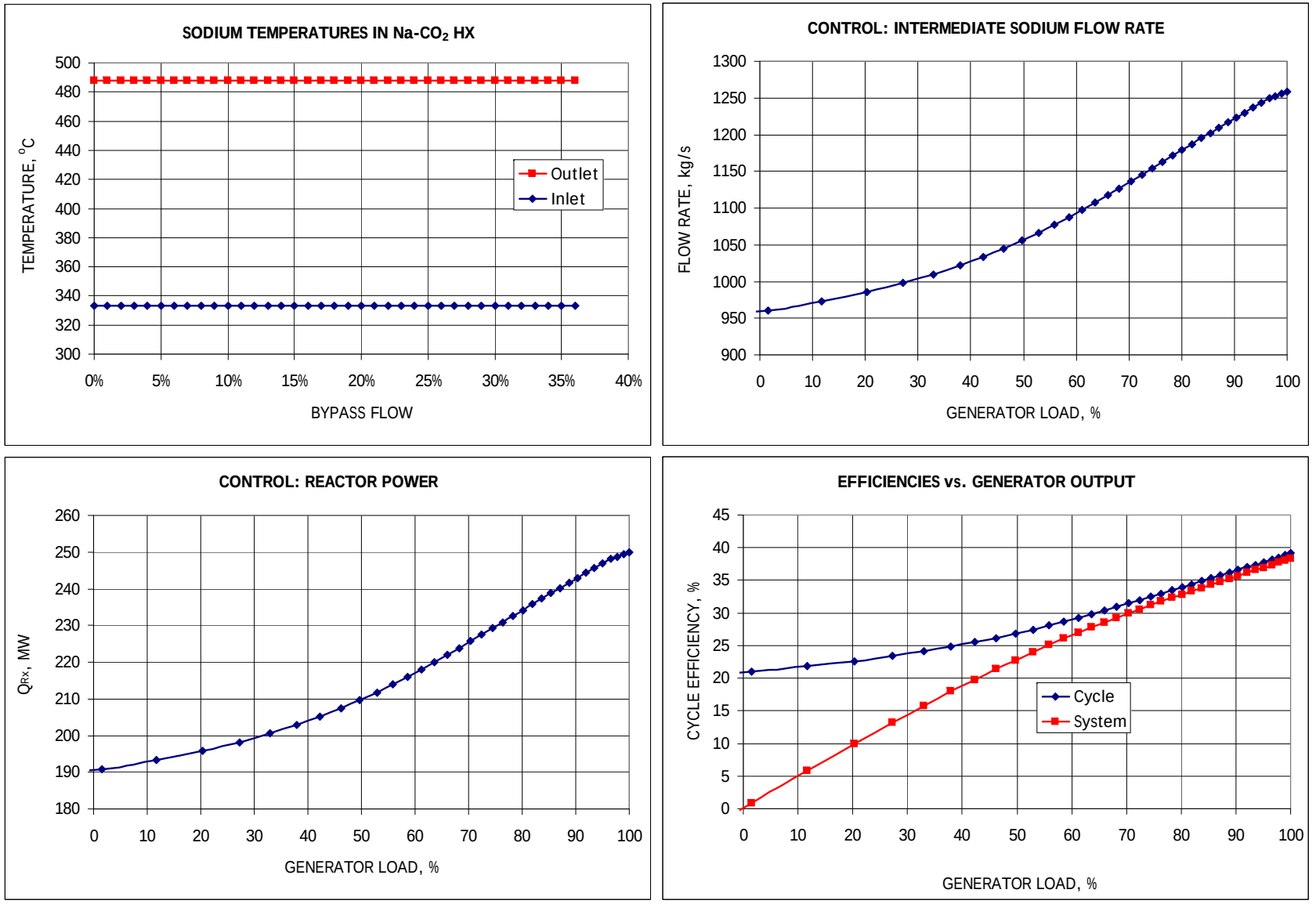

Figure A-4. Results of Turbine Bypass Control. (Continued)

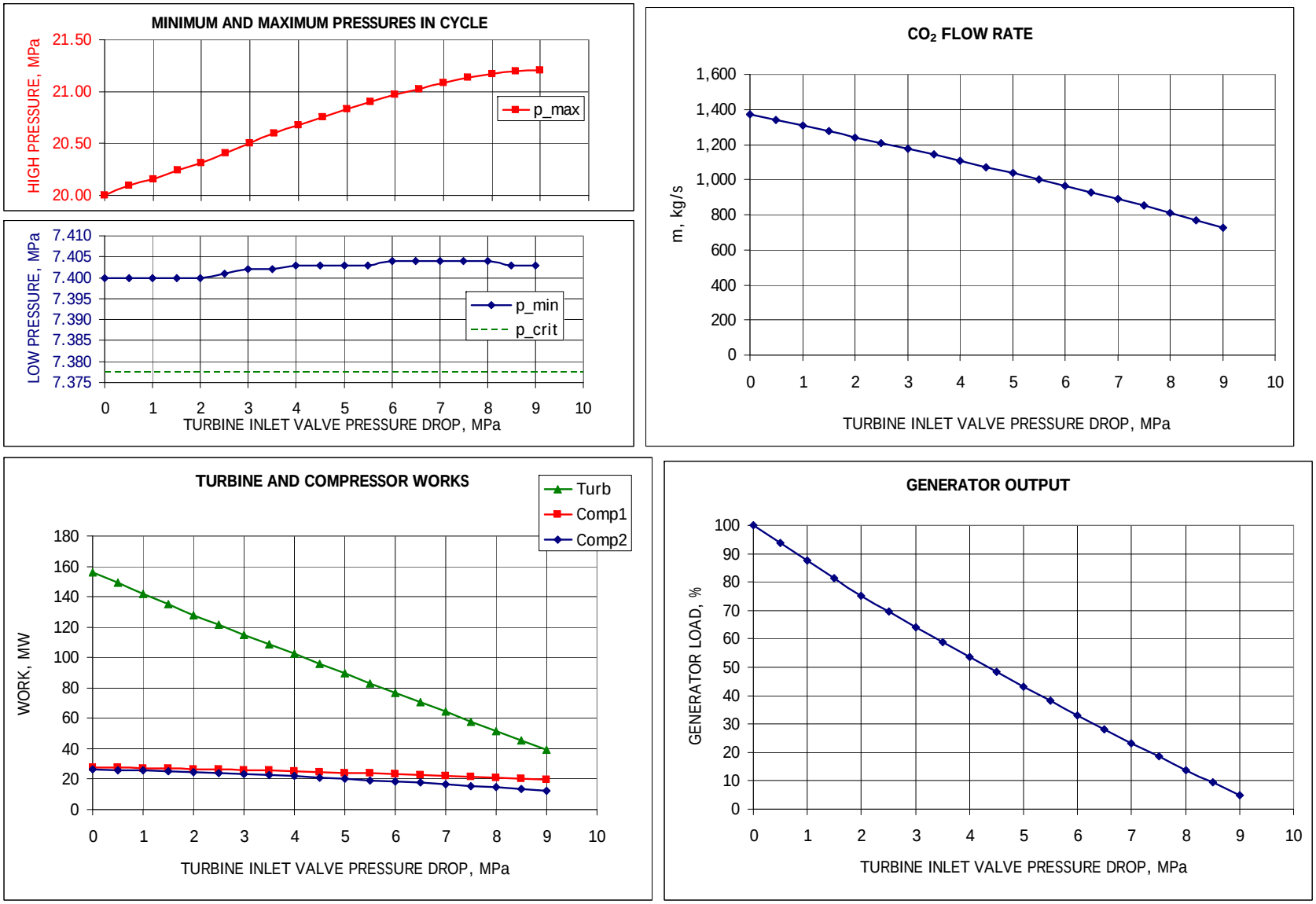

Figure A-5. Results of Turbine Inlet Throttling Control.

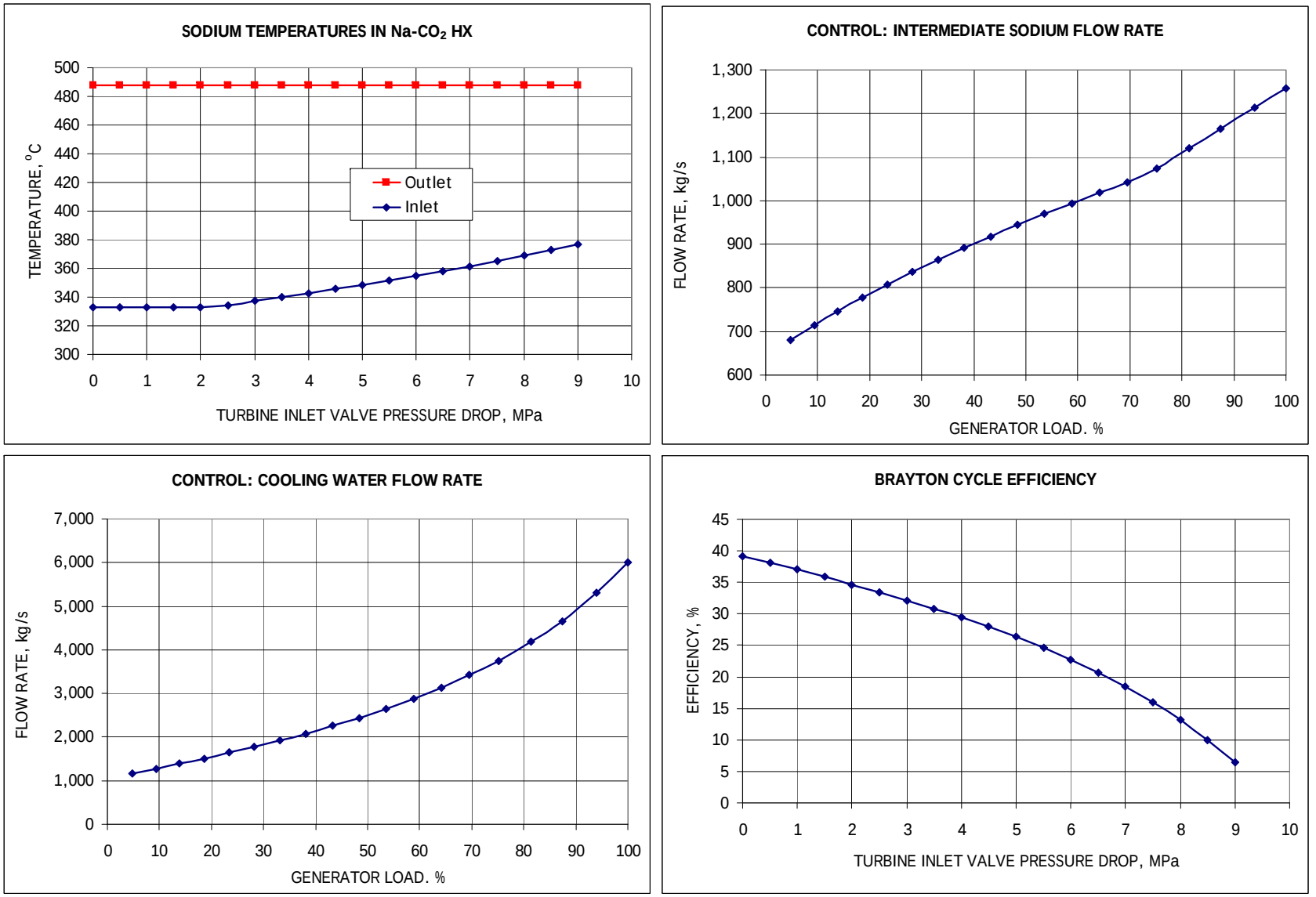

Figure A-5. Results of Turbine Inlet Throttling Control. (Continued)

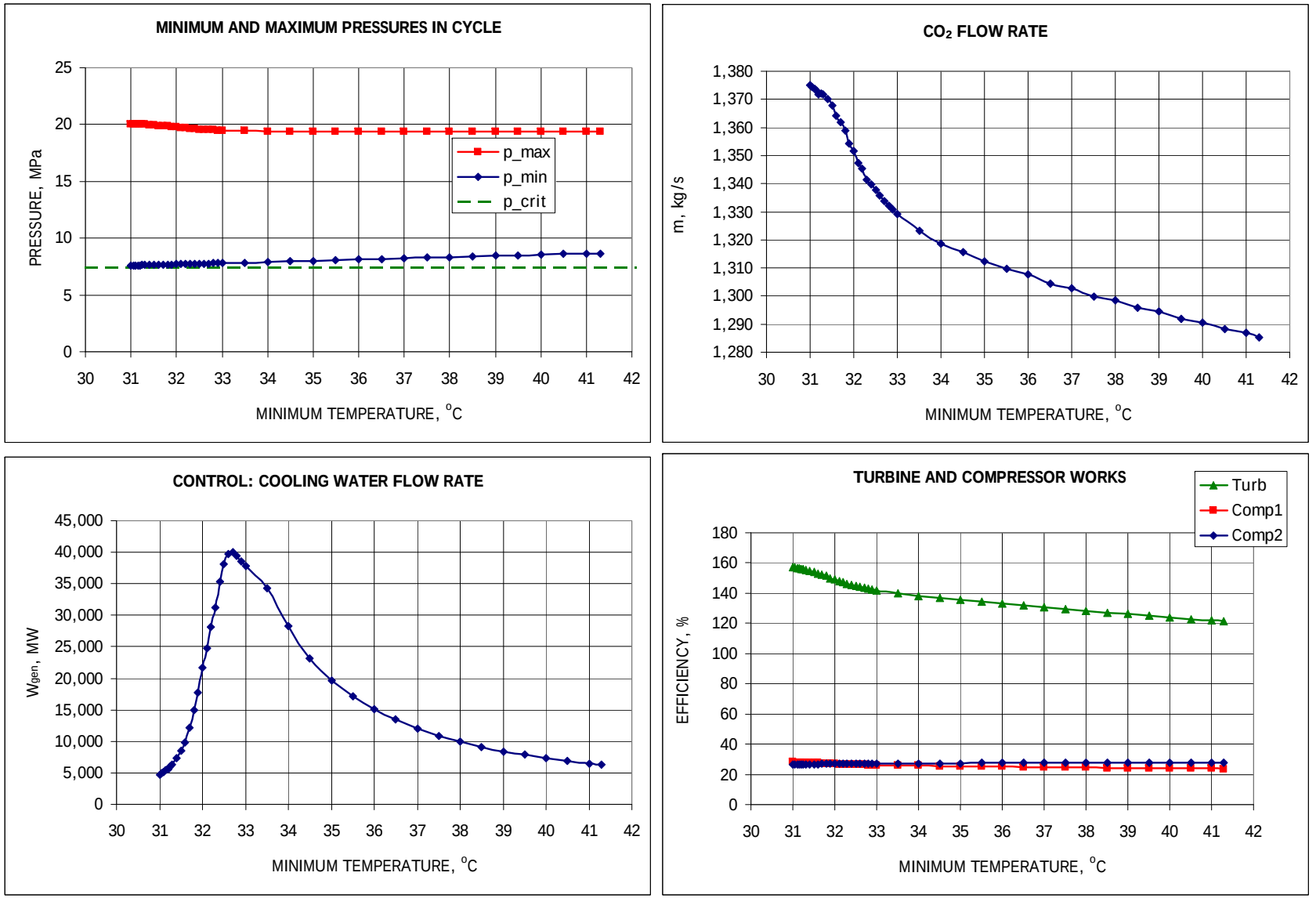

Figure A-6. Results of Minimum Temperature Control.

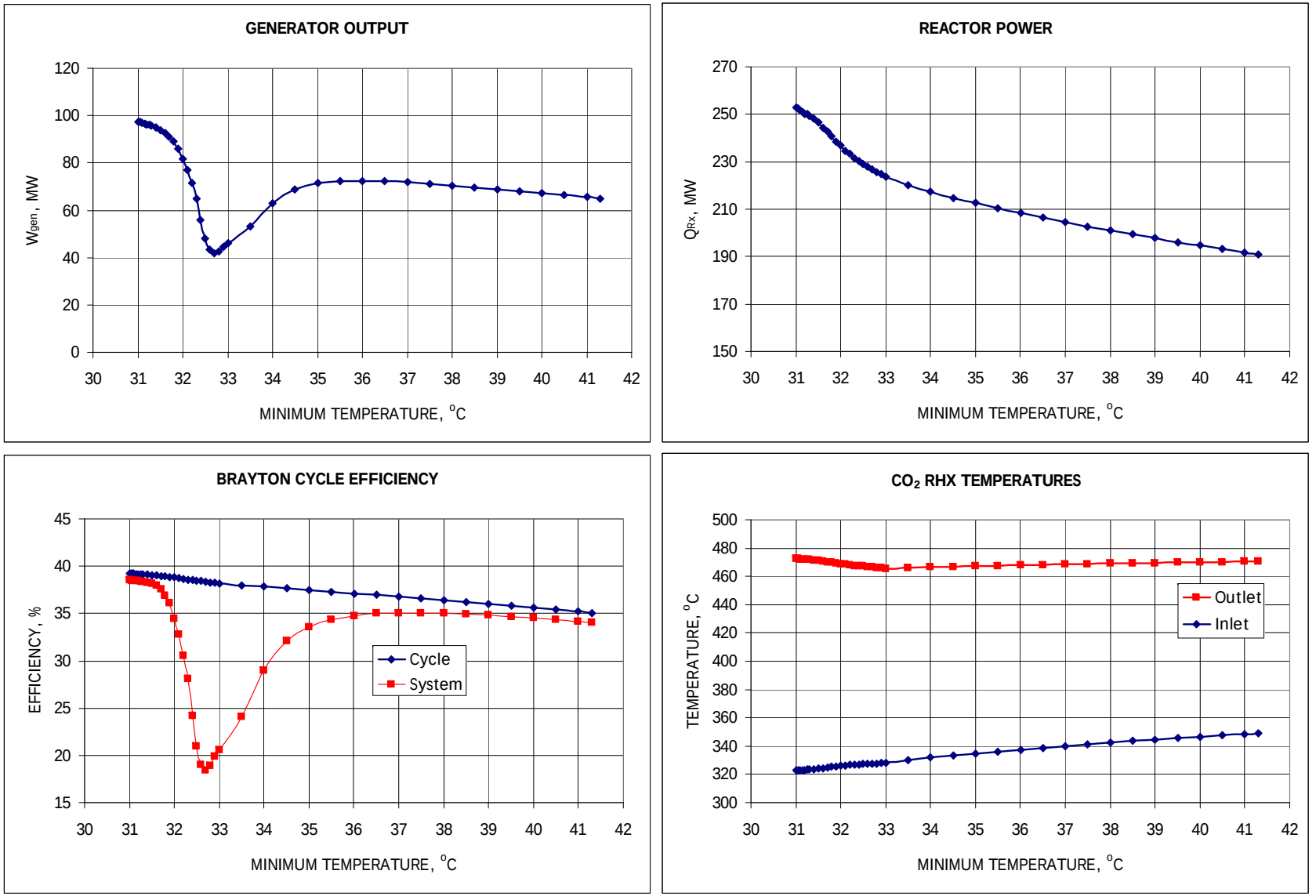

Figure A-6. Results of Minimum Temperature Control. (Continued)

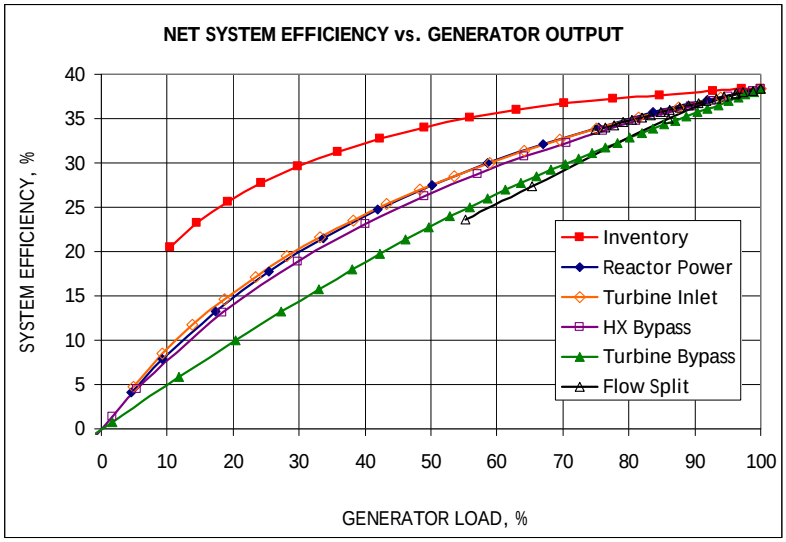

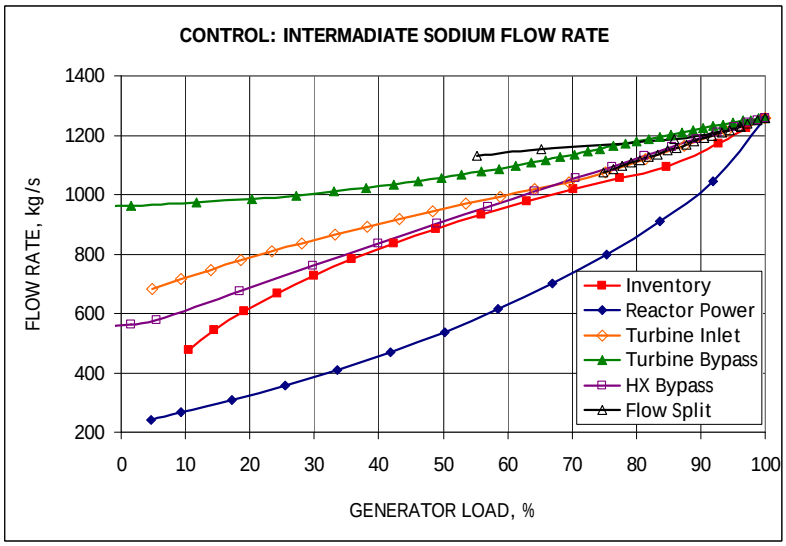

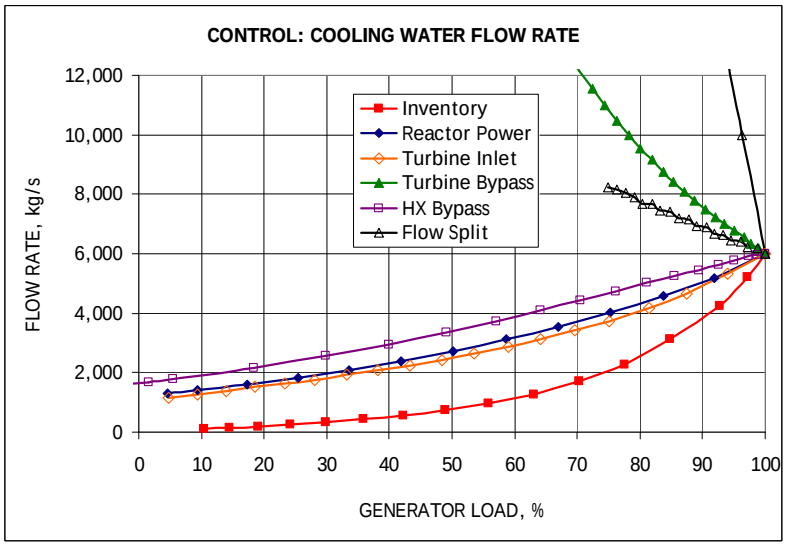

Figure A-7. Comparison of the Control Mechanisms.

The results of the analysis demonstrate that inventory control is a preferable control mechanism for the ABTR S-CO_2 cycle. However, the control relies on the inventory tanks to store the CO_2 mass removed from the cycle. In order for the control to operate in a passive mode (i.e. without boosting pumps), the pressure inside the tanks should not exceed the maximum system pressure. As the CO_2 mass is removed from the cycle, the cycle pressures are reduced while the inventory control tank pressure is increasing. The rate of the pressure increase in the tanks is defined by the tank total volume, as demonstrated in Figure A-8. The larger the tank volume, the lower the generator loads that can be achieved with inventory control. However, larger inventory tanks not only increase the capital cost of the S-CO_2 cycle, but also would require a larger building. It is estimated that for the tanks of total volume approximately equal to that of the high temperature recuperator (HTR), inventory control can be used from 100 % down to 30 % load.

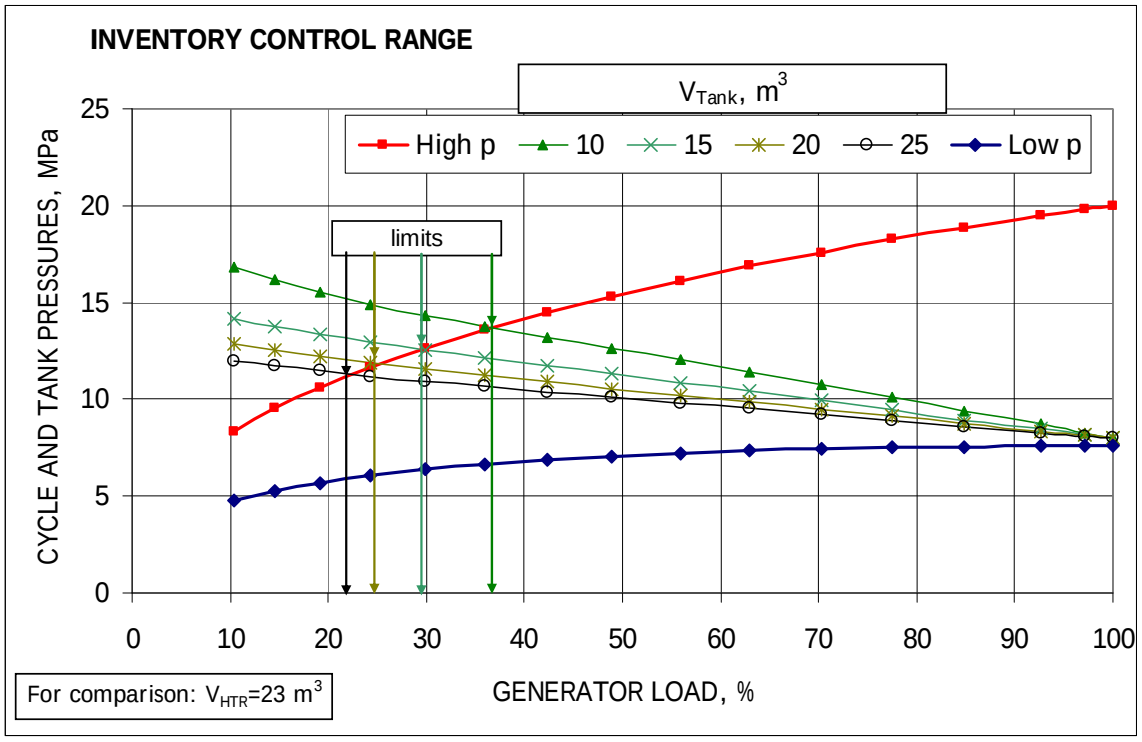

Figure A-8. Limits of the Inventory Control.

Below 30 % load, another control mechanism should be used. Both turbine bypass and reactor power control are suitable for these low loads, while the reactor power control produces slightly higher efficiency at low loads, as demonstrated in Figure A-7. Figure A-9 shows that the combination of the inventory control for loads between 100 % and 30 % and reactor power control below 30 % load can be used to control the ABTR S-CO_2 cycle over the entire range of load while providing the maximum cycle efficiency at reduced load.

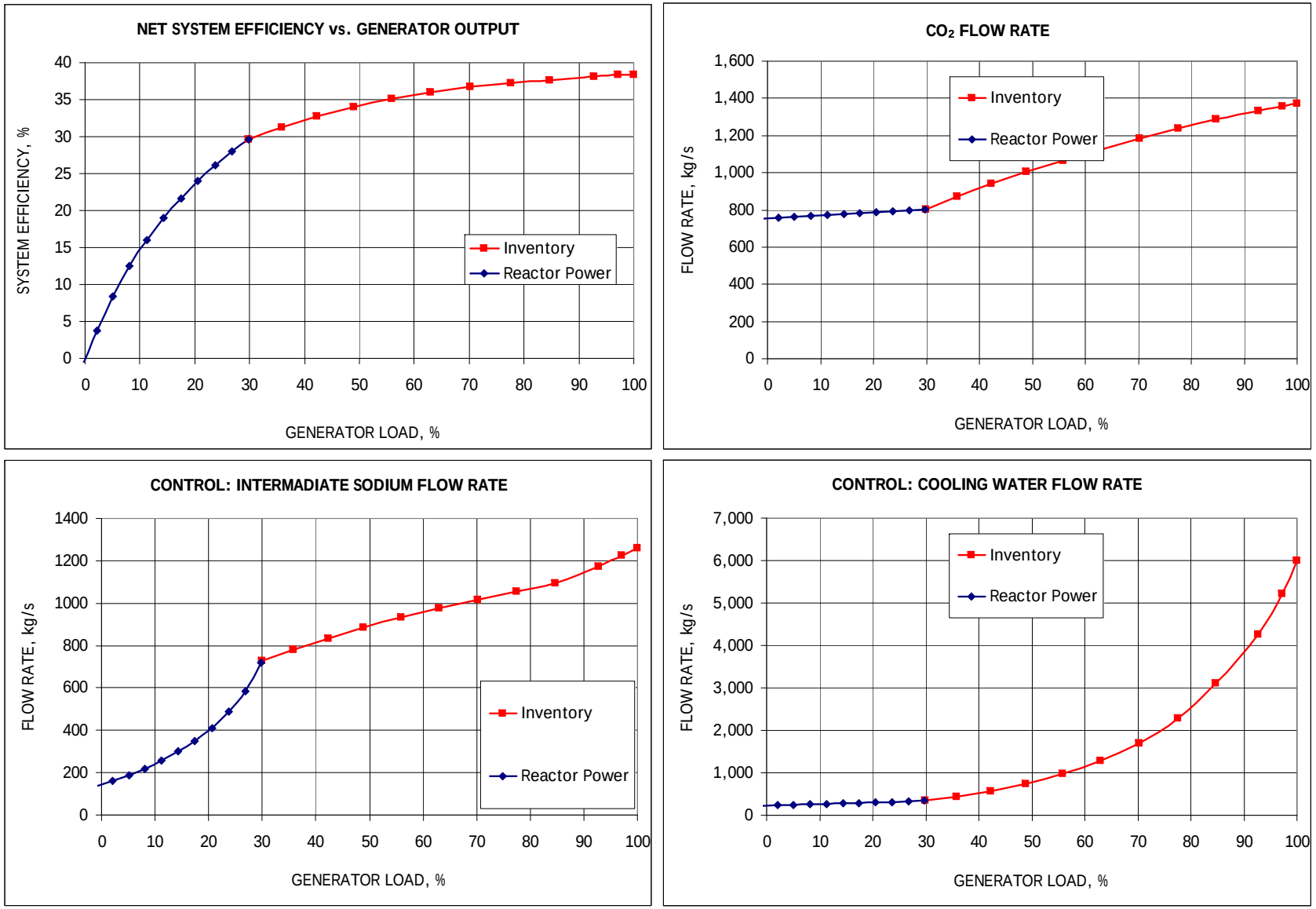

Figure A-9. Combination of Inventory and Reactor Power Controls.

References

A1. Chang, Y.I., et. al., "Advanced Burner Test Reactor Preconceptual Design Report," ANL-ABR-1 (ANL-AFCI-173), Argonne National Laboratory, September 5, 2006.

A2. Moisseytsev, A. and Sienicki, J. J., "Development of a Plant Dynamics Computer Code for Analysis of a Supercritical Carbon Dioxide Brayton Cycle Energy Converter Coupled to a Natural Circulation Lead-Cooled Fast Reactor," ANL-06/27, Argonne National Laboratory, July 2006.

A3. Moisseytsev, A. and Sienicki, J. J., "Supercritical CO_2 Brayton Cycle Control Strategy for Autonomous Liquid Metal-Cooled Reactors," Proceedings of Americas Nuclear Energy Symposium, ANES, Miami Beach, FL, October 3-6, 2004.

A4. Moisseytsev, A. and Sienicki, J. J., "Control of Supercritical CO_2 Brayton Cycle for LFR Autonomous Load Following," Transactions of the American Nuclear Society, Vol. 93, p. 342, American Nuclear Society 2005 Winter Meeting, Washington, DC, November 13-17, 2005.

A5. Moisseytsev, A. and Sienicki, J. J., "Automatic Control Strategy Development for the Supercritical CO_2 Brayton Cycle for LFR Autonomous Load Following," Paper 6074, Proceedings of 2006 International Congress on Advances in Nuclear Power Plants, ICAPP'06, Reno, NV, June 4-8, 2006.

Appendix B
A Utility for Piecewise Linear Fitting of Transient Data

A utility to convert arbitrary transient calculational results into a format suitable for a code input was developed. The codes considered in this work, SAS4A/SASSYS-1 and the Plant Dynamics Code, accept data in table form where the values of an input parameter are specified at fixed times and a linear fit is assumed between those time points. Therefore, the utility would need to fit the data with a piecewise linear function. It is assumed that the fit would be applied to a physical quantity such that a continuous function would be needed for the fit.

Suppose that there is a data set defined at certain values:

$$\{x_i, y_i\}, \quad i = 1,..., N .$$

For this application, y_i would be a value of the considered parameter (flow rate, temperature, etc.) at each time step x_i. A piecewise linear function needs to be found which accurately fits that data.

Suppose that the data is divided into n regions and a linear function is assumed inside each region j. It is assumed for the simplicity of the calculations that the border of each region would coincide with one of the data points, x_i. Denoting the region borders as $x_{0,j}$ and the values of linear fit at each border as f_j, the fit to the data on each region is found as following:

$$y_{fit,j}(x) = f_{j-1} + \frac{f_j - f_{j-1}}{x_{0,j} - x_{0,j-1}}\left(x - x_{0,j-1}\right), \quad x_{0,j-1} < x \le x_{0,j}$$

Assuming that the region j covers n_j data points, the difference between the data point and the fit for region j is defined as

$$\delta_i = y_i - y_{fit,j}(x_i) = y_i - \left[f_{j-1} + \frac{f_j - f_{j-1}}{x_{0,j} - x_{0,j-1}}\left(x_i - x_{0,j-1}\right)\right], \quad i = n_j + 1,..., n_{j+1}$$

Then, the least square fit is performed by calculating the total summation of the squared differences for all regions and all data points and minimizing that total summation:

$$R^2 = \sum_{j=1}^{n} \sum_{i=n_j+1}^{n_{j+1}} \delta_i^2 = \sum_{j=1}^{n} \sum_{i=n_j+1}^{n_{j+1}} \left\{ y_i - \left[f_{j-1} + \frac{f_j - f_{j-1}}{x_{0,j} - x_{0,j-1}}\left(x_i - x_{0,j-1}\right)\right]\right\}^2 = \min$$

$$\frac{\partial R^2}{\partial f_j} = 0$$

Since the fit in each region is done only based on two values f_{j-1} and f_j, the derivative of R^2 with respect to f_j has only two parts (and not the entire sum for j=1,…,n). The exception is for regions 1 and n, where only one part is present.

$$0 = \frac{\partial R^2}{\partial f_1} = -2\sum_{i=1}^{n_1}\left\{ y_i - \left[f_0 + \frac{f_1 - f_0}{x_{0,1} - x_{0,0}}\left(x_i - x_{0,0}\right)\right]\right\}\frac{x_i - x_{0,0}}{x_{0,1} - x_{0,0}}$$
$$-2\sum_{i=n_1+1}^{n_2}\left\{ y_i - \left[f_1 + \frac{f_2 - f_1}{x_{0,2} - x_{0,1}}\left(x_i - x_{0,1}\right)\right]\right\}\left(1 - \frac{x_i - x_{0,1}}{x_{0,2} - x_{0,1}}\right)$$

$$0 = \frac{\partial R^2}{\partial f_j} = -2\sum_{i=n_{j-1}+1}^{n_j}\left\{ y_i - \left[f_{j-1} + \frac{f_j - f_{j-1}}{x_{0,j} - x_{0,j-1}}\left(x_i - x_{0,j-1}\right)\right]\right\}\frac{x_i - x_{0,j-1}}{x_{0,j} - x_{0,j-1}}$$
$$-2\sum_{i=n_j+1}^{n_{j+1}}\left\{ y_i - \left[f_j + \frac{f_{j+1} - f_j}{x_{0,j+1} - x_{0,j}}\left(x_i - x_{0,j}\right)\right]\right\}\left(1 - \frac{x_i - x_{0,j}}{x_{0,j+1} - x_{0,j}}\right)$$

$$0 = \frac{\partial R^2}{\partial f_n} = -2\sum_{i=n_{n-1}+1}^{n_n}\left\{ y_i - \left[f_{n-1} + \frac{f_n - f_{n-1}}{x_{0,n} - x_{0,n-1}}\left(x_i - x_{0,n-1}\right)\right]\right\}\frac{x_i - x_{0,n-1}}{x_{0,n} - x_{0,n-1}}$$

Since the fit is made to the results of transient calculations, it is expected that the first point, $\{x_0, y_0\}$, represents the steady state value. Therefore, the steady state value should be the value of the fit function at the first time point such that

$$f_0 = y_0$$

Therefore, in the equations above, there are n unknowns – f_1,…,f_n – and n equations. Moreover, the equations are linear with respect to the f's such that a linear system of equations can be solved to find f_1,…,f_n:

$$\vec{A}\vec{f} = \vec{b}$$

where $\vec{A} = \left\{a_{i,j}, i = 1...n, j = 1...n\right\}$
$\vec{f} = \left\{f_j, j = 1...n\right\}$
$\vec{b} = \left\{b_i, i = 1...n\right\}$

The coefficients are found from the above equations:

$$a_{j,j-1} = \sum_{i=n_{j-1}+1}^{n_j}\left[1 - \frac{x_i - x_{0,j-1}}{x_{0,j} - x_{0,j-1}}\right]\frac{x_i - x_{0,j-1}}{x_{0,j} - x_{0,j-1}}$$

$$a_{j,j} = \sum_{i=n_{j-1}+1}^{n_j} \left[\frac{x_i - x_{0,j-1}}{x_{0,j} - x_{0,j-1}} \right]^2 + \sum_{i=n_j+1}^{n_{j+1}} \left[1 - \frac{x_i - x_{0,j}}{x_{0,j+1} - x_{0,j}} \right]^2$$

$$a_{j,j+1} = \sum_{i=n_j+1}^{n_{j+1}} \frac{x_i - x_{0,j}}{x_{0,j+1} - x_{0,j}} \left(1 - \frac{x_i - x_{0,j}}{x_{0,j+1} - x_{0,j}} \right)$$

with all other $a_{i,j}$=0 and $a_{j,j-1}$ and $a_{j,j+1}$ not needed for the first and last equations, respectively;

$$b_1 = -f_0 \sum_{i=1}^{n_1} \left[1 - \frac{x_i - x_{0,0}}{x_{0,1} - x_{0,0}} \right] \frac{x_i - x_{0,0}}{x_{0,1} - x_{0,0}} + \sum_{i=n_1+1}^{n_2} y_i \left(1 - \frac{x_i - x_{0,1}}{x_{0,2} - x_{0,1}} \right)$$

$$b_j = \sum_{i=n_{j-1}+1}^{n_j} y_i \frac{x_i - x_{0,j-1}}{x_{0,j} - x_{0,j-1}} + \sum_{i=n_j+1}^{n_{j+1}} y_i \left(1 - \frac{x_i - x_{0,j}}{x_{0,j+1} - x_{0,j}} \right), \quad j = 2,...,n-1$$

$$b_n = \sum_{i=n_{n-1}+1}^{n_n} y_i \frac{x_i - x_{0,n-1}}{x_{0,n} - x_{0,n-1}}.$$

The above system of linear equation is solved using a conjugate gradient solver. The pairs of the solution, in the form $\{x_{0,j}, f_j, j=0,\ldots,n\}$ are then supplied for the input to the transient code.

To find an optimal way to split the entire data into the specified number of region, the following procedure is implemented. First, the entire region is divided into two equal regions and the above system is solved with n=2. Then, the R^2 values are calculated for each region. The region with the largest R^2 is selected, divided into two equal regions, and the system is solved with three regions. The procedure is repeated until the specified number of regions is reached.

The utility was tested on the results of previous transient calculations where a transition from forced sodium flow to a natural circulation is calculated following the pump trip. Figure B-1 shows the calculated flow coastdown as a function of time during the first 2,000 seconds of the transient. This example was selected because it provides significant changes in the flow, by two orders of magnitude, and also shows highly non-linear behavior.

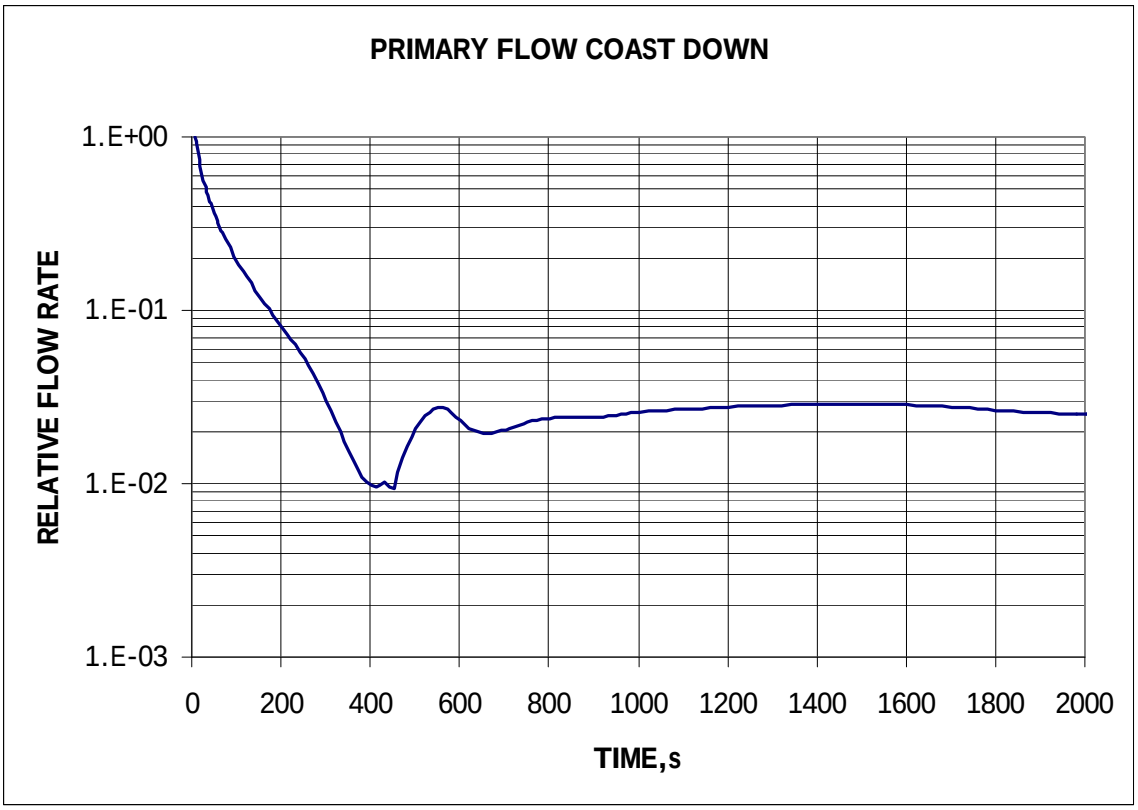

Figure B-1. Input Data for Utility Test.

Figures B-2 through B-4 show how the accuracy of the fit improves with an increase in the number of regions from 10 regions to 40 regions. All three graphs in each figure show the same data (Figure B-1) and fitting curves but plotted with the different scales. Except for the very small region in the middle, an almost perfect fit is achieved with 40 regions.

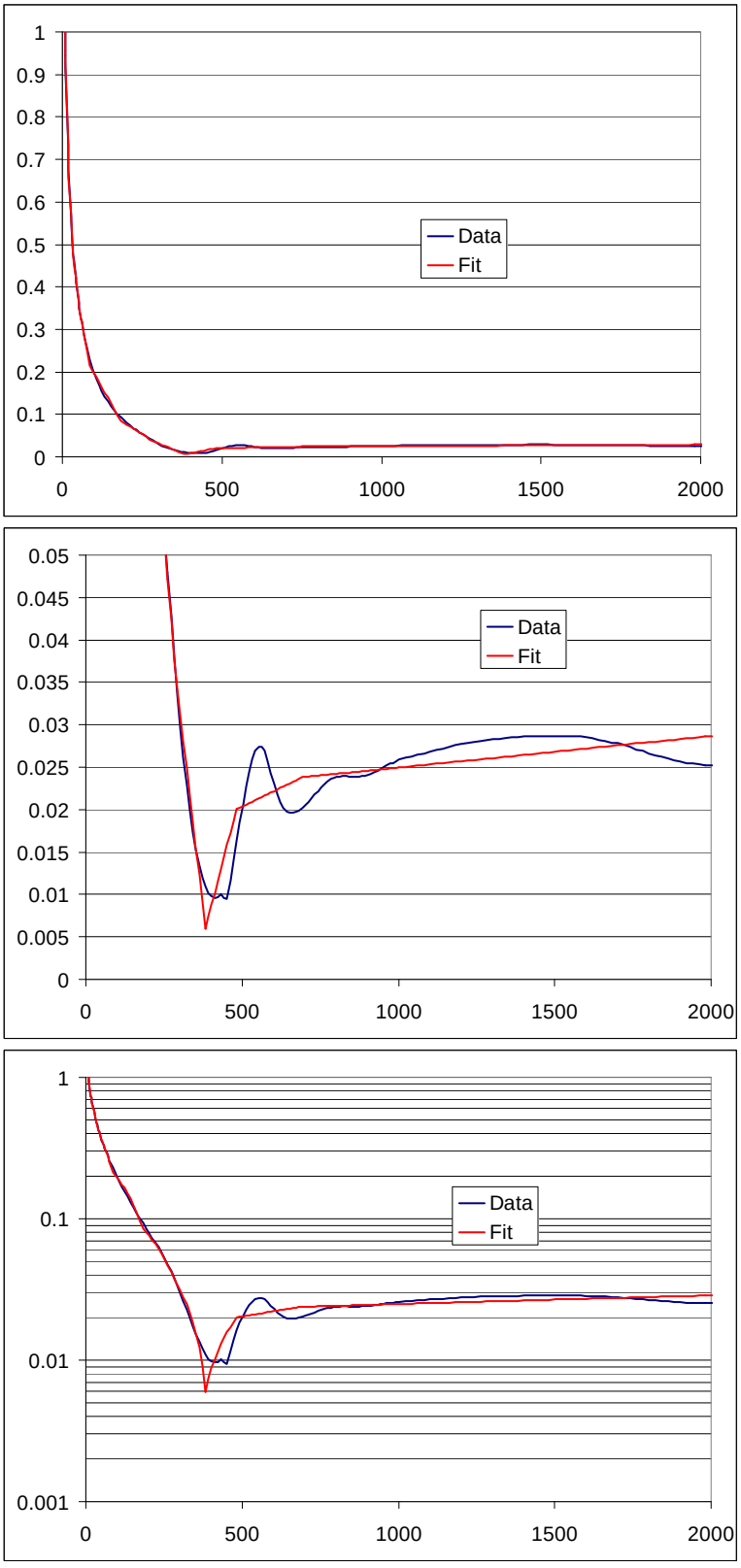

Figure B-2. Piecewise Linear Fit with 10 Regions.

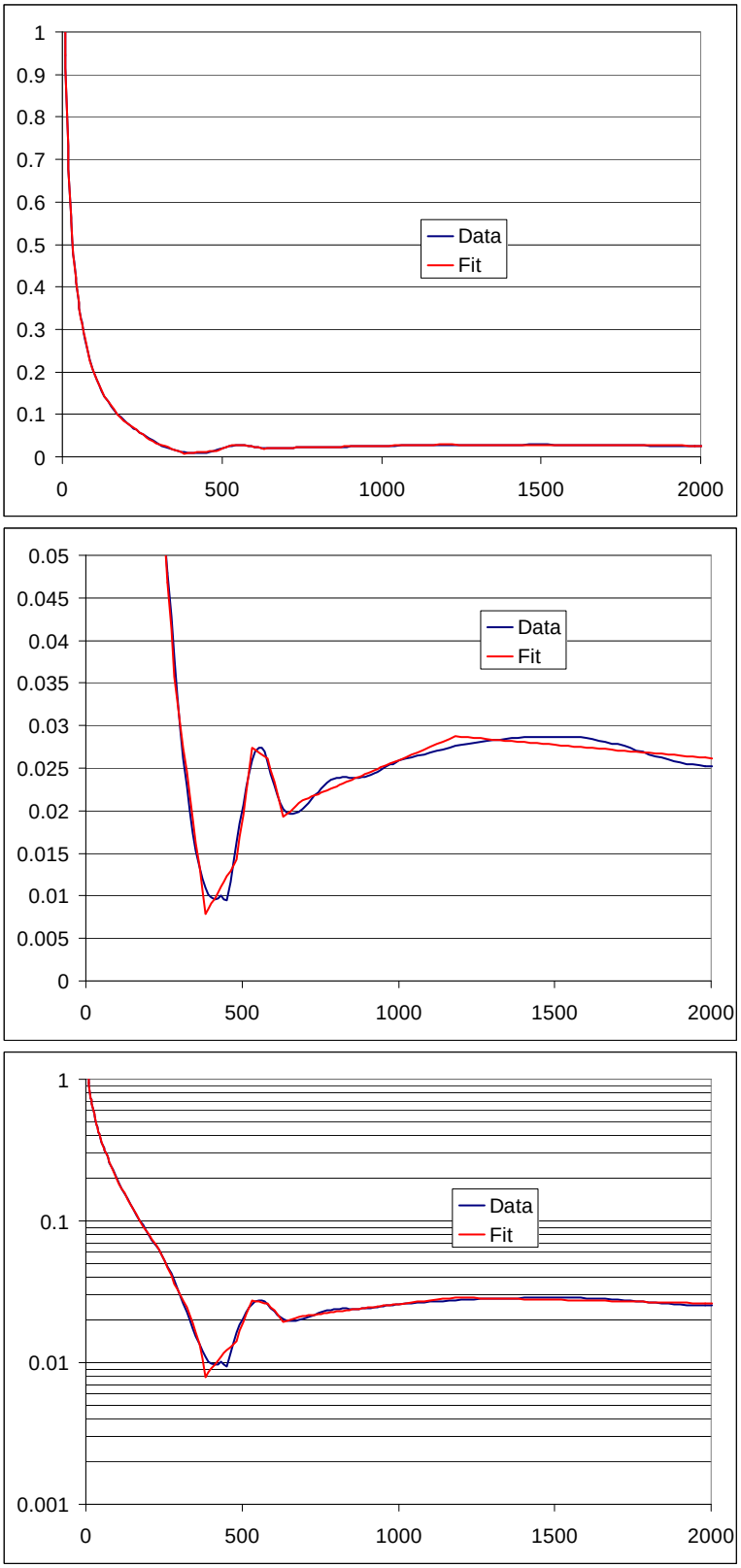

Figure B-3. Piecewise Linear Fit with 20 Regions.

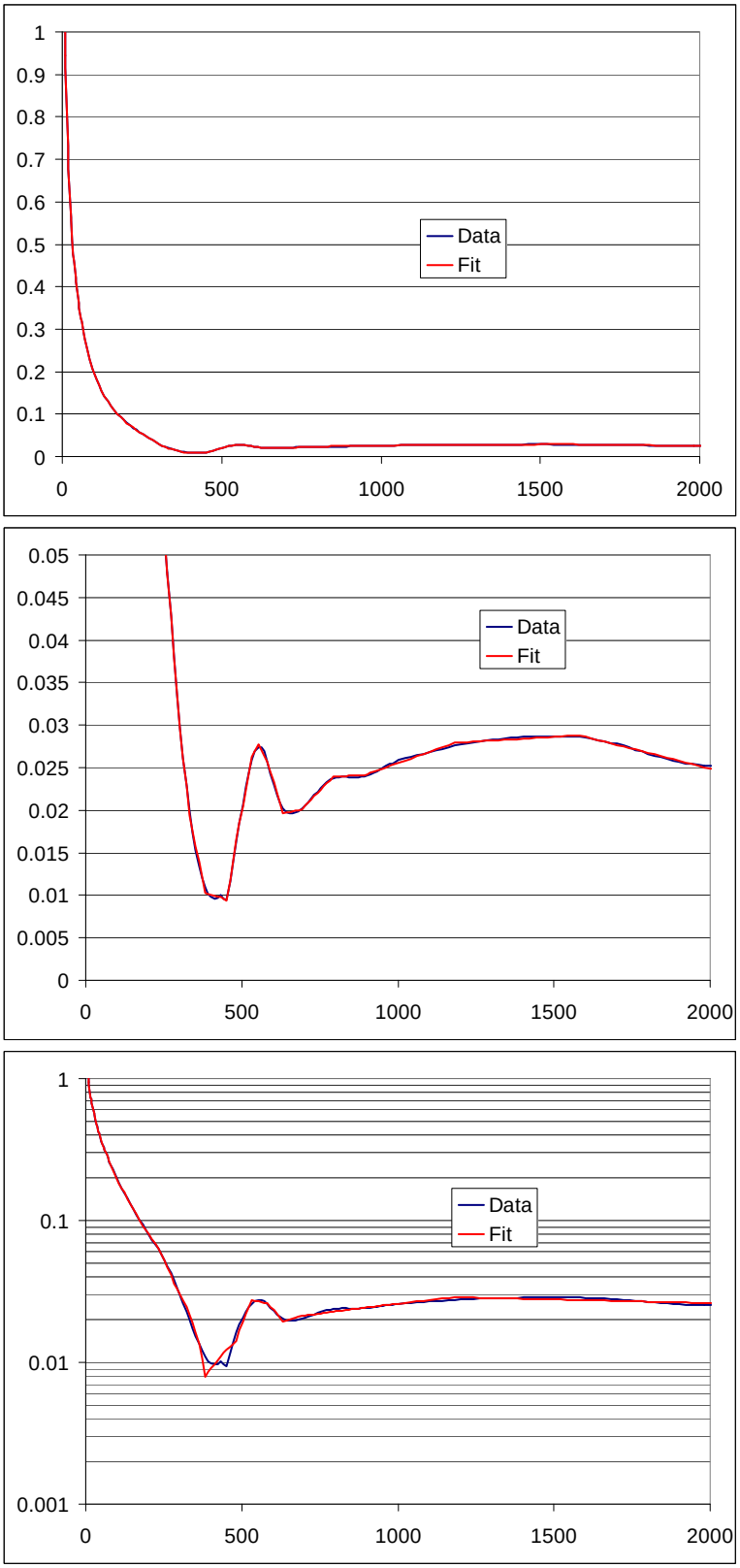

Figure B-4. Piecewise Linear Fit with 40 Regions.

It has been noticed in the above example that the fitted function was changing by two orders of magnitude (Figure B-1). At the same time, the fit has been done to minimize the absolute error between the data and the fit function. As a result, more significance is imposed on the high-flow regions (first few seconds of the transient), as opposed to the low-flow regions towards the end of the transient. Results in Figures B-2 through B-4 confirm that the fit for relatively high flows is much better than that for the relatively low flows. To address such situations, an option has been added to the utility to minimize relative rather than absolute error. The calculations in this case are similar to those described above, except that the error between the fit and the data is now calculated as:

$$\delta_i = \frac{y_i - y_{fit,j}(x_i)}{y_i} = 1 - \frac{1}{y_i}\left[f_{j-1} + \frac{f_j - f_{j-1}}{x_{0,j} - x_{0,j-1}}\left(x_i - x_{0,j-1}\right)\right], \quad i = n_j + 1,...,n_{j+1}.$$

Correspondingly, all of the coefficients in the equations and in matrices are normalized by y_i. Of course, in this option, the value of y_i should not be zero.

Figures B-5 and B-6 show the fits for the same data while the relative error is minimized for 10 and 20 regions, respectively. Compared to Figures B-2 and B-3, much better accuracy is achieved in the low flow regions, as expected. In fact, the fit with just 20 regions seems to be good enough such that 40 regions are not needed in this particular example.

The decision to minimize either absolute or relative error depends not only on the transient, but also on the importance of particular regions. For example, in the considered case, if a transition to the natural circulation is more important, than absolute error should be minimized. On the other hand, if long-term operation under the natural circulation is more important, then relative error should be minimized. The selection of number of regions is usually dictated by the format of the input file for a particular code and the limitations for that input.

The utility has a capability to provide the output in the format suitable for direct input for the considered codes (SAS4A/SASSYS-1 or the Plant Dynamics Code). It can also normalize the input to the steady state value.

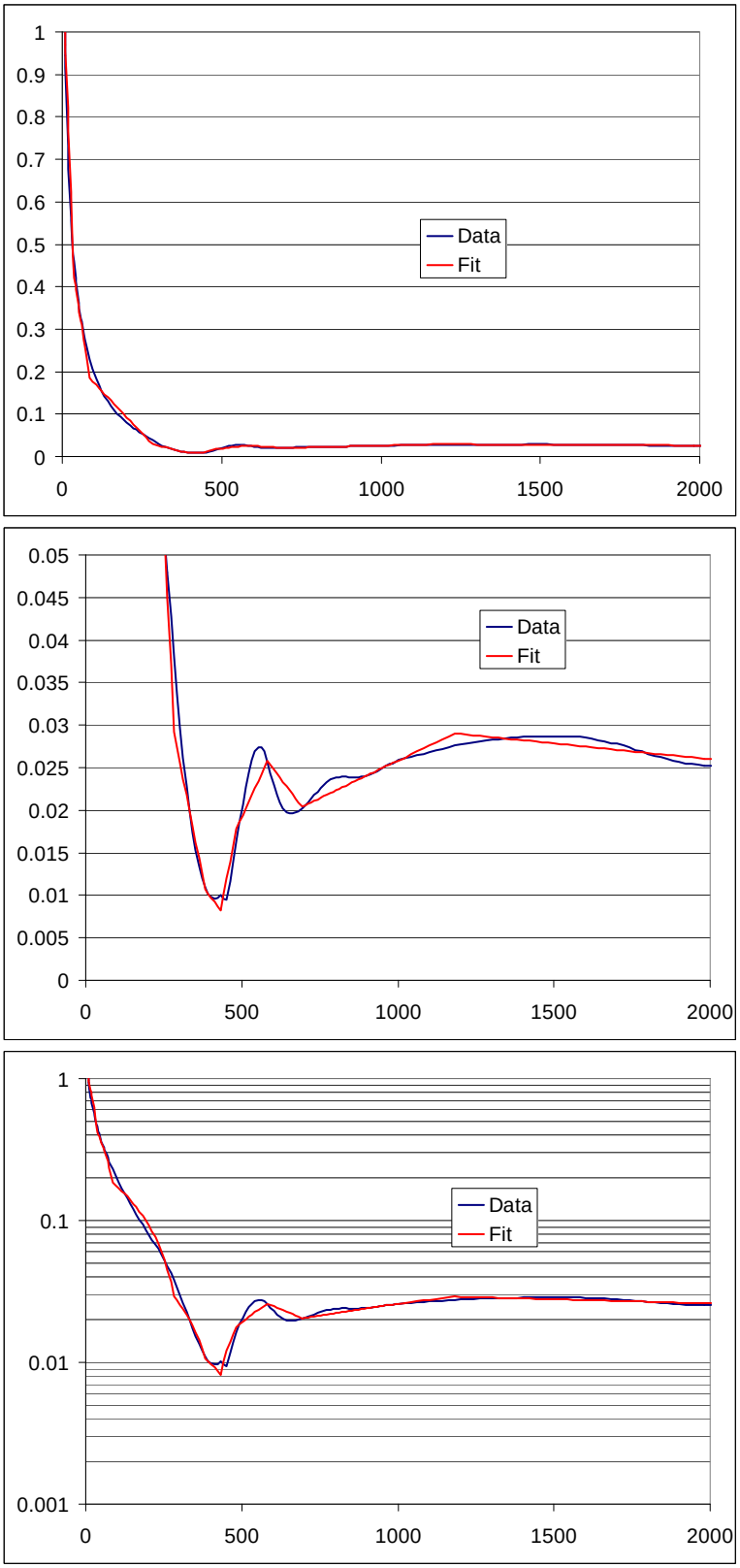

Figure B-5. Piecewise Linear Fit with 10 Regions, Relative Error.

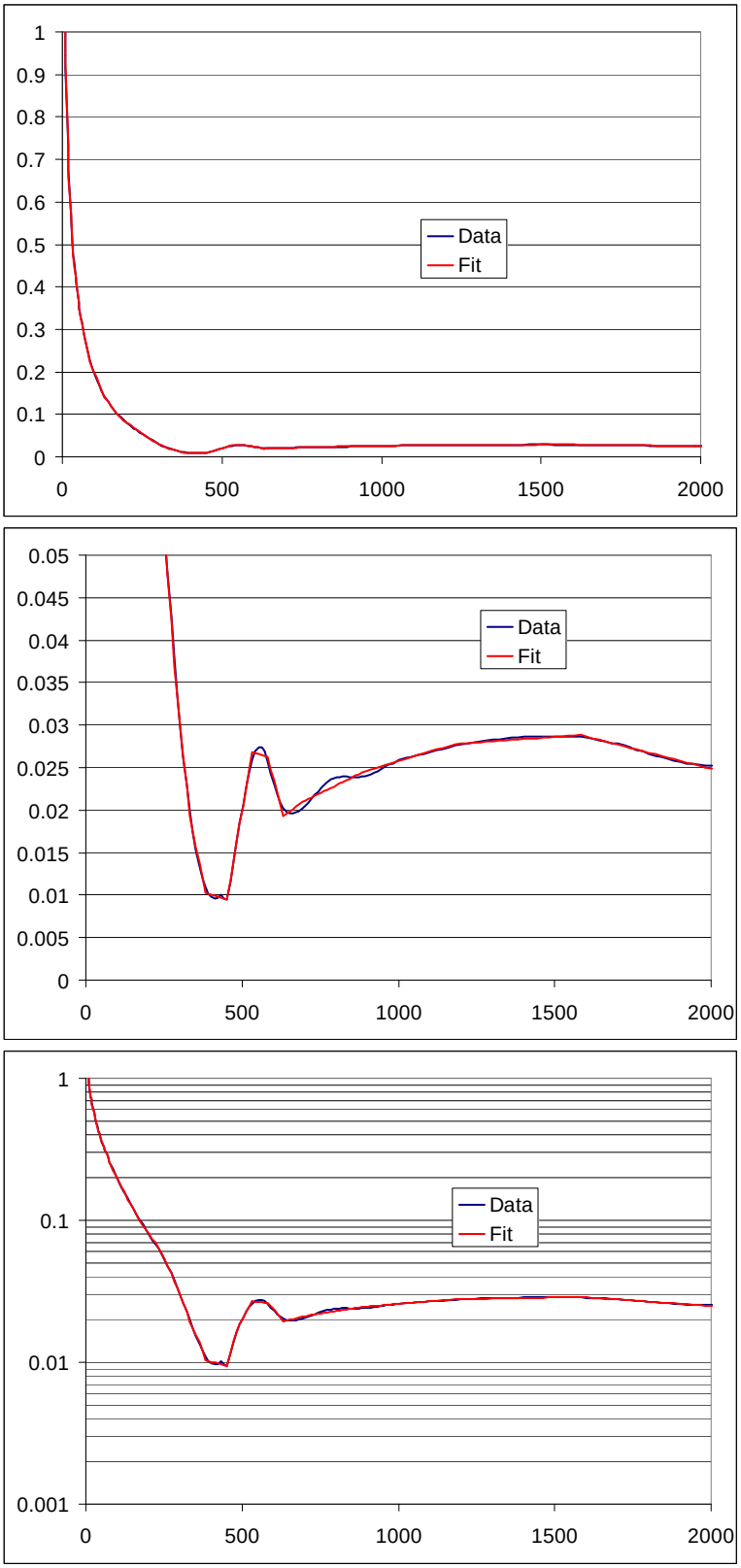

Figure B-6. Piecewise Linear Fit with 20 Regions, Relative Error.

Nuclear Engineering Division
Argonne National Laboratory
9700 South Cass Avenue
Argonne, IL 60439

www.anl.gov

A U.S. Department of Energy laboratory
managed by UChicago Argonne, LLC